Mechanism and Function of the Mitochondrial tRNA m^3C-Methyltransferase METTL8

DISSERTATION

ZUR ERLANGUNG DES DOKTORGRADES DER NATURWISSENSCHAFTEN (DR.RER.NAT)

DER FAKULTÄT FÜR BIOLOGIE UND VORKLINISCHE MEDIZIN DER

UNIVERSITÄT REGENSBURG

VORGELEGT VON

Eva Maria Schöller

AUS

Würzburg

IM JAHR

2021

Das Promotionsgesuch wurde eingereicht am:

19.11.2021

Die Arbeit wurde angeleitet von:

Prof. Dr. Gunter Meister

_____

Unterschrift

ABSTRACT

Mitochondria are the cell`s powerhouse with their own transcription and translation systems. The circular double-stranded DNA genome transcribes for two ribosomal RNAs (rRNAs), 22 transfer RNAs (tRNAs) and 13 messenger RNAs (mRNAs). The mt-mRNAs encode for 13 subunits of the respiratory chain embedded in the inner membrane. The inner and outer membrane of the mitochondrion form two internal compartments, the internal matrix and intermembrane space. For translation of the 13 mt-mRNAs mitochondria provide a complete und functional set of 22 mitochondrial encoded tRNAs (mt-tRNA). During their maturation from pre-tRNAs to their mature forms, mt-tRNAs undergo post-transcriptional modifications. Here, we identified the nuclear-encoded methyltransferase like 8 (METTL8) protein as a mitochondrial modifying enzyme that catalyzes m^3C_{32} methylation of mt-tRNA$^{Ser(UCN)}$ and mt-tRNA^{Thr}. Upregulating of METTL8 enhances respiratory activity, while it is reduces when METTL8 is lost. This dynamic regulation of METTL8 correlates with overall patient survival rates primarily in pancreatic cancer. Mitochondrial mitoribosomal profiling uncovered the molecular function of the METTL8-mediated m^3C_{32} methylation, which triggers mitoribosome stalling on mt-tRNA$^{Ser(UCN)}$ and mt-tRNA^{Thr} codons flanked by purine nucleotides. Proteomic analysis of respiratory chain complex I composition revealed that m^3C_{32} methylation balances the mitochondrial translation system by mostly affecting the mitochondrial encoded complex I subunits ND1 and ND6. Our data suggest that ND1 and ND6 levels may directly affect respiratory chain organization and thus its activity.

ZUSAMMENFASSUNG

Mitochondrien produzieren über ihr oxidatives Phosporylierungssytem (OXPHOS) Energie in Form von ATP. Die meisten Atmungskettenkomponenten sind Kern-codierte Proteine, 13 Untereinheiten sind jedoch mitochondrialen Ursprungs. Die zirkuläre doppelsträngige mitochondriale DNA codiert insgesamt für 2 ribosomale (rRNA), 22 transfer (tRNA) und 13 messenger RNAs (mRNA). Um ihre vollständige Funktion einnehmen zu können, müssen die 22 mitochondrialen tRNAs (mt-tRNA) post-transkriptionell modifiziert werden.

Dieser Arbeit charakterisiert die Funktion des METTL8-Proteins, eine RNA-spezifische Methyltransferase, die über ihre N-terminale Importsequenz ins Mitochondrium transportiert wird. Im Mitochondrium methyliert METTL8 die beiden mitochondrialen tRNAs mt-tRNA$^{Ser(UCN)}$ und mt-tRNA^{Thr} post-transkriptionell an der Anticodonschleifenposition 32. Physiologische Analysen zeigten, dass METTL8 die Atmungskettenfunktion beeinflusst. Zellen ohne jegliche METTL8-Expression haben eine verminderte Atmungskettenaktivität, Zellen mit erhöhter METTL8-Expression verzeichnen eine gesteigerte Atmungskettenaktivität. Eine erhöhte METTL8-Expression korreliert mitunter der Überlebensrate von Patienten, die an Bauchspeicheldrüsenkrebs leiden. Die molekulare Funktion dahinter konnte mittels *Ribosome Profiling* analysiert werden. Es stellte sich heraus, dass eine extreme METTL8-Expression bzw. eine fehlregulierte m^3C_{32} Methylierung das mitochondriale Ribosom pausieren lässt, wenn bestimmte mt-tRNA$^{Ser(UCN)}$ und mt-tRNA^{Thr} Codons erkannt werden. Eine weitere Analyse des Atmungskettenkomplex I ergab, dass eine fehlregulierte m^3C_{32}-Methylierung das mitochondriale Translationssystem bzw. die Translation der ND1- und ND6-Untereinheiten beeinflusst. Dadurch kann sich ein Translationsgleichgewicht zwischen den 13 mitochondrial-codierten Proteinen einstellen, dass die Atmungskettenkomposition und Atmungskettenaktivität verbessert.

PUBLICATIONS AND AUTHOR CONTRIBUTIONS

Parts of this thesis have been published in the following article:

Schöller, Eva; Marks, James; Marchand, Virginie; Bruckmann, Astrid; Powell, Christopher A.; Reichold, Markus et al. (2021): Balancing of mitochondrial translation through METTL8-mediated m(3)C modification of mitochondrial tRNAs. In: *Molecular cell. DOI:* 10.1016/j.molcel.2021.10.018.

Author contribution to this thesis:

James Marks and Markus Hafner performed ribosomal profiling data and analysis, Virginie Marchand and Yuri Motorin performed AlkAnilineSeq experiments and analysis, Christopher A. Powell, Christian Daniel Mutti and Michal Minczuk performed ^{35}S-methionine metabolic labelling of mitochondrial proteins. Regina Feederle generated monoclonal antibodies, Markus Reichold contributed to respiratory measurements, Stefan Hüttelmaier contributed to the cancer-associated aspects, Astrid Bruckmann, Peter Oefner and Katja Dettmer performed mass spectrometry.

CONTENTS

1 INTRODUCTION

1.1 The Biology of RNA Modifications

RNAs are modified post-transcriptionally by processes such as splicing, capping, polyadenylation, editing or chemical modifications. More than 170 (Esteve-Puig et al. 2020) chemically distinct RNA modifications on all four nucleotide (Motorin und Helm 2011) are known and highly conserved in all kingdoms of life. The most heavily modified RNA species are non-coding RNAs like ribosomal RNA (rRNA), transfer RNA (tRNA) and small nuclear RNA (snRNA). The functionality of RNA modifications ranges from RNA metabolism including mRNA splicing, translation and decay (Chatterjee et al. 2021), RNA fine tuning (Schwartz 2016) including dynamic RNA folding (Mugridge et al. 2018), stability (Tudek et al. 2019) and activity (Roundtree et al. 2017).

Two third of the 170 RNA modifications comprise RNA methylation. Preferred methylation sites are nucleophilic sites like nitrogens, oxygens of the 2`OH and carbon atoms at position 5 in pyrimidines and at positions 2 and 8 in adenosines (Motorin und Helm 2011) (Figure 1.1).

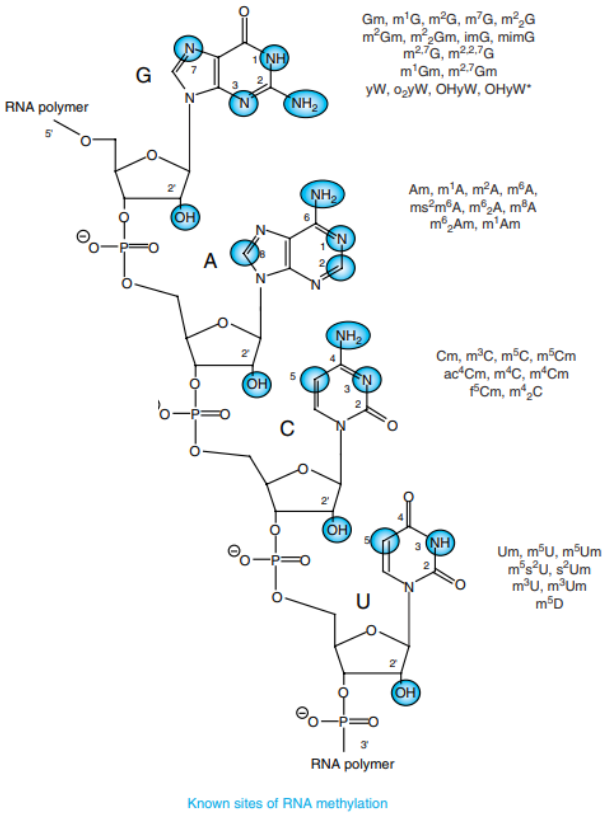

Figure 1.1: Overview of methylated nucleotide sites (Motorin und Helm 2011)
Chemical structure of all four ribonucleotides with their methylations sites highlighted in blue (left panel). Right panel lists all known modifications according to the ribonucleotide.

1.2 The tRNA Epitranscriptome

The classical tRNA function is linking the genetic code to its respective protein sequence. During translation, charged tRNAs transfer the mRNA encoded amino acid to a poly-peptide chain using the ribosome as mediator platform. For proper and efficient translation, functional tRNAs are essential. The maturation of tRNAs is a multi-step process starting with a tRNA precursor, which is further modulated and at least heavily modified by post-transcriptional modifications. 90 out of the overall 170 post-transcriptional modifications occur in tRNAs (Machnicka et al. 2013; Cantara et al. 2011), which accumulate in the tRNA core and the anticodon loop (Machnicka et al. 2014). Modifications in tRNAs control mainly the tRNA structure and its decoding fidelity. To ensure tRNA translation accuracy most of the tRNA modifications in the anticodon loop are found preferentially at the positions 34, 37 or 39 (Figure 1.2).

The great diversity of tRNA positions 34 and 37

Modifications at or next to the anticodon are one of the most functionally important and conserved modified residues. Particularly, the tRNA position 34, the wobble base complement, is frequently modified to restrict or increase wobbling (Krüger und Sørensen 1998; Murphy, 4th. et al. 2004). Wobbling allows tRNAs to recognize two to four nucleotides at the third position of the mRNA codon, which increase the tRNA capacity to decode synonymous mRNA codons and thus the translation of the degenerate genetic code. Nucleotide modifications at the wobble complement position 34 are for example queuine (Q_{34}), 5-methyl-cytosine (m^5C_{34}) or 5-methoxycarbonylmethyl-2-thiouridine ($mcm^5s^2U_{34}$), which support translational efficiency and fidelity (Figure 1.2) (Agris et al. 2007). Queuine is a guanine analogue and is found in tRNAs encoding for tyrosine (Tyr), histidine (His), aspartate (Asp) and asparagine (Asn) (Vinayak und Pathak 2009). This hypermodification is detectable in eukaryotes, prokaryotes as well in plants and affects anticodon flexibility and might regulate codon biased translation of discrete mRNA transcripts (Vinayak und Pathak 2009; Morris et al. 1999). Another modified residue at position 34 is uridine (U), which is universally hypermodified to $mcm^5s^2U_{34}$ particularly in higher eukaryotes and yeast. This modification appears in tRNAs encoding for lysine (Lys/UUU), glutamine (Gln/UUG) and glutamate (Glu/UUC) (Takai und Yokoyama 2003) and ensure proper decoding of the synonymous adenine (A) - and guanine (G) -ending codons (Rezgui et al. 2013). Further, the $mcm^5s^2U_{34}$ modification stabilizes the codon-anticodon pairing by enhancing the stacking interaction within the base pair (Hou et al. 2015).

The modified or hypermodified residue at position 37, adjacent to the wobble base (Figure 1.2), is known to restructure the anticodon loop to prevent binding to a fourth mRNA base, which ensure correct anticodon-codon pairing (Agris et al. 2007). Curiously, position 37 encodes exclusively for the purine bases guanine and adenine. Guanines are frequently methylated at N^1 (m^1G_{37}) and further hypermodified

to wybutosine (Cantara et al. 2011), which impedes ribosome slippage on phenylalanine codons (Tuorto und Lyko 2016a). Adenines are methylated at N^6 (m^6A_{37}), C^2 (m^2A_{37}) or thiomethylated at C^2 (ms^2i^6A, ms^2t^6A, ms^2io^6A, ms^2hn^6A) (Crécy-Lagard et al. 2010).

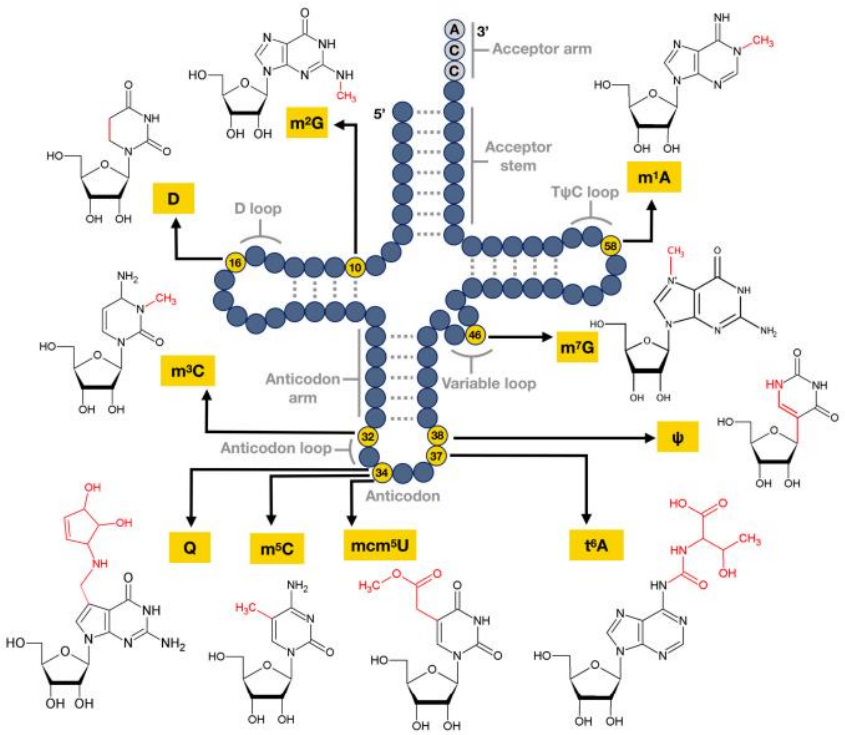

Figure 1.2: tRNA cloverleaf with the crucial modified positions (Huber et al. 2019)
tRNA cloverleaf with all known single methylation and hypermethylation sites in eukaryotes. Structural elements are appointed to the side of the tRNA cloverleaf. Crucial modified positions are highlighted in yellow, the modified residue of the nucleosides are indicated in red.

Structural impact of tRNA modifications

Functional tRNAs rely on simple ribose or nucleotide methylations and complex hypermodifications in the anticodon loop. In addition to decoding functions discussed before, hypermodifications support correct folding of the anticodon loop structure, which is vital for proper translation (Agris et al. 2007). Ribose 2`- *O* methylations, which are absent in mitochondrial tRNAs (Suzuki und Suzuki 2014), or nucleotide methylations occur mostly in the tRNA core region supporting the tertiary interaction between D and T arm and stabilize the three-dimensional fold (Lorenz et al. 2017)(Figure 1.3). Modifications in the core region, particularly m^5C modification at the positions 40, 51, 55 or 56 further affect the binding of magnesium (Mg^{2+}) ions. Fully or none modified tRNAs bind Mg^{2+} ions differently

and thus modulate the acceptor-anticodon interstem angle (Friederich et al. 1995; Friederich und Hagerman 1997; Friederich et al. 1998), which affects tertiary folding transitions. Under physiological Mg^{2+} concentrations, only fully methylated tRNAs obtain their functional optimum.

The structural impact of post-transcriptional tRNA modifications is demonstrated, for instance, by the loss of N^1-methyladenosine at position 9 (m^1A_9) in the mitochondrial $tRNA^{Lys}$ (Alexandrov et al. 2006; Kadaba et al. 2004). This modification blocks the alternative Watson-Crick base pairing to U_{64} and thus enables aminoacylation (Helm et al. 1998; Helm et al. 1999). This mechanism implicates that the tRNA structure heavily depends on specific modification patterns.

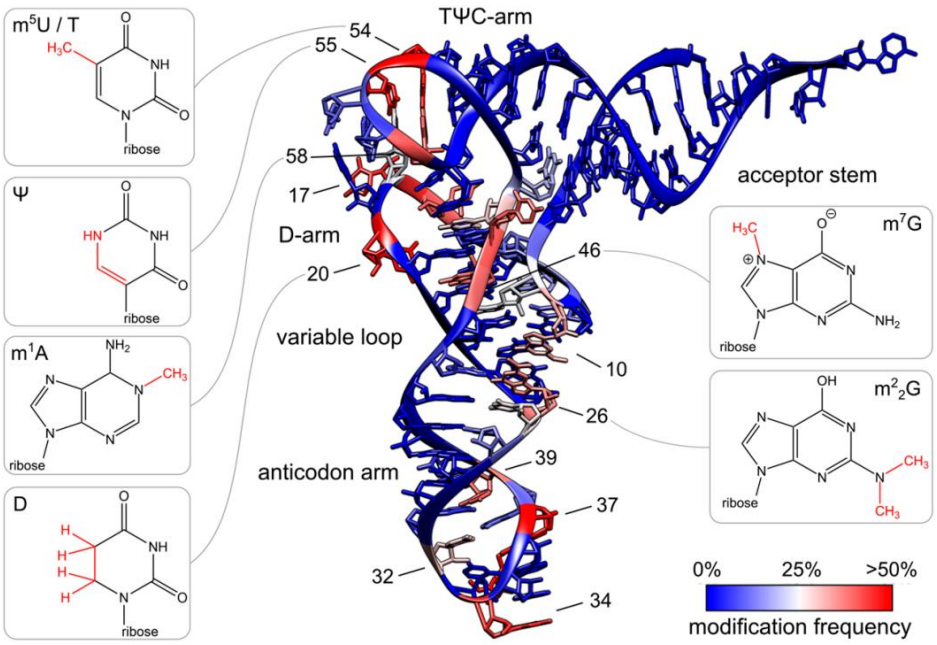

Figure 1.3: 3D tRNA cloverleaf with structurally crucial post-transcriptional modification (Lorenz et al. 2017)

Crystal structure of $tRNA^{Phe}$ from *S.cerevisiae*. Color indicates modification level of each nucleoside. Respective scale is shown at the bottom right. Chemical structure of the individual modification hotspots are shown to the side of the structure. Structural elements of the tRNA are named to the side.

During the establishment of the characteristic cloverleaf structure, multiple modifications are installed in a certain order and create an interdisciplinary network (Arimbasseri et al. 2016; Lin et al. 2018). This circuitry has been shown for the cytoplasmic $tRNA^{Ser}$ and the mitochondrial $tRNA^{Thr}$. Sequencing data revealed that patients with loss of N^6-isopentenyladenosine (i^6A_{37}) in $tRNA^{Ser}$ or N^6-treonylcarbamoyladeonsine (t^6A_{37}) in mt-$tRNA^{Thr}$ also lack the 3-methylcytidine (m^3C) modification at position 32 (Lin et al. 2018; Arimbasseri et al. 2016). Although most modifications are needed, a few

modifications can removed without structural collapse for adopting the correct tRNA structure (Helm 2006; Motorin und Helm 2010).

Diseases linked to tRNA modification defects

In 1990, human disorder were associated with hypo- or hypermodified tRNAs for the first time (Kobayashi et al. 1990). Analysis of patient samples confirm that loss of certain tRNA modifications cause metabolic or neurodegenerative disorders (Bento-Abreu et al. 2018; Guy et al. 2015; Abbasi-Moheb et al. 2012; Cohen et al. 2015; Davarniya et al. 2015; Simpson et al. 2009). Contrary, hypermodified tRNAs were detected in a variety of cancer types (Huang et al. 2018; Rapino et al. 2017). Further disorders linked to tRNA modification dysregulation are mitochondrial myopathy, encephalopathy, lactic acidosis and stroke-like episodes (MELAS) and myoclonus epilepsy with ragged red fibers (MERRF). Both disorders rely on A3243G mutations in mt-tRNA$^{Leu(UUR)}$ and A8344G mutations in mt-tRNA^{Lys} implicating loss of the taurine-derived modifications (τm^5U and $\tau m^5s\,^2U$) at the wobble position U_{34} (Schaffer et al. 2014). Mutation in the respective $m^5s\,^2$ modifying enzyme methylaminomethyl-2-thiouridylatemethyltransferase (TRMU) (Meng et al. 2017) causes a similar phenotype. Here, the lack of the $m^5s\,^2$ hypermodifcation in the mt-tRNAs Lys, Glu and Gln impair mitochondrial translation and enhance the reactive oxygen species (ROS) production (Guan et al. 2006; Meng et al. 2017).

Furthermore, loss of the anticodon loop modifications t^6A_{37} and $ms^2t^6A_{37}$ are associated with metabolic disorders like diabetes (Palmer et al. 2017) and imbalanced proteostastis, which results in neurodegeneration and MERRF (Edvardson et al. 2017; Lin et al. 2018). Patients suffering from neurodegenerative defects or MERRF display a lack of the t^6A modification at position 37, which is based on either the A15923G mutation in mt-tRNA^{Thr} or on mutation in the OSGEP protein (Edvardson et al. 2017; Lin et al. 2018). OSGEP is part of the KEOPS complex, which catalyze the t^6A modification. Loss of this universally conserved modification impair overall protein synthesis and activate the unfolded protein response (UPR) due to the accumulation of aberrant proteins in the ER lumen (Rojas-Benítez et al. 2017). The development of type 2 diabetes is caused by loss of the methyltiotransferase CDKAL1, which catalyze the ms^2 hypermodification of t^6A in the cytoplasmic tRNA$^{Lys(UUU)}$ (Arragain et al. 2010; Wei et al. 2011). In the absence of the ms^2 hypermodification, the translation of the respective lysine codons AAA and AAG in proinsulin is impaired, which reduced insulin β-cell secretion and endoplasmatic reticulum (ER) stress.

An additional disorder linked to tRNA modification defects is the non-syndromic X-linked intellectual disability, which correlates in particular with dysregulated ribose methylation (Guy et al. 2015; Dai et al. 2008). This brain disorder is caused by mutations in the modifying enzyme FTSJ1, which catalyze the 2`-*O*-methylcytidine (Cm) modification at position 32 and 2`-*O*-methylguanosine (Gm) at position 34 in the cytoplasmic phenylalanine tRNA (Phe).

Apart from modulating codon fidelity and tRNA structure, post-transcriptional modifications also affect the generation and accumulation of tRNA-derived fragments in human disorders (Soares und Santos 2017). Under stress conditions, mature tRNAs can be cleaved and the tRNA-derived fragments function as signal molecules in a variety of cellular processes, like gene expression, translation initiation and elongation and stress granule assembly. Some tRNA-derived fragments can also act as miRNAs (Hasler et al. 2016; Lee et al. 2009; Maute et al. 2013; Martens-Uzunova et al. 2014; Shen et al. 2018; Yeung et al. 2009). Usually tRNA fragments are cleavage products of abundant tRNAs and comprise 14- to 32-nucleotides. The tRNA- derived fragment can include either the extreme 5`- or 3` end of the respective mature tRNA or only an internal sequence. This alterative function of tRNAs is an issue in cancer, neurodegenerative disorders and infection (Martens-Uzunova et al. 2014; Yeung et al. 2009; Maute et al. 2013; Lee et al. 2009). Alterations in tRNA fragment levels are linked in particular to m^5C-, m^1G_9- and pseudouridine (Ψ)-tRNA hypomodifications. For instance, loss of m^5C due to the lack of the respective modifying enzyme NSUN2 triggers the accumulation of 5`tRNA-derived fragments in brain, which activates cellular stress response (Blanco et al. 2014; Flores et al. 2017). This intracellular stimulus reduce protein synthesis and thus impair brain development in mice (Blanco et al. 2014). In the absence of the tRNA methyltransferase TRMT10A, tRNAs miss the m^1G_9 modification, which initiates $tRNA^{Gln}$ cleavage in lymphoblast and iPSC-derived β-liked cells. The 5`$tRNA^{Gln}$-derived fragments of at least 22 nucleotides benefit β-cell apoptosis and therefore contribute to both type 1 and 2 diabetes (Cosentino et al. 2018). Contrary to the tRNA fragment accumulation described before, the Ψ-hypomodified tRNAs alanine (Ala), cysteine (Cys) and valine (Val) reduce the cleavage of their respective 5`tRNA fragments. In emybryonic human stem cells (hESCs), low levels of Ψ-5´tRNA-derived fragments leads to an inefficient translation initiation and affect stem cell fate determination (Guzzi et al. 2018). Of note, this hypomodification is caused by the lack of the pseudouridylate synthase PUS7 (Guzzi et al. 2018).

1.3 SAM-dependent Methyltransferases 'write' RNA methylations

SAM-dependent enzymes use the metabolite S-adensoyl-methionine (SAM or AdoMet) to transfer a methyl group to their acceptors producing S-adenosyl-homocysteine (SAH) as a by-product. The largest SAM-dependent enzyme family are SAM-dependent methyltransferases (MTases), which are classified in at least five independent structural classes (Struck et al. 2012). Class I, the Rossmann-fold MTases (RFM), is the largest superfamily and includes the most DNA methyltransferases as well as a few protein methyltransferases. RFMs act mostly as monomer, however di-, tri- and tetramers were also observed (Motorin und Helm 2011). Class II-IV combine MTases with less common structural elements like MTases containing MetH reactivation domain (class II), precorrin-4 MTases (class III) or the SPOUT family of RNA MTases (class IV), which represents the second largest group of RNA-MTases. SPOUT MTases act as dimers and catalyze the formation of N^3-methyluridine (m^3U), N^3-methylpseudouridine ($m^3\Psi$), N^1-methylpseudouridine ($m^1\Psi$), N^1-methylguanosine (m^1G), N^1-methyladenosine (m^1A) and 2´-*O*-ribose methylation. The interface of the two monomers forms the catalytic site (Motorin und Helm 2011). Class V consists of protein methyltransferases (PTM), primarily protein lysine methyltransferases (PKMTs), also known as SET-domain protein methyltransferases.

SAM-dependent RNA MTases share among themselves some additional catalytic features, like the acid-base catalysis meaning removal of at least one proton at its target site (Figure 1.4 A). Endocyclic nitrogen target sites (guanine *N*7; adenine *N*1 and cytosoine *N*3), however, are positively (+1) charged and are excluded from acid-base catalysis (Swinehart und Jackman 2015)(Figure 1.4B).

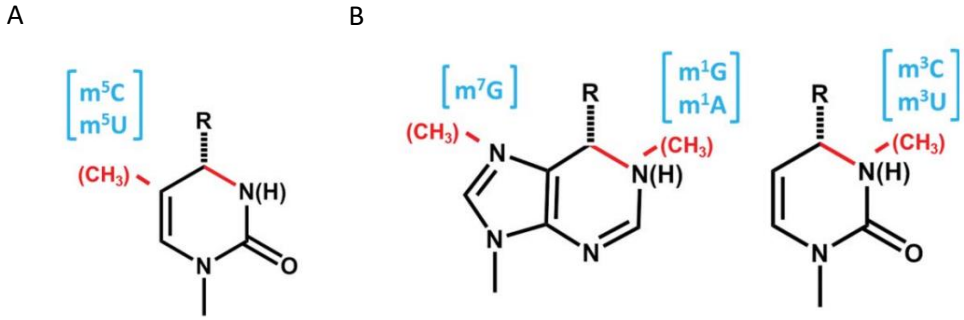

Figure 1.4: Acid-base catalysis and exceptions (Swinehart und Jackman 2015)
(A) Methylation at the carbon *C*5 in pyrimidines. Methylation sites are indicated in red as well the single/double bonds. Resulting modification is shown in brackets, the acid-base affected proton at *N*3 in parentheses. The remaining nucleotide at *N*4 is indicated by R.
(B) Methylation at the endocyclic nitrogens *N*7, *N*1 and *N*3 of purines and pyrimidines. Affected positions and single/double bond are indicated as described in (A). At physiological pH methylated endocyclic nitrogens *N*7, *N*1 and *N*3 are positively charged.

The probably most popular SAM-dependent RNA MTase is the methyltransferase-like 3 protein (METTL3), member of the supercomplex catalyzing the internal N^6-methyladenosine (m^6A) on messenger RNAs (mRNA) (Bokar et al. 1997; Bokar et al. 1994). The m^6A mehyltransferase supercomplex (MTC) composed of METTL3, METTL14, WTAP, VIRMA, ZC3H13, RBM15/15B and HAKAI plays a crucial role in human biology and is still highly investigated (Liu et al. 2013; Ping et al. 2014; Schwartz et al. 2014; Wang et al. 2014; Liu et al. 2014; Patil et al. 2016; Wen et al. 2018; Yue et al. 2018; Schöller et al. 2018). So far, its biochemical mechanism is well established. The modification is encoded within the consensus RRACH motif (R = A/G, H = A/C/U) by the catalytic component METTL3, whereas METTL14 regulates in return RNA binding. RRACH motifs in the coding sequence (CDS) and 3` untranslated region (3`UTR) next to the stop codon are preferentially modified (Huang et al. 2020; Delaunay und Frye 2019a; Deng et al. 2018; Dominissini et al. 2012; Jia et al. 2011; Meyer et al. 2012; Pan et al. 2018). Strikingly, the modification can be removed by the demethylases FTO and ALKBH5, so called erasers (Jia et al. 2011; Zheng et al. 2013). Longstanding, modifications were considered as static and stable however, in 2010 it was observed that yeast modulates its modification pattern due environmental cues such stress or nutrition (Endres et al. 2015; Chan et al. 2015; Chan et al. 2010) and benefits cell survival (Damon et al. 2015). The dynamic regulation of the m^6A mark catalyzed by the MTC affects particularly mRNA splicing, mRNA nuclear export, stability and localization (Parnell et al. 2021). This dynamic interplay between writer and erasers suggest further, that m^6A plays a crucial role in human diseases. Dysregulated METTL3/METTL14 expression results in severe developmental defects including embryonic lethality and misbalancing of the circadian period (Batista et al. 2014; Fustin et al. 2013; Geula et al. 2015). In cancer however, METTL3 is upregulated solely and triggers cancer cell growth, survival and invasion. Intriguingly, in cancer the catalytic activity of METTL3 is not essential suggesting the METTL3 N terminus acts as a mediator between the translation initiation factor 3 and the translation initiation complex supporting the translation of oncogenic transcripts (Hua et al. 2018; Lin et al. 2016).

The reversibility and dynamic of tRNA modification is demonstrated for example by the writer complex TRMT6/TRMT61A catalyzing m^1A using SAM as methyl donor and the eraser ALKBH1 (Liu et al. 2016). This reversible and dynamic system allows cells to adapt cellular functions to the environment affecting development and growth (Tuorto und Lyko 2016b; Kirchner und Ignatova 2015). Interestingly, cells with certain dysregulated writer expression have no clear phenotype under cell culture conditions. The missing tRNA modification is compensate by an upregulated tRNA expression pretending a functional tRNA (Esberg et al. 2006; Cload et al. 1996). This compensating effect impede the analysis of biological functions of RNA writers and modifications particularly for tRNAs.

1.4 Incomplete landscape of cytoplasmic and mitochondrial tRNA 'writers'

Human tRNA modifications are studied already for a long time. However, the knowledge on human tRNA modifying enzymes is incomplete. Currently, only the tRNA modifying proteome of *Saccharomyces cerevisiae* is almost complete (Crécy-Lagard et al. 2019). For humans, it has been suggested that approximately ~135 different tRNA writers are needed to modify all cytoplasmic and mitochondrial tRNAs (Crécy-Lagard et al. 2019), but so far, only few genes encoding for tRNA modification enzymes are listed in the MODOMICS database (Boccaletto et al. 2018). Of note, 20 different mitochondrial tRNA writers are already confirmed (Suzuki und Suzuki 2014; Suzuki et al. 2020). Crécy-lagard et al. tried to fill this gap by matching cytosolic and mitochondrial tRNA modification genes to their respective modifications (Figure 1.5) using public available sequencing data and databases (Crécy-Lagard et al. 2019). This approach enables to map tRNA modifications to tRNA writer candidates, which were mainly uncharacterized methyltransferases, pseudouridine synthases or THUMP-domain-containing proteins. However, few modifications could still not be allocated to any writer candidate and have to be identified first (Figure 1.5, highlighted in red) (Crécy-Lagard et al. 2019). The annotation of several different isoforms of tRNA modifying enzymes or the dynamic modification system complicate this process.

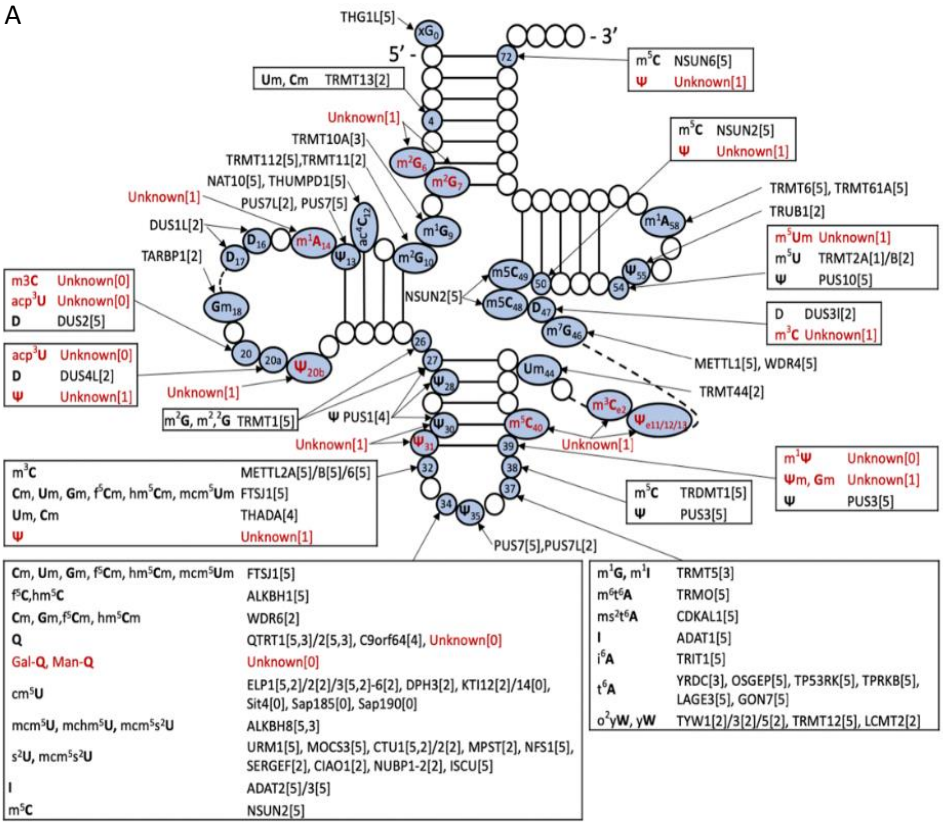

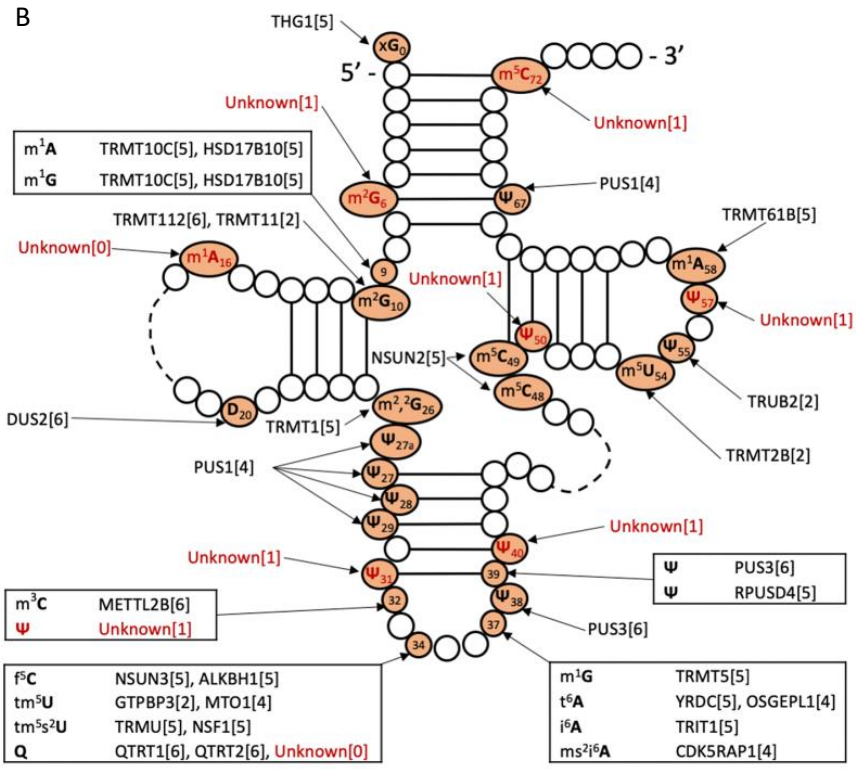

Figure 1.5: Cloverleaf of cytoplasmic and mitochondrial tRNA with indicated modified residues (Crécy-Lagard et al. 2019)

(A) Cloverleaf structure of cytoplasmic tRNA and its modified residues (blue). Respective modifying enzymes are indicated and valued with an evidence code, shown in brackets. [0] suggested candidate [1] potential, not verified candidate [2] non-mammalian validated candidate [3] human *in vitro* validated candidate [4] mammalian candidate validated in a heterologous host [5] mammalian *in vivo* validated candidate. Unknown writers are highlighted in red.

(B) Cloverleaf structure of cytoplasmic tRNA and its modified residues (orange). Respective modifying enzymes are indicated and valued with an evidence code, shown in brackets. [0] suggested candidate [1] potential, not verified candidate [2] non-mammalian validated candidate [3] human *in vitro* validated candidate [4] mammalian candidate validated in a heterologous system [5] mammalian *in vivo* validated candidate [6] cytoplasmic counterpart. Unknown writers are highlighted in red. Of note, QTRT1 and QTRT2 are validated as mammalian mt-tRNA writers, responsible for Q34 formation (Suzuki et al. 2020)

AIM OF THIS THESIS

During maturation, tRNAs undergo several processing steps including post-transcriptional modifications. Various sequencing strategies identified potentially all post-transcriptionally modified residues in cytoplasmic and mitochondrial tRNAs. However, the knowledge of their respective modifying enzymes is incomplete. To identify potential tRNA writers, uncharacterized methyltransferases, pseudouridine synthases or THUMP-domain containing proteins were matched to the post-transcriptional tRNA landscape, which in part were confirmed in separate studies. The methyltransferase like proteins (METTL) METTL2A/B and METTL6 were characterized and validated as cytoplasmic tRNA writers catalyzing the formation of 3-methylcytidine (m^3C). Their homolog METTL8 was identified as an m^3C mRNA writer, a second study postulate METTL8 is involved in R-loop formation in the nucleus. At the beginning of this thesis work, the predicted methyltransferase METTL8 was fully uncharacterized. It was therefore the aim of this thesis to identify and characterize its catalytic activity, the type of modification it is catalyzing, its natural substrate RNA as well as its cellular functions.

2 RESULTS

2.1 Establishment of monoclonal antibodies against METTL8

An essential basis for the investigation of METTL8 are well-characterized and specific biochemical reagents. Therefore, we initiated out work with creating a toolbox including antibodies. Monoclonal antibodies were generated by rat immunizations with a 13 amino acid (aa) METTL8 peptide (Figure 2.1A). Hybridomas were generated by our collaborator Regina Feederle from the Monoclonal Antibody Core Facility, Helmholtz-Zentrum in Munich (Monoclonal Antibody Core Facility, Institute for Diabetes and Obesity, Helmholtz-Zentrum München, German Research Center for Environmental Health, 85764 Neuherberg, Germany). Hybridomas were subsequently selected and tested in immunoprecipitation (IP) and western blot. We fused an FLAG/HA (F/H)-tag to the C terminus of METTL8, overexpressed the construct in Flp-In TREx293 cells and performed IP experiments using different hybridomas. METTL8-F/H was immunoprecipitated successfully by the antibody clones 16A7 and 19A10. An anti-FLAG IP was used as control (Figure 2.1B). The signal intensities of the anti-FLAG antibody in the control und test IPs were comparable. Furthermore, the antibody clones 16A7 and 19A10 were verified in an endogenous METTL8 IP (Figure 2.1C). The endogenous METTL8 IP in presence of RNaseA was equivalent to the IP without RNaseA. The RNase treatment indicated that the METTL8 IP is an RNA-independent enrichment and further not influenced by additional RNA-protein interactions. Simultaneously, the affinity of the antibody clone 19A10 was confirmed in western blots (Figure 2.1C, top). To validate the specificity of the detected METTL8 signal, we rerun the METTL8 IP with three additional METTL8 knock-out clones (KO) (Figure 2.1C, bottom). No signal was detected in all three METTL8 KO clones. In the third step, the detected signal was authenticated as METTL8 by mass spectrometry (Figure 2.1D). For identification, HeLa S3 lysate was used and separated on a sucrose gradient (data not shown). Fractions including METTL8 were pooled and METTL8 IP of the pooled fractions was performed by the anti-METTL8 clone 16A7. Indeed, the band migration at the expected position was identified as METTL8 by mass spectrometry. This analysis was performed by our collaborator Astrid Bruckmann (Regensburg Center for Biochemistry (RCB), Laboratory for RNA Biology, University of Regensburg, 93053, Regensburg, Germany). In addition, the mass spectrometry data was screen for METTL8 interaction partners. Unfortunately, no specific interaction partner could be identified in these assays (data not shown).

A

METTL8 (NM_024770.4)

MNMIWRNSISCLRLGKVPHRYQSGYHPVAPLGSRILTDPAKVFEHNWDHQWSKEEEAA
ARKKVKENSAVRVLLEEQVKYEREASKYWDTFYKIHKNKFFKDRNWLLREFPEILPVDQK
PEEKARESSWDHVKTSATNRFSRMHCPT**VPDEKNHYEKSS**GSSEGQSKTESDFSNLDSEK
HKKGPMETGLFPGSNATFRILEVGCGAGNSVFPILNTLENSPESFLYCCDFASGAVELVK
SHSSYRATQCFAFVHDVCDDGLPYPFPDGILDVILLVFVLSSIHPDRMQGVVNRLSKLLK
PGGMLLFRDYGRYDKTQLRFKKGHCLSENFYVRGDGTRAYFFTKGEVHSMFCKASLDEKQ
NLVDRRLQVNRKKQVKMHRVWIQGKFQKPLHQTQNSSNMVSTLLSQD

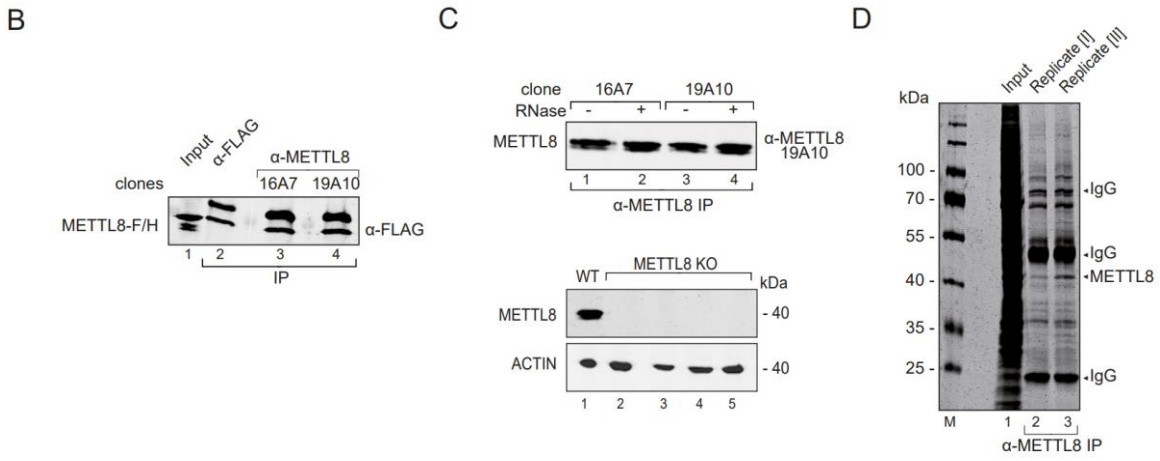

Figure 2.1: Establishment of monoclonal antibodies against METTL8
(A) Protein sequence of METTL8 (Uniprot: B3KW44) including peptide sequence for immunization (highlighted in green)
(B) Validation of the METTL8 monoclonal antibody clones 16A7 and 19A10 in immunoprecipitation (IP) using Flp-In TREx293 overexpressing METTL8-F/H. α-Flag IP was used as control.
(C) Top: IP of endogenous METTL8 using monoclonal METTL8 antibody clones 16A7 and 19A10 and RNaseA. Monoclonal METTL8 antibody clone 19A10 was used for western blotting. Bottom: α- METTL8 IP of Flp-In TREx METTL8 WT and three METTL8 KO Flp-In TREX clones.
(D) Coomassie Blue gel after α-METTL8 IP in HeLa S3 cells using METTL8 antibody clone 19A10. Lysate was purified by a sucrose gradient before. Indicated METTL8 protein was validated by LC-MS/MS analysis.

2.2 METTL8 is a mitochondrially localized protein

In 2017 and 2020 it was reported that METTL8 modifies mRNAs or RNAs within nuclear R-loop structures (Xu et al. 2017; Zhang et al. 2020). According to this RNA species and localization, METTL8 should localized either in the cytoplasm or in the nucleus. While antibody testing for immunofluorescence (IF) in Flp-In TREx293 cells overexpressing METTL8-F/H we observed a specific granular cytoplasmic pattern (Figure 2.2A) reminiscent of a classical mitochondrial localization. Thus, we assumed that METTL8 might be a mitochondrial protein and co-stained METTL8-F/H or -GFP either with the antibody against the mitochondrial outer membrane protein TOMM20 (Figure 2.2B,

upper panel) or MitoTracker, which specifically labels mitochondria (Figure 2.2B, lower panel). In both panels we observed a 100 % overlay of the fluorescence signals of the METTL8-F/H or -GFP construct and TOMM20 or MitoTracker. The mitochondrial localization was further validated by biochemical fractionation experiments (Figure 2.2C). We purified mitochondria of Flp-In TREx cells mechanically and through several centrifugation steps and tested each fraction (debris including nuclei, cytosol and mitochondria) for the nuclear marker protein NRB54, the cytoplasmic marker ACTIN and the mitochondrial inner membrane marker TIMM44. Endogenous METTL8 was enriched in each fraction by IP prior to western blotting. METTL8 was barely or not present in debris and cytosol fractions, but clearly detectable in the mitochondrial fraction (Figure 2.2C). A proteinase K (PK) treatment exclude an unspecific or specific binding to the mitochondrial surface. The METTL8 signal intensities of the untreated and PK-treated fraction are equivalent and proves METTL8 localizes to mitochondria.

Most nuclear encoded mitochondrial proteins are translated as precursor proteins with an N-terminal cleavable mitochondrial targeting sequence (MTS) in the cytosol (Abe et al. 2000; Roise und Schatz 1988; Roise et al. 1986; Roise et al. 1988; Heijne 1986). The MTS can be predicted by different algorithms. We used MitoFates (Fukasawa et al. 2015) and found a potential N terminally mitochondrial import motif of METTL8 with a probability of almost 0.9 (Figure 2.3A). Of note, there is no MTS prediction for the METTL8 homologs METTL2A/B and METTL6. Usually the import into the mitochondria is mediated by binding of the hydrophobic MTS residues to TOMM20 (Abe et al. 2000). To directly test this, we mutated consecutively the hydrophobic isoleucines (Ile) and leucine (Leu) in the predicted TOMM20 recognition site to glutamines (Gln) (Figure 2.3A). The GFP-tagged METTL8 mutants were transfected into HEK 293 cells and co-stained with the MitoTracker (Figure 2.3B). The single METTL8 mutant (Ile^{4}) mainly localized to the mitochondria but also to the cytoplasm (panel I). Loss of two isoleucine residues ($Ile^{4,9}$) in the TOMM20 recognition site results in a diffuse cytoplasmic pattern (panel II) and the mitochondria start to fragmentate. Taken together, the predicted MTS signal is active based on the hydrophobic residues Ile^{4} and Ile^{9}. Biochemical fractionations of the corresponding F/H-tagged METTL8 mutants confirm the IF results (Figure 2.3C). The triple mutation $Ile^{4,9}$ and Leu^{12} leads to a clear mis-localization to nucleoli (Figure 2.3B, panel III), which might be based on the predicted METTL8 N terminally nuclear localization sequence (NLS). Moreover, we observed apoptosis in cells with METTL8 nucleoli mis-localization (panel IV). Interestingly, both targeting signals, MTS and NLS are conserved in mammalian METTL8 isoforms. For example, in mice the MTS is detectable N terminally in all isoforms, the NLS in three of six isoforms placed at the nearer C-terminus. Summarizing, we found that METTL8 is a mitochondrially localized protein.

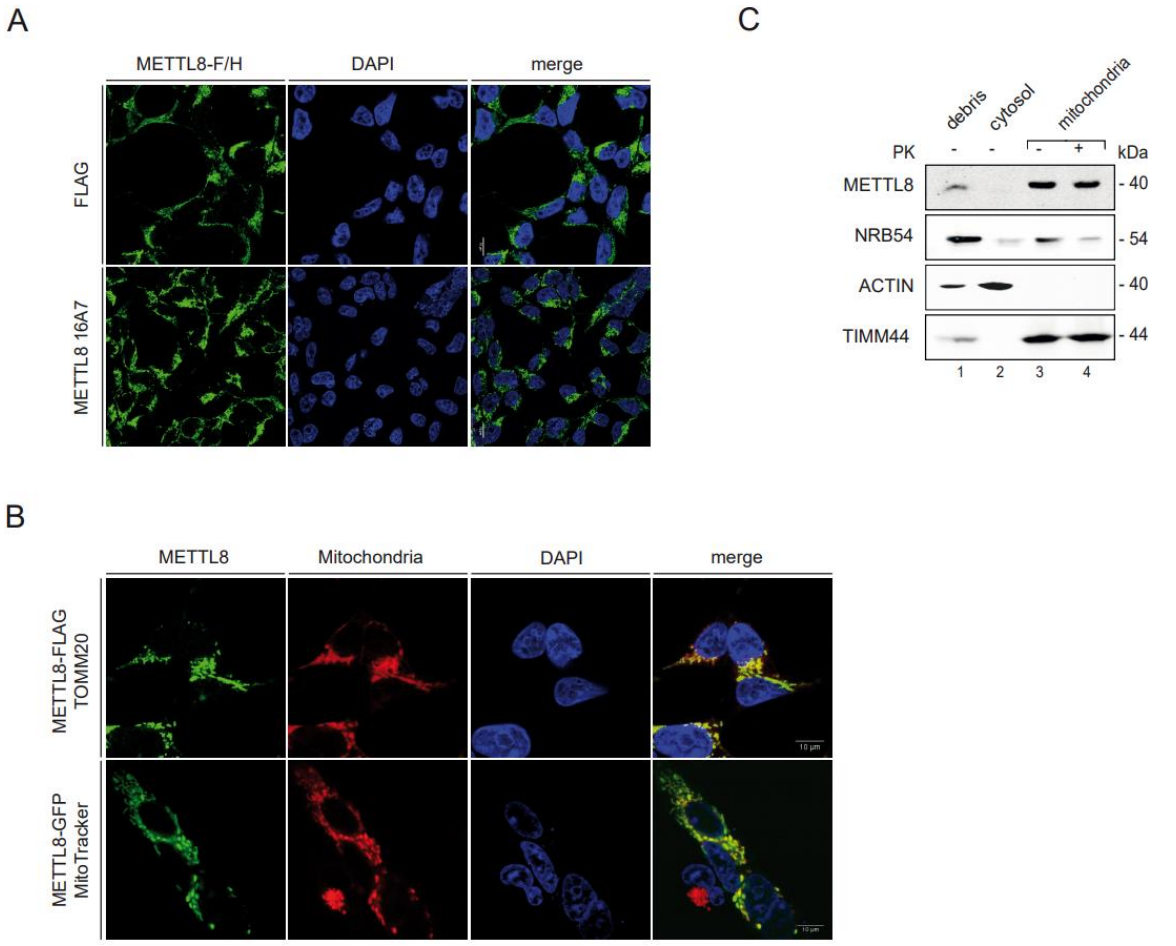

Figure 2.2: METTL8 is a mitochondrially localized protein
(A) Immunofluorescence detection of METTL8-F/H by anti-FLAG (green, left panel) and anti-METTL8 16A7 (green, right panel) in Flp-In TREx293 cells. Nuclei were stained with DAPI (blue) (scale bars: 10 µm)
(B) Subcellular localization of METTL8-F/H (green, upper panel) and METTL8-GFP (green, lower panel) in Flp-In TREx293 cells. Top: immunofluorescence detection of METTL8-F/H (green), mitochondrial import receptor subunit TOMM20 (red), and DAPI (blue). Bottom: fluorescence imaging of METTL8-GFP (green), MitoTracker Deep Red (red) and Hoechst 33342 (blue) (scale bars: 10 µm)
(C) Subcellular fractionation of Flp-In TREx293 cells into debris/nuclei (NRB54), cytosol (ACTIN) and mitochondria (TIMM44). Mitochondria were treated with ProteinaseK. Endogenous METTL8 was detectable after anti-METTL8 IP.

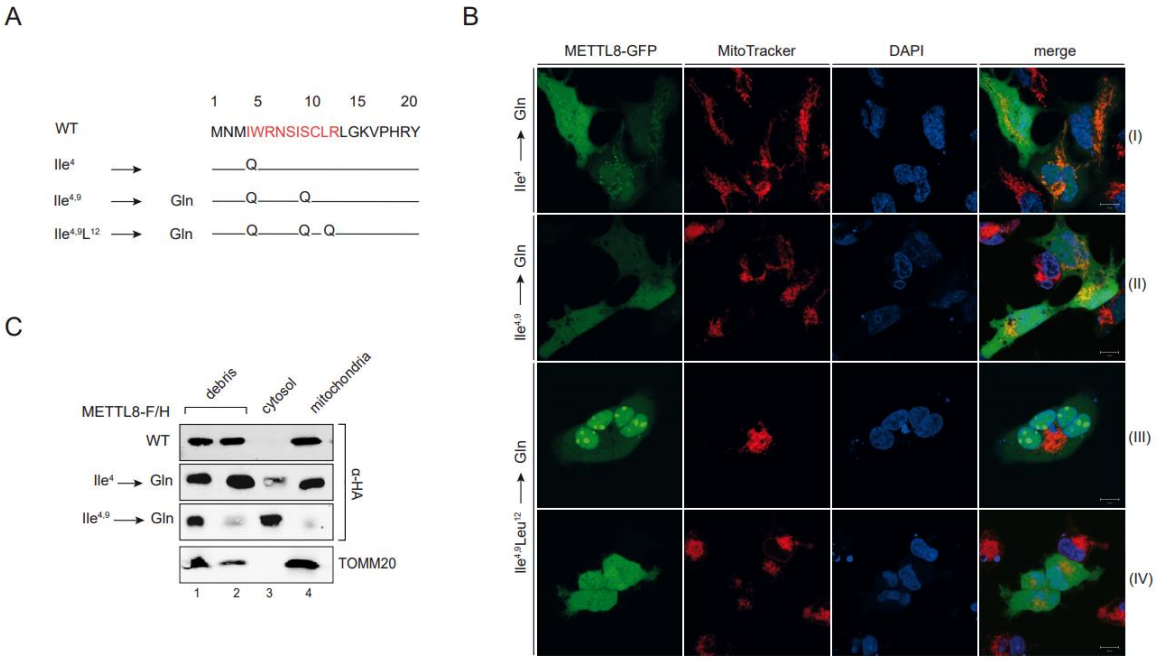

Figure 2.3: Mitochondrial localization of METTL8 via N terminally MTS
(A) Snapshot of predicted MTS pre-sequence with MPP (mitochondrial-processing peptidase) cleavage site (position 20) and mutation of amino acids Ile4,9 and Leu12 to glutamines.
(B) *Live cell imaging* of modified METTL8-GFP (green) by fluorescence detection of MitoTracker Deep Red (red) and Hoechst 33342 (blue). Fluorescence detection of METTL8-GFP single (panel I). double (panel II) and triple MTS mutant (panel III-IV) (scale bars: 10 µm).
(C) Subcellular fractionation of Flp-In TREx293 cells overexpressing METTL8-F/H constructs into debris/nuclei, cytosol and mitochondria. METTL8-F/H was detected by anti-HA, and TOMM20 served as mitochondrial marker.
.

2.3 METTL8 binds to mt-tRNAs and does not influence aminoacylation

Since it has been reported that METTL8 binds mRNAs (Xu et al. 2017), we tested whether METTL8 might be associated with mitochondrial mRNAs due its mitochondrial localization. For identifying METTL8 mt-mRNA targets, we performed METTL8 IPs from METTL8 wilde type (WT) and KO Flp-In TREx293 cells and purified co-immunoprecipitated RNAs. 13 transcripts are encoded in the mitochondrial genome and we analyzed all of them by qPCR but no transcript was specifically enriched after METTL8 IP (Figure 2.4A). On that account, we concluded that METTL8 does not bind mt-mRNA stably. The publication defining METTL8 as an mRNA methyltransferase, characterized the METTL8 homologs METTL2A/B and METTL6 as tRNA methyltransferases acting on $tRNA^{Thr/Ser}$ isoacceptors and $tRNA^{Arg(CCU)}$. Hence, we tested binding to mt-tRNAs. We reran the experimental setup and included two additional METTL8 KO Flp-In TREx293 clones and METTL8-F/H overexpressing Flp-In TREx293 cells (Figure 2.4B). The co-purified tRNAs were analyzed by northern blotting and show an

enrichment of mt-tRNA$^{Ser(UCN)}$, mt-tRNA^{Arg}, mt-tRNA^{Thr} and mt-tRNA^{Trp} in presence of overexpressed METTL8-F/H (Figure 2.4B). Under endogenous conditions, just mt-tRNA$^{Ser(UCN)}$ and mt-tRNA^{Arg} were efficiently co-immunoprecipitated. The remaining 18 mt-tRNAs did not show any signal after METTL8 IP (Figure 2.4B and data not shown). Of note, mt-tRNA^{Thr} is either low abundant or hardly detectable as evidence from the weak signal already in the input samples (Figure 2.4B). A solid conclusion about mt-tRNA^{Thr} enrichment under normal conditions is therefore rather difficult. Interestingly, in the absence of METTL8, the mt-tRNA^{Thr} appears to be upregulated in the input samples suggesting that the interplay between METTL8 and mt-tRNA^{Thr} appears to be much more complex. We further corroborate the observed mt-tRNA^{Thr} expression phenomena comparing mt-tRNA^{Thr} signal intensities from different amount of total RNA of METTL8 WT, KO and overexpressing METTL8-F/H Flp-In TREx 293 cells by northern blot (Figure 2.4C, left panel). Quantification analysis showed a two-fold higher mt-tRNA^{Thr} signal intensity in the METTL8 KO cells resulting the mt-tRNA^{Thr} level depends on METTL8 availability (Figure 2.4C, right panel). To confirm that METTL8 is acting exclusively on a subset of mitochondrial tRNAs, we performed an anti-FLAG-METTL2 IP, which is known to modify the cytoplasmic counterparts like the isoacceptor tRNA$^{Thr(AGT)}$ (Figure 2.3E). Northern blot analysis shows that F/H-METTL2 enriches tRNA$^{Thr(AGT)}$ efficiently whereas mt-tRNA^{Thr} is not bound by F/H-METTL2. Furthermore METTL8 does not interact with the METTL2 tRNA target tRNA$^{Thr(AGT)}$ (Figure 2.4D).

During the aminoaclytion process tRNAs are charged (aminoacyl-tRNA, aa-tRNA) and active for protein synthesis on the ribosome. Since METTL8 binds mt-tRNAs, we analyzed potential METTL8 effects on the aminoacylation efficiency of bound tRNA targets by an aminoacylation assay using acid gels (Varshney et al. 1991) (Figure 2.4E). To keep charged tRNAs, total RNA was purified und separated under acid conditions. Deacylated, meaning uncharged tRNAs were used as control. The aminoacylation and deacylation in all three independent METTL8 KO clones were unchanged compared to the METTL8 WT indicating METTL8 does not influence aminoacylation of its mt-tRNA interaction partners.

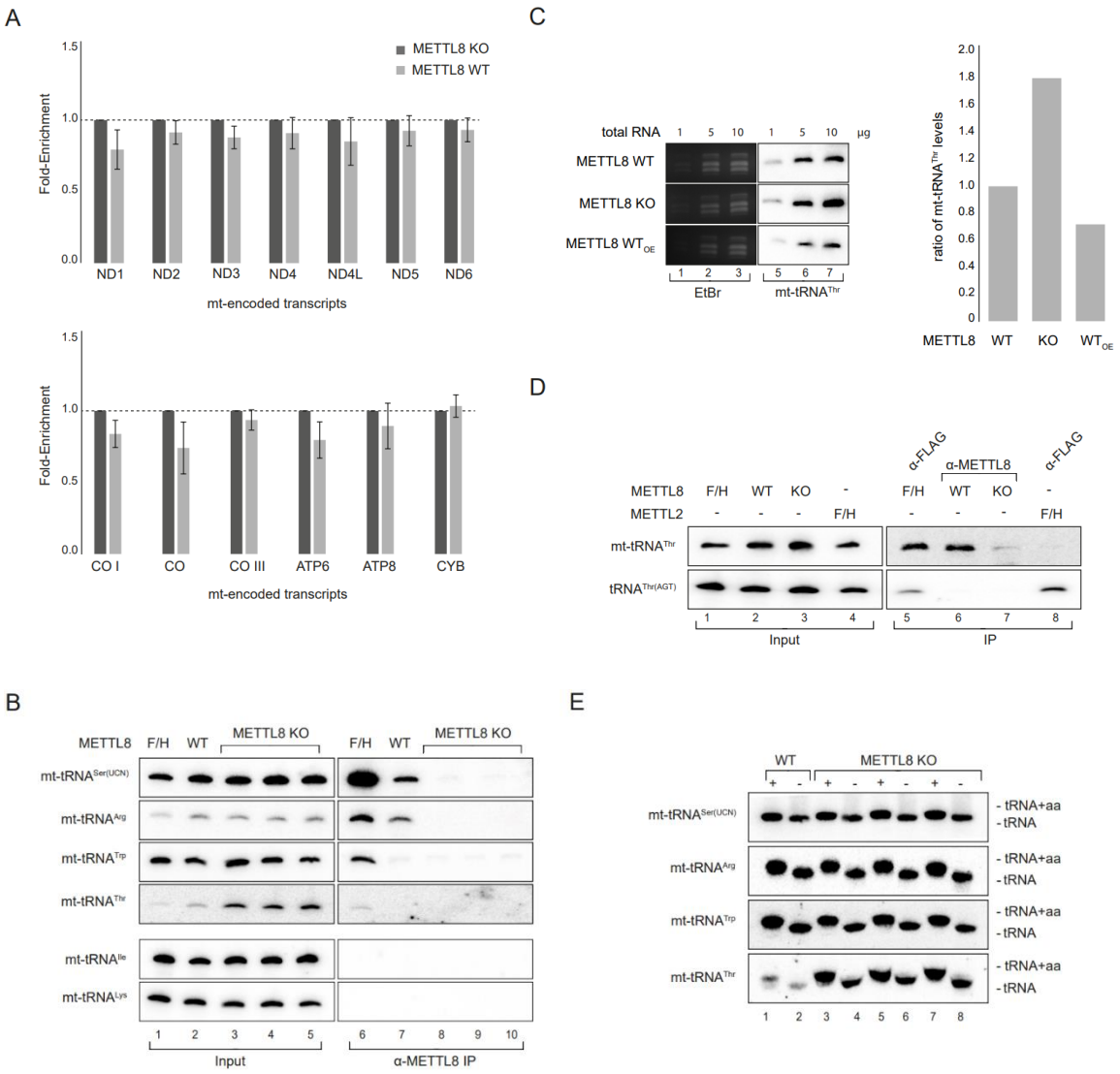

Figure 2.4: METTL8 interacts with mitochondrial tRNAs

(A) METTL8 RNA immunoprecipitation (RIP)-qPCR of METTL8 WT and METTL8 KO Flp-In TREx293 cell lines. METTL8 KO cell line was used as control. Mean ± standard error of difference (SED) of three independent measurements are plotted.

(B) Northern Blot analysis of RNA co-immunoprecipitated with METTL8. METTL8 KO cell lines and 0.5 µg total RNA for input were used as controls.

(C) Left: Northern Blot analysis of mt-tRNA^{Thr} levels in overexpressing METTL8 WT, METTL8 WT and KO cell lines. EtBr staining served as loading control. Right panel: corresponding phosphor imaging quantification is shown.

(D) Northern Blot analysis of RNA co-immunoprecipitated with METTL8 and METTL2. METTL8-F/H and F/H-METTL2 were immunoprecipitated by using anti-FLAG. 0.5 µg total RNA was used as input control.

(E) Mitochondrial tRNA aminoacylation (+) and deacylation (-) levels in METTL8 WT and METTL8 KO cell lines.

2.4 METTL8 methylates m^3C_{32} in mt-tRNA$^{Ser(UCN)/Thr}$

In 2018, the AlkAnilineSeq approach for genome-wide m^3C profiling was published and established (Marchand et al. 2018) (Figure 2.5A). This technique gave us the option to directly investigate whether METTL8 is an m^3C methyltransferase as has been suggested by others, doing the conformation of this work (Xu et al. 2017) and define its modification site in more detail. Another benefit of this method is the unbiased detection of m^3C alterations in METTL8 KO Flp-In TREx293 cells. We teamed up with the lab of Yuri Motorin and Virginie (Université de Lorraine, CNRS, INSERM, UMS2008/US40 IBSLor, EpiRNA-Seq Core facility, F-54000 Nancy, France; Université de Lorraine, CNRS, UMR7365 IMoPA, F-54000 Nancy, France) performing the AlkAnilineSeq experiments. The AlkAnilineSeq data revealed in the absence of METTL8 an m^3C depletion in the mitochondrial tRNAs mt-tRNA$^{Ser(UCN)}$ and mt-tRNA^{Thr} at position 32 (Figure 2.5B).

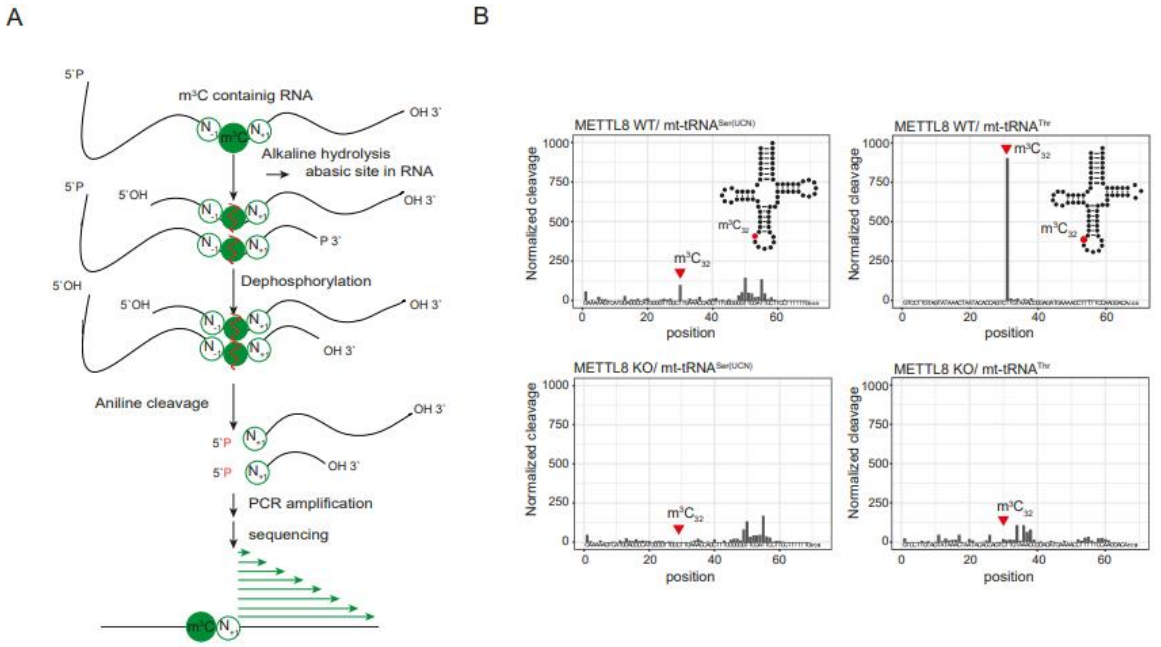

Figure 2.5: METTL8 methylates position C_{32} in mt-tRNA$^{Ser(UCN)}$ and mt-tRNA^{Thr}
(A) Illustration of the AlkAniline-Seq mechanism starting with RNA strand cleavage induced by alkaline hydrolysis generating a basic site. N_{+1} reads are enriched by primer ligation and sequencing strategy. M^3C modification is represented as green dot, a basic site as broken dot.
(B) AlkAniline-Seq analysis of METTL8 WT and METTL8 KO cell lines. Top: m^3C cleavage profiles of mt-tRNA$^{Ser(UCN)}$, mt-tRNA^{Thr} in METTL8 WT. Bottom: m^3C cleavage profiles in METTL8 KO.

The cytoplasmic counterparts were unaffected in the METTL8 KO cells indicating METTL8 acting specifically on the two mitochondrial tRNAs (Figure 2.6A). Furthermore, we observed that the mitochondrial tRNAs mt-tRNA^{Arg} and mt-tRNA^{Trp} were unchanged in the absence of METTL8 (Figure 2.6B and C), even though both mt-tRNAs were co-immunoprecipitated during METTL8 IP (Figure 2.4B). Mt-tRNA^{Arg} contains a U nucleotide at position 32, which is according to the literature not methylated at all similary, the nucleotide C at position 32 in mt-tRNA^{Trp}, which has been not been found methylated so far (Suzuki und Suzuki 2014; Suzuki et al. 2020). Taken together, we can confirm METTL8 as an m^{3}C methyltransferase acting specifically on the mitochondrial tRNAs mt-tRNA$^{Ser(UCN)}$ and mt-tRNA^{Thr}.

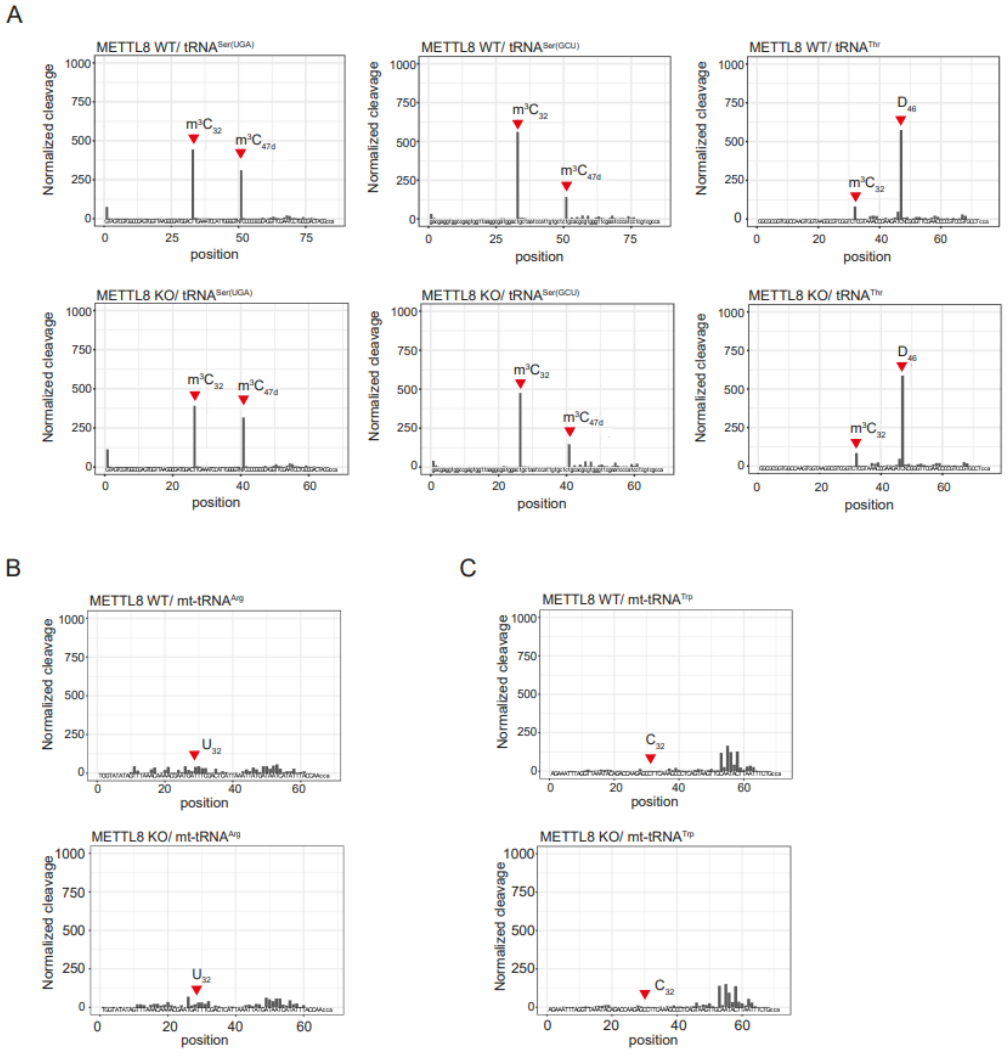

Figure 2.6: METTL8 is a mitochondrial m^{3}C specific methyltransferase
(A) AlkAniline-Seq analysis of METTL8 WT and METTL8 KO cell lines. Left: m^{3}C cleavage profile of the cytoplasmic tRNA$^{Ser(UGA/GCU)}$ and tRNA^{Thr} in METTL8 WT. Right: m^{3}C cleavage profiles in METTL8 KO cell line.
(B) AlkAniline-Seq analysis of METTL8 WT and METTL8 KO cell lines. Top: m^{3}C cleavage profiles of mt-tRNA^{Arg} in METTL8 WT. Bottom: m^{3}C cleavage profiles of mt-tRNA^{Arg} in METTL8 KO
(C) AlkAniline-Seq analysis of METTL8 WT and METTL8 KO cell lines. Top: m^{3}C cleavage profiles of mt-tRNA^{Trp} in METTL8 WT. Bottom: m^{3}C cleavage profiles of mt-tRNA^{Trp} in METTL8 KO

2.5 METTL8-mediated m^3C_{32} methylation depends on A_{37} isopentenylation

To understand the biochemical mechanism of the METTL8 activity, we reconstitute the m^3C methylation at position 32 on mt-$tRNA^{Ser(UCN)}$ *in vitro*, the position 32 initiating the anticodon loop arm. For the *in vitro* methylation approach, we first purified the C-terminally GST-tagged METTL8 protein from bacteria (Figure 2.7A) and synthesized the mt-$tRNA^{Ser(UCN)}$ substrate by *in vitro* transcription. According to the PFAM domain prediction, METTL8 contains a SAM-binding domain (Figure 2.7B). Therefore, we used radioactively labeled SAM as methyl donor. To introduce the m^3C modification in the mt-$tRNA^{Ser(UCN)}$ substrate, we set up an methylation reaction of radioactively labeled SAM, recombinant METTL8 and the RNA substrate.

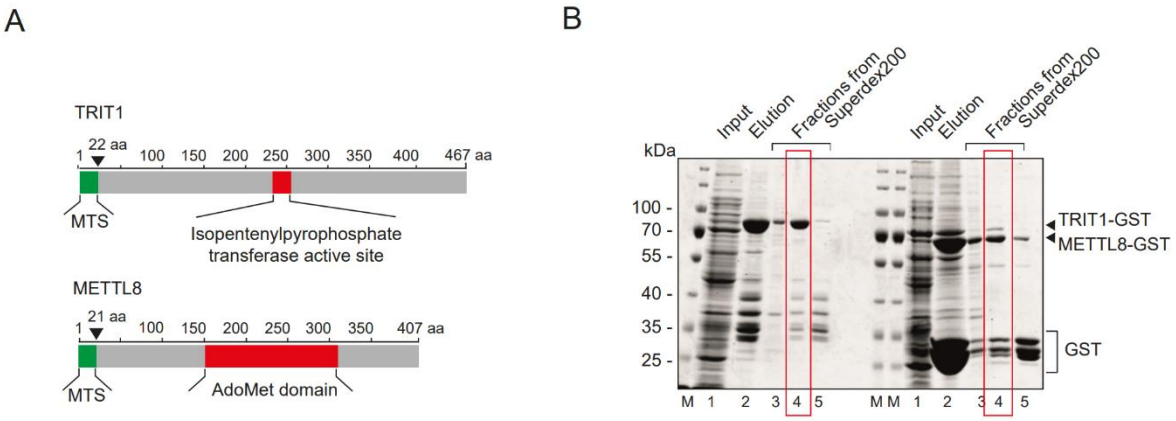

Figure 2.7: Recombinant METTL8 and TRIT1 purification
(A) Left: cartoon of METTL8 (UniProt: B3KW44) and TRIT1 (UniProt: Q9H3H1) protein domains. Catalytic domains (S-Adenosyl-Methionine binding site/ Isopentenylpyrophosphate transferase active site) highlighted in red and mitochondrial targeting signal (MTS) in green.
(B) Recombinant TRIT1-GST and METTL8-GST proteins after individual purification steps. Protein used for analysis is marked in red.

Unfortunately we did not detect any activity on the RNA substrate (Figure 2.8A (I) and B). Interestingly, it has been figured out that tRNAs containing adenosines at positions 36 and 37 are isopentenylated (i^6A) or treonylcarbamoylated (t^6A) at position 37 (El Yacoubi et al. 2012; Miyauchi et al. 2013; Kimura et al. 2014; Lamichhane et al. 2013; Cabello-Villegas et al. 2002). Furthermore patients lacking the t^6A_{37} modification showed a loss of m^3C_{32} (Arimbasseri et al. 2016; Lin et al. 2018). Therefore, we introduced prior the METTL8 methylation assay the i^6A_{37} modification into our RNA substrate by TRIT1, the human mitochondrial i^6A modifying enzyme (Lamichhane et al., 2013), in an isopentenylation reaction. The C terminally GST-tagged TRIT1 was purified from bacteria before (Figure 2.7B). We reran the methylation assay with radioactively labeled SAM, recombinant METTL8 and the i^6A_{37} pre-modified

RNA substrate. We observed an efficient methylation of the i^6A_{37} pre-modified mt-tRNA$^{Ser(UCN)}$ substrate (Figure 2.8A, (II) and B), which was abolished in the corresponding r.32C>G mt-tRNA$^{Ser(UCN)}$ mutant (Figure 2.8A, (III) and B). The *in vitro* methylation specificity of METTL8 was further validated. In control methylation reactions, METTL8 did not show any methylation activity on the i^6A_{37} pre-modified mitochondrial tRNAs phenylalanine (Phe), tryptophan (Trp) and serine (AGY) (Ser(AGY))), which also contain a C_{32} (Figure 2.8B (ctrl.)). The *in vitro* reconstitution revealed that METTL8 activity on the m^3C_{32} mark needs prior isopentenylation at position 37.

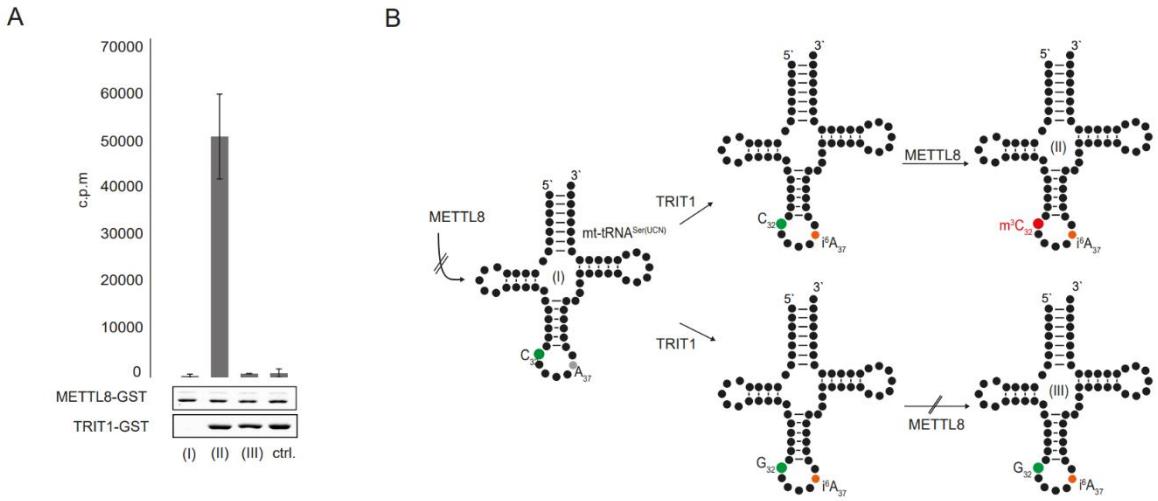

Figure 2.8: METTL8 methylates position C_{32} in mt-tRNA$^{Ser(UCN)}$ and mt-tRNA^{Thr} *in vitro*
(A) Methyltransferase activity assay of METTL8-GST. Full-length, unmodified mt-tRNA$^{Ser(UCN)}$ (column I), i^6A_{37} preo-modified mt-tRNA$^{Ser(UCN)}$ (column II), i^6A_{37} pre-modified mt-tRNA$^{Ser(UCN)}$ C32G mutant (column I) were used as substrates. Mitochondrial i^6A_{37} pre-modified tRNAs Phe, Trp and Ser(AGY) were used as negative controls. Mean ± SED of three to six independent measurements are plotted. As loading control 1 µg recombinant protein was separated on a 10 % SDS gel and stained by Coomassie Blue.
(B) Cartoon of the m^3C formation on mt-tRNA$^{Ser(UCN)}$. Position 32 (green) is methylated (red) after position 37 (black) is isopentenylated (orange).

To set up further controls, we generated a catalytically inactive METTL8 mutant. First, we aligned the three human homologs METTL2B, 6 and 8 and predicted the conserved potential catalytically residues D230, D260, F253, D272, L299 in the AdoMet domain as catalytically relevant residue (Figure 2.9A). Of note, the residue D260 is not highly conserved. We mutated all residues to alanine (D230A; D260A; F253A; D272A, L299A) und unfortunately struggled to purify all mutants recombinantly except METTL8 D260A. Thus, we expressed all other mutants in Flp-In TREx293 cells, however the METTL8 mutants D230A as well L299A were less expressed than the WT and METTL8 F253A variant was not expressed at all (Figure 2.9B). Furthermore, the METTL8 mutants D272A as well as L299A affected

cell viability negatively (data not shown). Therefore, we performed methylation assays with the immunoprecipitates of METTL8 WT and METTL8 D230A Flp-In TREx293 cells (Figure 2.9C, left panel) as well with recombinant METTL8 WT and D260A variant (Figure 2.9C, right panel). The METTL8 D260A variant was still active in the methylation assay but to a lesser extent than the METTL8 WT. In the methylation reaction with METTL8 variant D230A we couldn`t detect any enzymatic activity (Figure 2.9C, left panel) and to that end we postulate residue D230 is a catalytically relevant residue.

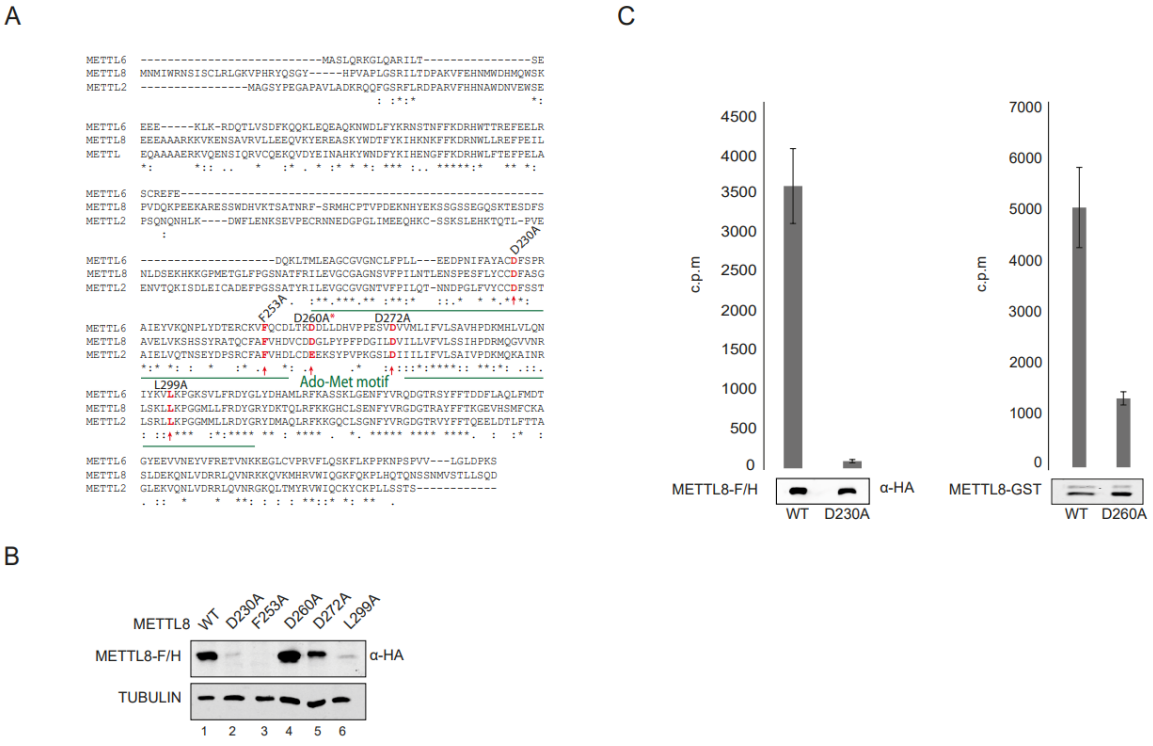

Figure 2.9: Generation of a METTL8 catalytic inactive mutant
(A) Multiple sequence alignment of human METTL2B (GenBank: NM_018396.2), METTL6 (GenBank: NM_152396.3), and METTL8 (GenBank: NM_024770.4). Conserved S-Adenosyl-Methionine binding site is highlighted in green. Conserved predicted catalytically residues are highlighted in red.
(B) METTL8-F/H expression of potential METTL8 catalytically inactive mutants in Flp-In TREx cell lines. TUBULIN was used as control.
(C) Left: methylation assay of WT METTL8-F/H and METTL8-F/H D230A variant. Both constructs were enriched by an anti-FLAG IP. Methylation activity was adjusted to western blot signals. Right: methyltransferase activity assay of WT METTL8-GST and METTL8 D260A variant. As loading control 1 µg recombinant protein was separated on a 10 % SDS gel and stained by Coomassie Blue (right panel). I^6A_{37} pre-modified mt-tRNA$^{Ser(UCN)}$ was used as substrate. Mean values ± SED of three independent measurements are plotted.

2.6 Loss of METTL8 affects respiratory chain activity

The mitochondrial respiratory chain generates cellular energy in form of adenosine triphosphate (ATP) via its oxidative phosphorylation system (OXPHOS), which is highly connected to the cytosolic sugar metabolism. Even if METTL8 does not modify mt-mRNAs and is dispensable for aminoacylation, we assume a potential METTL8 influence on the respiratory complex activity, because several studies have already shown the link between loss of tRNA modifications and mitochondrial diseases (Fakruddin et al. 2018; Yarham et al. 2014). To get an overview on metabolism in general, we analyzed the main intra- (Figure 2.10A) and extracellular (Figure 2.10B) carbon sources of cytosolic and mitochondrial metabolism using gas chromatography-mass spectrometry (Figure 2.10). Loss of METTL8 leads to a mild intracellular increase of succinate, which was reproducible (data not shown) but statistically not significant (Figure 2.10A). The extracellular levels of pyruvate, lactate and glucose in METTL8 KO were unchanged (Figure 2.10B). A succinate accumulation would be consistent with in a model of a respiratory chain with a deficient complex II activity. We conclude complex II may not regenerate $FADH_2$ efficiently anymore and downshift of the TCA cycle maybe resulting in an overall reduced cytosolic and mitochondrial metabolism.

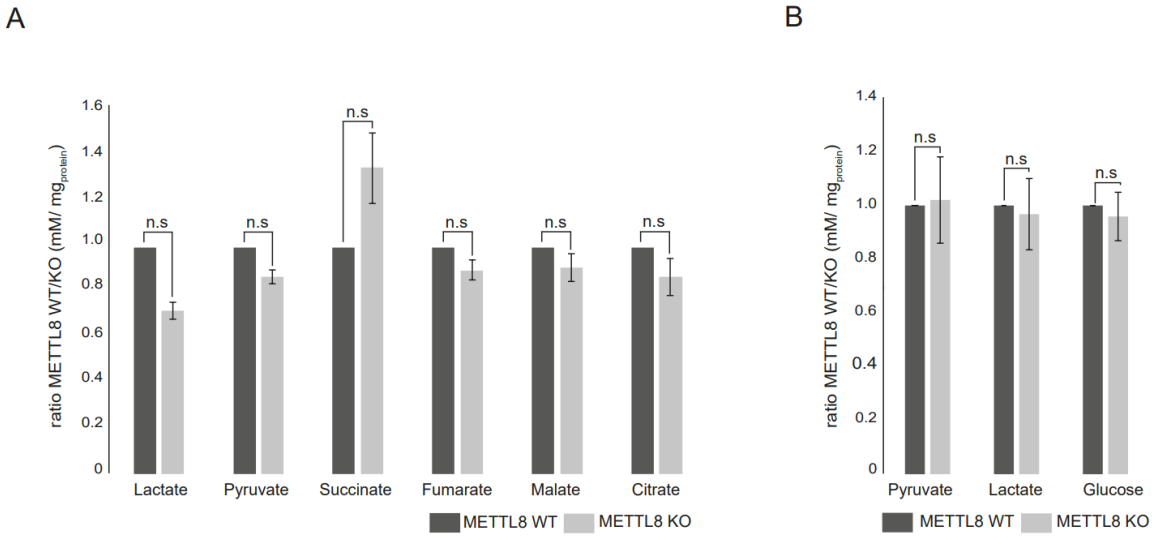

Figure 2.10: Loss of METTL8 disturbs metabolic balancing
(A) Glycolysis and TCA-cycle intermediates in METTL8 WT (dark grey) and METTL8 KO (light grey) cell lines. Mean values ± SED of three independent measurements are plotted. n.s $p > 0.05$ in *t* test.
(B) Metabolic footprinting of the primary glycolysis carbon sources in METTL8 WT (dark grey) and METTL8 KO (light grey) cell lines. Mean values ± SED of three independent measurements are plotted. n.s $p > 0.05$ in *t* test.

To understand the physiological mechanism of METTL8 in more detail, we performed high-resolution respirometry (Oroboros-2k) (Figure 2.11). Using specific substrate-uncoupler-inhibitor titration (SUIT) protocols, we analyzed different coupling control state like ROUTINE respiratory activity, OXPHOS capacity and Leak state. During the uncoupling state we evaluated the electron transport system (ETS). All described parameters were reduced in the absence of METTL8 (Figure 2.11, left panel) based on impaired complex I and II activities (Figure 2.11, right panel).

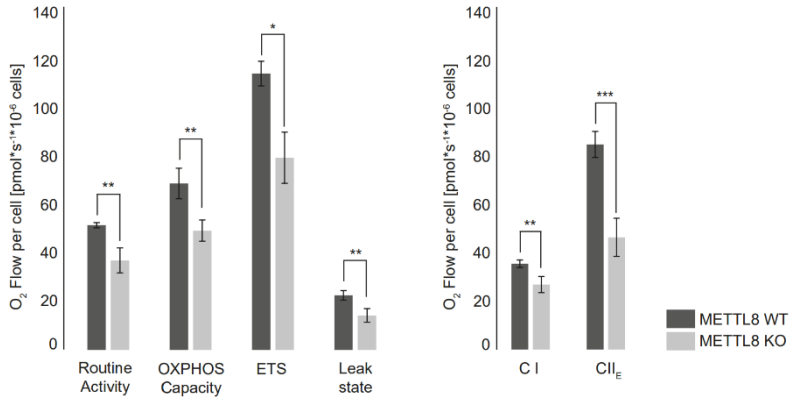

Figure 2.11: Loss of METTL8 disturbs reduces OXPHOS activity
Oxygraph-2k measurements of WT METTL8 (dark grey) and METTL8 KO (light grey) Flp-In-TREx293 cell lines. Respiratory activity analysis was performed using the substrate-uncoupler-inhibitor-titration-protocol (SUIT) with carbonyl caynid 4-(trifluoromethoxy)phenylhydrazone (FCCP). Mean values ± SED of four independent measurements are plotted. * $p < 0.05$, ** $p < 0.01$, *** $p < 0.001$ in *t* test.

To confirm that the reduced respiratory activity is caused by loss of the METTL8 catalytic activity, we reran the Oroboros-2k measurements with rescued Flp-In TREx293 METTL8 KO cells either with METTL8 WT or with its catalytic mutant (D230A) (Figure 2.12). When we looked at rescue activity of METTL8 WT and METTL8 D230A, we observed METTL8 WT rescued OXPHOS capacity and ETS highly efficient, however, ROUTINE respiratory activity and leak state were less rescued (Figure 2.12, left panel). Furthermore, we detected a high rescue efficiency of complex I and II in METTL8 WT compared to METTL8 D230A (Figure 2.12, middle panel). Of note, in METTL8 WT rescued Flp-In TREx293 METTL8 KO cells complex I activity was increased compared to complex I activity in Flp-In TREx293 cells. This effect might be based on the increased METTL8 expression level in METTL8 WT rescued Flp-In TREx293 METTL8 KO cells (data not shown). However, complex I activity in METTL8 KO and METTL8 D230A-rescued Flp-In TREx293 METTL8 KO cells were identical.

Accordingly, we postulate that METTL8 affects via its catalytic activity on mt-tRNA$^{Ser(UCN)}$ and mt-tRNA^{Thr} respiratory chain activity in a particular way.

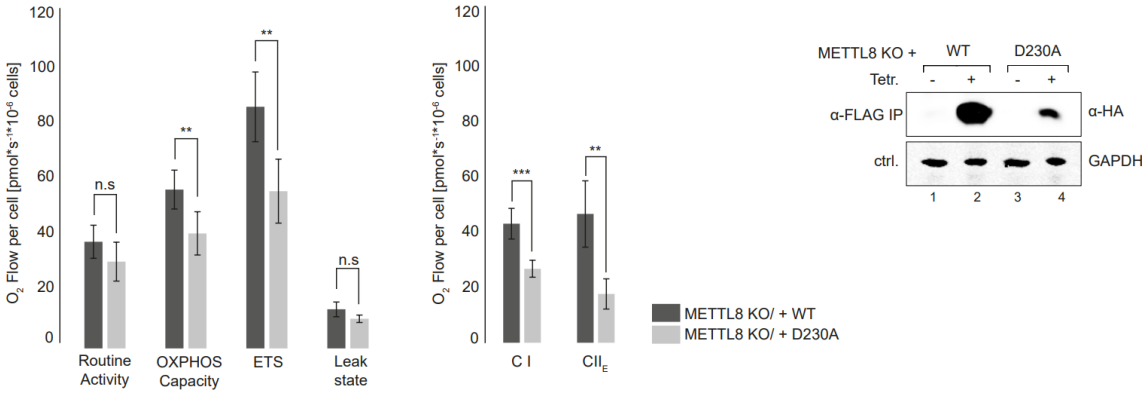

Figure 2.12: METTL8 catalytic activity influences OXPHOS activity
Left Oxygraph-2k measurements of Flp-In-TREx293 METTL8 KO rescue variants. Respiratory activity analysis of METTL8 KO_WT-F/H (dark-grey) and METTL8 KO_D230A-F/H (light grey) was performed as described in (C). Mean values ± SED of four independent measurements are plotted. n.s $p > 0.05$, ** $p < 0.01$, *** $p < 0.001$ in *t* test. Right: expression of METTL8 WT-F/H and METTL8 D230A-F/H rescued METTL8 KO Flp-In TREx cell lines after anti-FLAG IP. GAPDH served as control.

2.7 METTL8 levels affect cell growth and patient survival in pancreatic cancer

So far, the biological function of METTL8 is unknown, however several studies linked an upregulated METTL8 expression level to several cancer types (Begik et al. 2020; Zhang et al. 2020). To confirm this correlation, we monitored in a first step cell proliferation under different METTL8 expression conditions (Figure 2.13A). Loss of METTL8 affected Flp-In TREx293 cell growth not significantly (Figure 2.13A, upper panel) but we observed in WT METTL8-rescued Flp-In TREx293 METTL8 KO cells a highly efficient growth rate in contrast to the corresponding catalytic mutant METTL8 D230A (Figure 2.13A, lower panel). Due to the fitter growth of WT METTL8 rescued Flp-In TREx293 METTL8 KO cells and the unchanged proliferation rate between Flp-in TREx293 METTL8 KO and rescued METTL8 D230A we assumed METTL8 catalytic activity promotes cell proliferation.

To align upregulated METTL8 expression with common cancer types we used the public data bank TCGA. According to TCGA METTL8 is up-regulated in diffuse large B cell carcinoma (DLBC), glioblastoma (GBM), low grade glioma (LGG), lung squamous cell carcinoma (LUSC), pancreatic adenocarcinoma (PAAD), stomach adenocarcinoma (STAD) and thyroid carcinoma (THYM) (Figure 2.13B, C) which also fits to previous studies (Begik et al., 2020). Typically, the overall gene expression in cancer is changed. Nonetheless, each mis-regulated gene might not necessarily be essential for cancer development, maintenance or growth. Due to this reason, we looked at the Kaplan-Meier curves of the appropriate cancer types based on the TCGA data reflecting correlation of gene expression with overall patient survival (Figure 2.13D). The overall survival rate of patients suffering from DLBC, GBM, LGG, LUSC, THYM and STAD was independent of METTL8 expression. Interestingly, the survival of PAAD patients showing a high METTL8 expression level was significantly reduced (Figure 2.13D, righter upper panel). Based on this observation, we assumed that METTL8 might be relevant for pancreatic cancer pathology.

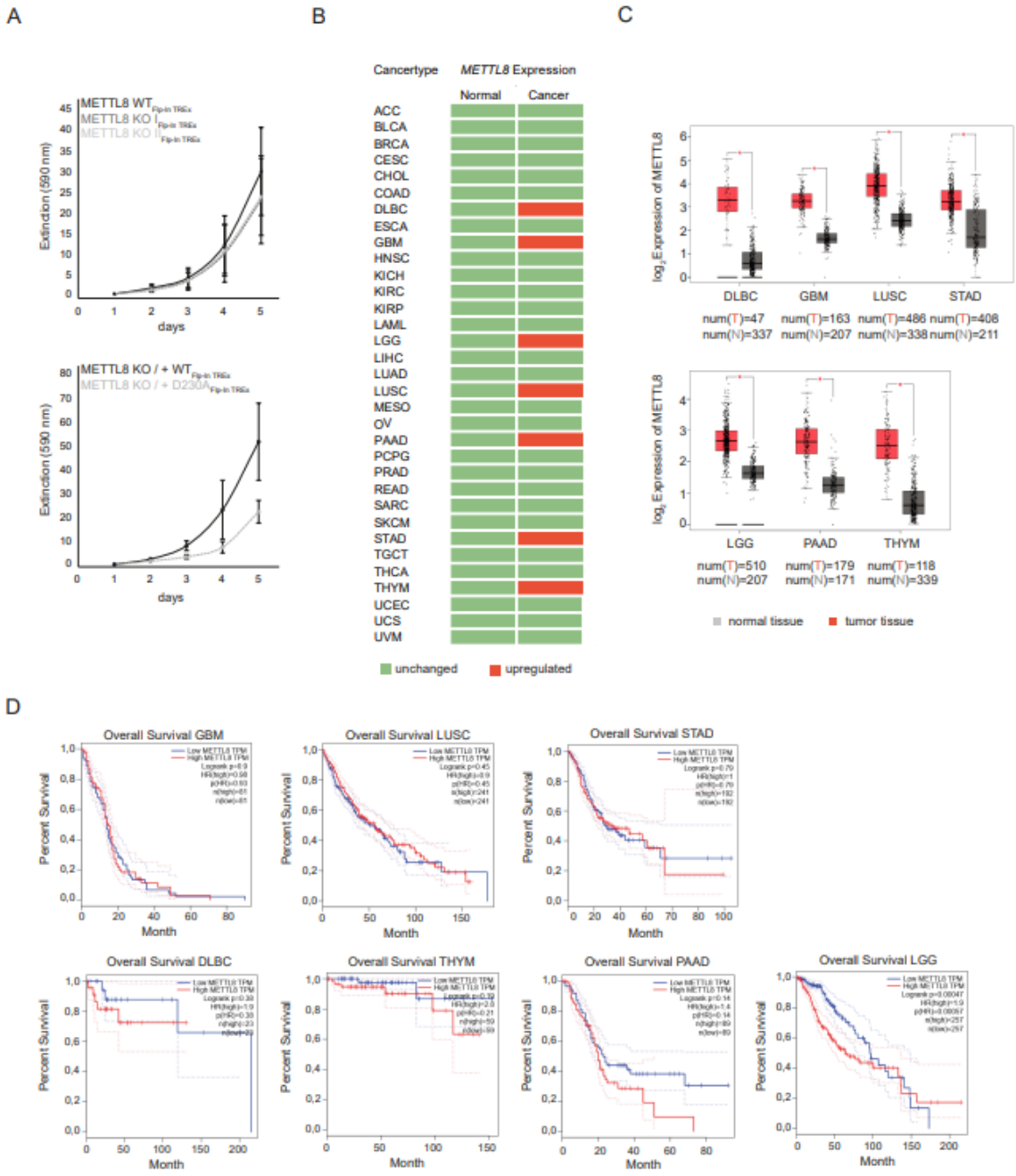

Figure 2.13: Upregulated METTL8 expression correlates with survival rate in PAAD cancer
(A) The top diagram shows Flp-In TREx293 METTL8 WT cell proliferation in black and METTL8 KO in gray, and the bottom diagram shows growth curves of the Flp-In TREx293 METTL8 KO rescue variants METTL8 KO_WT-F/H (black) and METTL8 KO_D230A-F/H (gray). Cells were grown in presence of high glucose. Mean values ± SED of four independent measurements are plotted.
(B) List of cancer types from GEPIA database (Database: GEPIA). Cancer types with upregulated *METTL8* expression are highlighted in red.
(C) Box plot of METTL8 expression in DLBC, GBM, LGG, LUSC, PAAD, STAD, THYM cancer (red) and normal tissue (grey) based on the GEPIA data set (Database: GEPIA). $p < 0.05$.
(D) Correlation of METTL8 expression and patients overall survival in DLBC, GBM, LGG, LUSC, PAAD, STAD, THYM cancer. Correlation with overall survival with low METTL8 expression (blue) and high METTL8 expression level (red).

We deeper investigated this correlation by knocking out METTL8 in the pancreatic cancer cell line PANC-1 (Figure 2.14A) and monitored those proliferation rates over five days (Figure 2.14B, left panel). The loss of METTL8 in PANC-1 cells impaired an efficient cell growth compared to Flp-In TREx293 cells. To mimic the PANC-1 METTL8 expression level in Flp-In TREx293 cells we overexpressed METTL8 in those additionally to the METTL8 WT expression level (Figure 2.14B, right panel). When METTL8 was overexpressed, we observed a strong accelerated cell proliferation bolstering our assumption that METTL8 promotes cell growth in certain cancer types like pancreatic cancer.

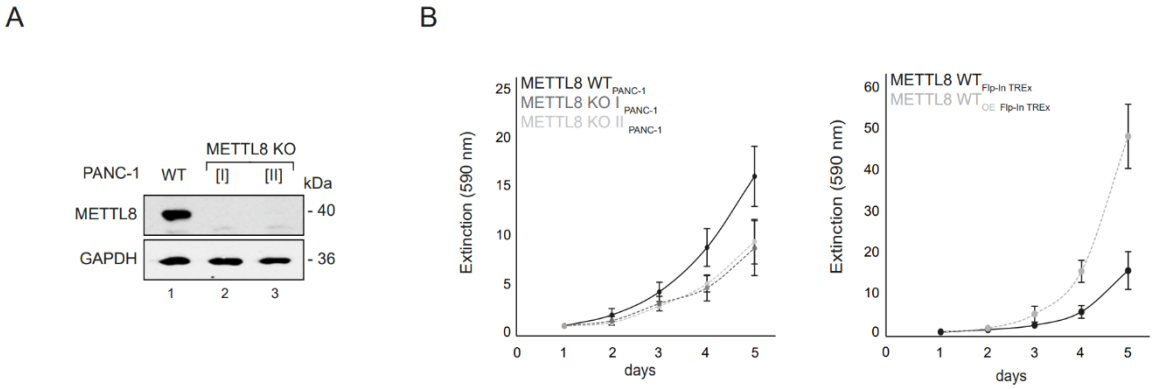

Figure 2.14: METTL8 expression influences proliferation rate in PAAD cancer
(A) Detection of METTL8 in PANC-1 METTL8 WT and METTL8 KO cell lines after anti-METTL8 IP. GAPDH was used as control.
(B) Left: growth curves of PANC-1 METTL8 WT in black and METTL8 KO in gray. Right: proliferation of tetracycline treated METTL8 WT (black) and METTL8 overexpressing (WT_{OE}) (gray) Flp-In TREx293 cells. Cells were grown in presence of high glucose. Mean values ± SED of four independent measurements are plotted.

2.8 Aberrant m^3C_{32} methylation pattern stimulates OXPHOS activity in PANC-1

To better understand a potential role of METTL8 conduct in pancreatic cancer, we analyzed the m^3C_{32} methylation pattern in pancreatic cell lines PANC-1 and CAPAN-1 by AlkAnilineSeq (Figure 2.8A). To evaluate conspicuous features in pancreatic cancer we compared the m^3C_{32} methylation of PANC-1 and CAPAN-1 with Flp-In TREx293 cells (Figure 2.15A). At a first glance, it seems that the methylation pattern of mt-$tRNA^{Thr}$ between the three cell lines is similar. The mt-$tRNA^{Thr}$ methylation level in Flp-In TREx293, PANC-1 and CAPAN-1cells was > 750 Units (U) meaning that the tRNA population is almost fully methylated (Figure 2.15A, panel I-III). In contrast, the methylation of mt-$tRNA^{Ser(UCN)}$ in Flp-In TREx293 cells just counted 150 Units (panel IV) suggesting that only 5-10 % of the whole $tRNA^{Ser(UCN)}$ population is methylated and the main population is unmethylated at position C_{32}.

Surprisingly, the C_{32} methylation status of mt-tRNA$^{Ser(UCN)}$ in PANC-1 is at least 2.5-fold increased (380 U, panel V) compared to Flp-In TREx293 cells. Of note, the normalized cleavage is not linear in the range of around 150 Units. Curiously, the mt-tRNA$^{Ser(UCN)}$ m^3C_{32} level in the CAPAN-1 cell line (panel VI) counted 150 Units as well like in Flp-In TREx293 cells although this cell line apparently derived from PAAD cancer. When we analyzed the METTL8 expression level in the three used cell lines by western blotting, we observed that the METTL8 expression level was much lower in CAPAN-1 cells compared to the PANC-1 cells (Figure 2.15B). This strengthened our hypothesis that m^3C_{32} methylation level correlates with METTL8 expression. Even though PANC-1 and CAPAN-1 originate from the pancreatic ductus, they develop differently and have to adapt to their specific environment. Of note, CAPAN-1 cells are isolated from a liver metastasis, PANC-1 from pancreatic ductus.

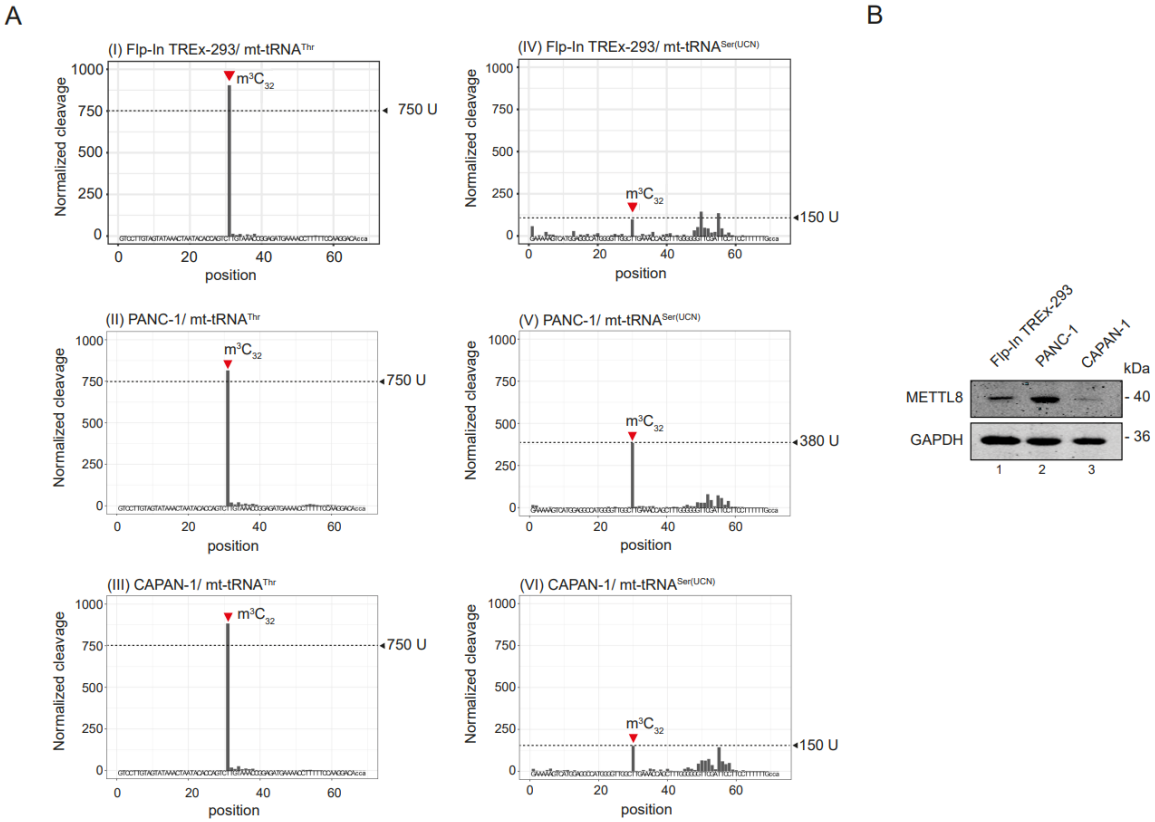

Figure 2.15: METTL8 expression correlates with m3C32 level of mt-tRNASer(UCN)
(A) AlkAniline-Seq analysis of mt-tRNA^{Thr} and mt-tRNA$^{Ser(UCN)}$ in Flp-In TREx293, PANC-1 and CAPAN-1 cell lines. Top. m^3C cleavage profiles of mt-tRNA^{Thr}. Bottom: m^3C cleavage profiles of mt-tRNA$^{Ser(UCN)}$
(B) METTL8 expression level in Flp-In TREx293, PANC-1 and CAPAN-1 cell lines after anti-METTL8 IP. GAPDH was used as control.

We assume that METTL8 up-regulation affects mainly the mt-tRNA$^{Ser(UCN)}$ methylation status and this might stimulate or reduce respiratory chain activity. For this reason, we assessed the standard Oroboros parameters in both pancreatic cancer cell lines PANC-1 and CAPAN-1 and the non-pancreatic cell line A549 (Figure 2.16A). In PANC-1 cells, we observed a higher ROUTINE activity and OXPHOS capacity as well as a more active ETS compared to CAPAN-1 and A549 cells (Figure 2.16A). The PANC-1 Leak state was enlarged additionally (Figure 2.16A). Strikingly, PANC-1 complex I activity was at least three-fold increased, while complex II was mildly elevated compared to CAPAN-1 cells (Figure 2.16A, left panel). In line with our hypothesis, higher respiratory activity was linked with METTL8 up-regulation (Figure 2.16B) meaning the respiratory activity pattern correlates with METTL8 expression level. Further, we analyzed PANC-1 respiratory activity under METTL8 KO conditions (Figure 2.16C) and observed that loss of METTL8 reduced all respiratory chain parameters moderately (Figure 2.16C). According to the AlkAnilineSeq and Oroboros results, we suggest METTL8 upregulation beneficial for PANC-1 cells.

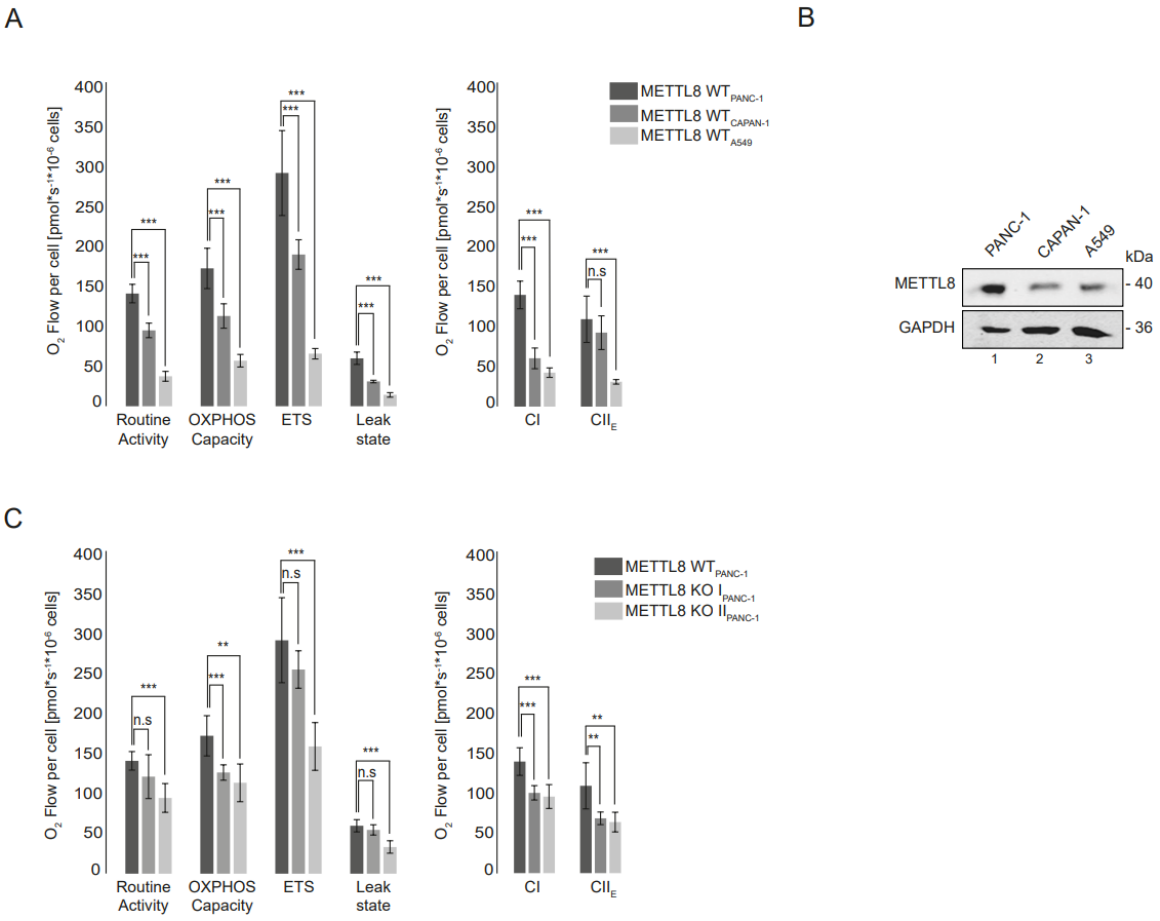

Figure 2.16: METTL8 expression correlates with respiratory chain activity in PANC-1 cells
(A) Oxygraph-2k measurements of PANC-1 (dark gray), CAPAN-1 (gray) and A549 (light gray) cell line using the SUIT protocol with FCCP. Mean values ± SED of four independent measurements are plotted. n.s $p > 0.05$, ** $p < 0.01$, *** $p < 0.001$ in *t* test.

(B) METTL8 expression level in PANC-1, CAPAN-1 and A549 cell line after anti-METTL8 IP. GAPDH was used as control.
(C) Oxygraph-2k measurements of WT METTL8 (dark gray) and METTL8 KO (light gray) PANC-1 cell lines. Respiratory activity analysis was performed as described in (C). Mean values ± SED of four independent measurements are plotted. n.s $p > 0.05$, ** $p < 0.01$, *** $p < 0.001$ in *t* test.

To confirm that the increased m^3C_{32} level in PANC-1 is based on METTL8 up-regulation, we mimiced the PANC-1 conditions in Flp-In TREx293 cells by METTL8 overexpression. The AlkAnilineSeq data revealed an m^3C_{32} boost of mt-tRNA$^{Ser(UCN)}$ from 150 Units to 280 Units under METTL8 overexpression conditions (Figure 2.17A, lower panel), while mt-tRNA^{Thr} methylation level seemed to be unchanged (> 750 U) (Figure 2.17A, upper panel). We next asked whether the m^3C_{32} boost of mt-tRNA$^{Ser(UCN)}$ can stimulate respiratory activity in Flp-In TREx293 cells (Figure 2.17B). We observed a mild increase of OXPHOS capacity and complex I activity under METTL8 overexpression conditions (Figure 2.17B). Surprisingly, the Leak state was reduced when METTL8 was upregulated (Figure 2.17B). The remaining Oroboros parameters as routine activity, ETS and complex II activity were unchanged (Figure 2.17B) suggesting that METTL8 is a bottleneck for respiratory chain function through mt-tRNA$^{Ser(UCN)}$ methylation.

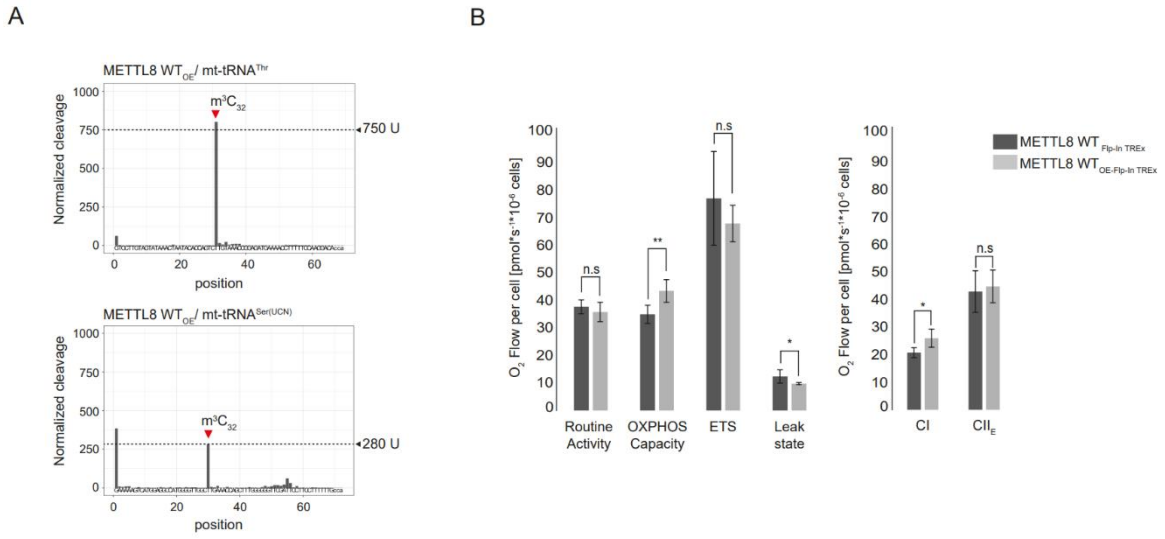

Figure 2.17: METTL8 upregulation increases m^3C_{32} methylation of mt-tRNA$^{Ser(UCN)}$
(A) m^3C cleavage profiles of mt-tRNA^{Thr} (top panel) and mt-tRNA$^{Ser(UCN)}$ (bottom panel) in Flp-In TREx293 cells overexpressing METTL8 WT .
(B) Respiratory activity of METTL8 WT (dark gray) and METTL8 overexpressing (WT_{OE}) (light gray) Flp-In TREx293 cell line analyzed by high-resolution respirometer Oxygraph-2k as described in (C). Mean values ± SED of four independent measurements are plotted. n.s $p > 0.05$, * $p < 0.05$, ** $p < 0.01$ in *t* test

2.9 METTL8 affects complex assembly by balancing mitochondrial translation

Prior to analyzing the impact of the mt-tRNA$^{Ser(UCN)}$ and mt-tRNA^{Thr} m^3C_{32} methylation on mitochondrial translation, we first checked their codon distribution among all 13 mitochondrial transcripts (Figure 2.18). Surprisingly, all codons of both mt-tRNAs appear in all transcripts randomly meaning there is no bias towards a specific mt-mRNA (Figure 2.18A). An unbiased metabolic labeling approach of mitochondrial proteins in the cell lines Flp-In TREx293 and PANC-1 performed by our collaborators Chris Powell, Chris Mutti and Michal Minczuk in Cambridge (Medical Research Council Mitochondrial Biology Unit, University of Cambridge, Hills Road, Cambridge, CB2 0XY, UK) confirmed that none of the 11 mitochondrial gene was specifically affected under METTL8 KO conditions (Figure 2.18B and C). Unfortunately, the expression levels of the mitochondrial proteins ND4L and ND6 remained unclear because they were not detectable after the gel electrophoresis (Figure 2.18C). The specificity in detecting mitochondrial proteins was ensured by emetine dihydrochloride blocking cytoplasmic translation.

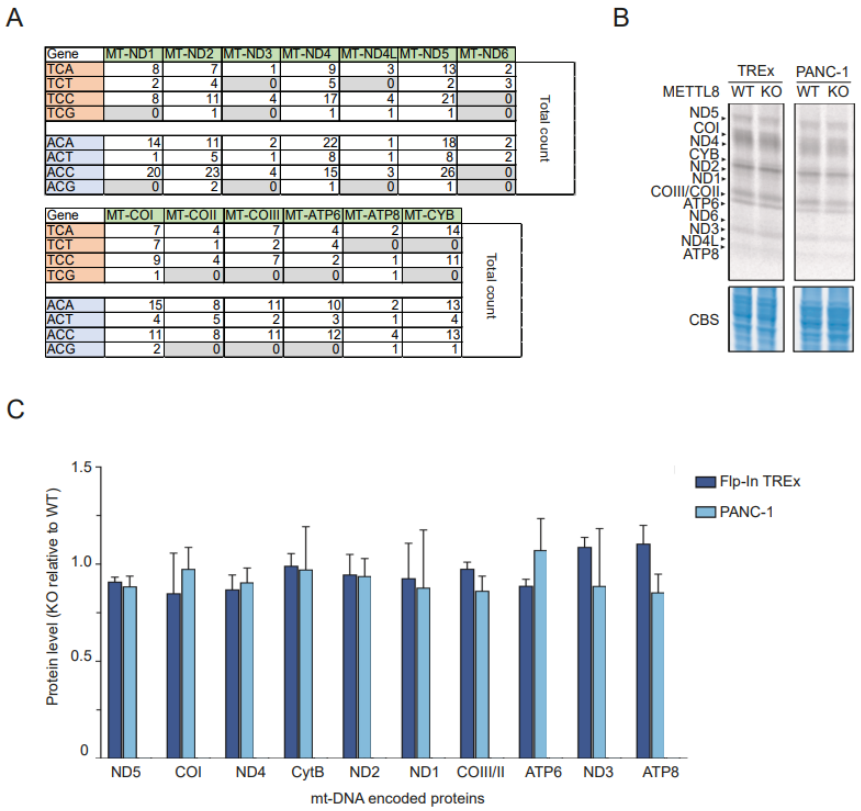

Gene	MT-ND1	MT-ND2	MT-ND3	MT-ND4	MT-ND4L	MT-ND5	MT-ND6	
TCA	8	7	1	9	3	13	2	Total count
TCT	2	4	0	5	0	2	3	
TCC	8	11	4	17	4	21	0	
TCG	0	1	0	1	1	1	0	
ACA	14	11	2	22	1	18	2	
ACT	1	5	1	8	1	8	2	
ACC	20	23	4	15	3	26	0	
ACG	0	2	0	1	0	1	0	

Gene	MT-COI	MT-COII	MT-COIII	MT-ATP6	MT-ATP8	MT-CYB	
TCA	7	4	7	4	2	14	Total count
TCT	7	1	2	4	0	0	
TCC	9	4	7	2	1	11	
TCG	1	0	0	0	1	0	
ACA	15	8	11	10	2	13	
ACT	4	5	2	3	1	4	
ACC	11	8	11	12	4	13	
ACG	2	0	0	0	1	1	

Figure 2.18: m^3C_{32} unbalancing in mt-tRNA$^{Ser(UCN)}$ and mt-tRNA^{Thr} affects respiratory complex assembly
(A) Codon distribution of mt-tRNA$^{Ser(UCN)}$ (red) and mt-tRNA^{Thr} (blue) in the 13 mt-DNA encoded transcripts. Codons not available in a gene highlighted in gray.
(B) Radioactive pulse labeling of *de novo* mitochondrial protein synthesis. Flp-In TREx293 and PANC-1 METTL8 WT and METTL8 KO cell lines were labeled with [^{35}S] methionine after cytoplasmic protein synthesis was

blocked by emetine dihydrochloride. Total lysates were separated by Tricine-SDS-PAGE and stained with Coomassie Blue as a loading control (left panel).
(C) Phosphor imaging quantification of the radioactive pulse labeling experiment shown in (B). Mean values ± SED of two independent measurements are plotted.

Due to the respiratory phenotype and the fact that complex I is the largest enzyme of the respiratory chain containing seven of the 13 mitochondrially encoded transcripts, we analyzed complex I assembly and composition by blue native gel electrophoresis followed by mass spectrometry (Figure 2.19A, top panel). To separate the individual sub-complexes of complex I and II, we purified mitochondria from METTL8 WT, KO and METTL8 overexpressing Flp-In TREx293 cells and retained the sub-complex assemblies by non-denaturating lysis conditions. The identified proteins were matched based on their size to the corresponding sub-complexes (Figure 2.19A), which were subsequently compared between the three cell lines (Figure 2.19B). Under METTL8 WT conditions, we did not detect all described components of the complex I assembly, which has not been unexpected. To separate the single complex I sub-complexes (ND units), hydrophobic high molecular mass proteins have to been solubilized which generally is challenging (Barros and McStay, 2020). Not-detectable components in our analysis under METTL8 WT conditions were listed in table 1 in HEK293T WT (Figure 2.19B, "HEK293T WT"). Compared to METTL8 WT, under METTL8 overexpressing conditions, we were able to detect all components of the respiratory complex I (Figure 2.19B, "METTL8 WT_{OE}"). Due to this striking effect, we assume METTL8 up-regulation supports specific ND subunit's abundance or stability. Interestingly, under METTL8 KO conditions, four additional proteins compared to METTL8 WT were not incorporated into complex I sub-complexes (Figure 2.19B, "METTL8 KO", highlighted in red). Surprisingly, two of them are nuclear encoded (NDUFA6 and SDHD), while ND1 and ND6 are mt-DNA encoded. Parallel to the blue native approach we performed proteomics of mitochondria purified from METTL8 WT, KO and WT_{OE} Flp-In TREx293 cells under denaturating conditions (data not shown). In presence of METTL8 either expressed normally or up-regulated, we identified all 13 mitochondrially encoded transcripts, however in METTL8 KO cells ND6 was missing (data not shown). In the analysis after the blue native gel electrophorese, ND6 and ND1 were not detectable might be consistent to their neighboring positions in the fully assembled complex I (Figure 2.19C).

A

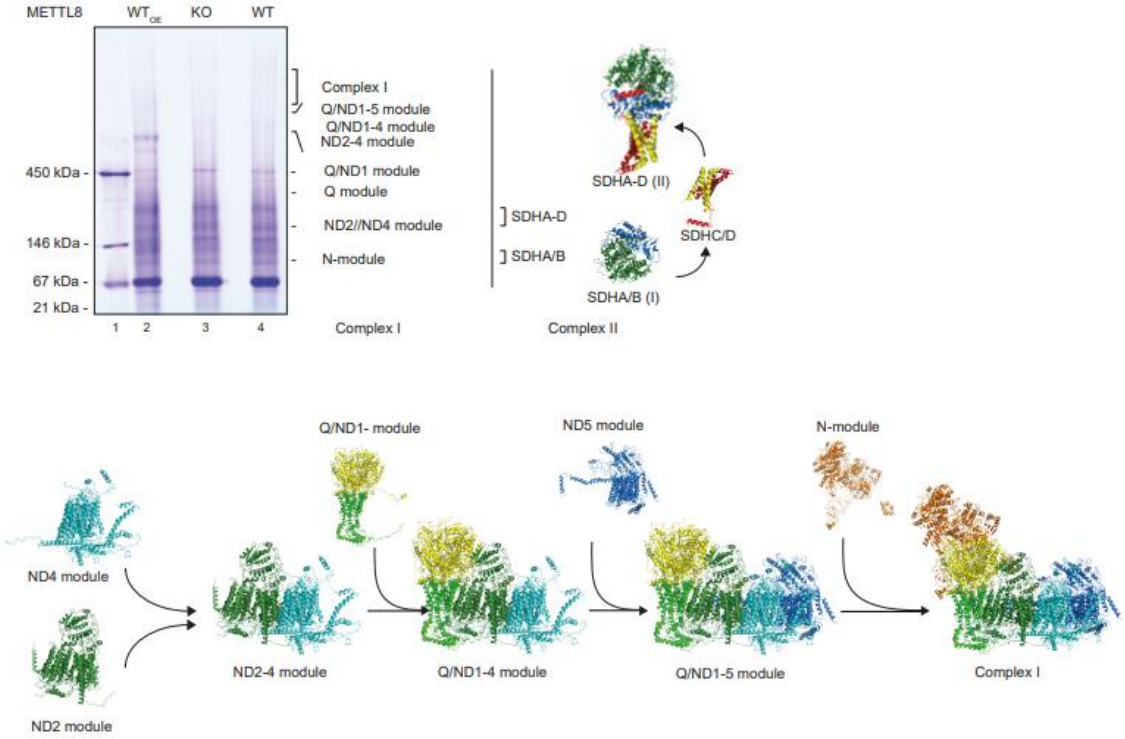

B

Table 1. Not-detecteable proteins in LC-MS/MS analysis according to their complex submodule

Module	HEK293T WT	METTL8 WT$_{OE}$	METTL8 KO
N - module	- NDUFS4 - NDUFS6		- NDUFS4 - NDUFS6 - NDUFA6
Q/ND1 module	- NDUFA3		- NDUFA3 - MT-ND1
ND2 module	- NDUFAFA1 - NDUFA1 - NDUFA10		- NDUFAFA1 - NDUFA1 - NDUFA10 - MT-ND6
ND4 module	- NDUFB3 - NDUFAB1		- NDUFB3 - NDUFAB1
ND5 module	- NDUFB5 - NDUFB11		- NDUFB5 - NDUFB11
SDHA-D			- SDHD

C

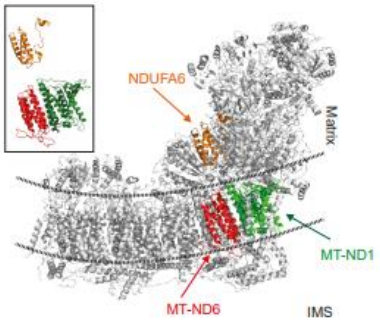

Figure 2.19: m^{3}C$_{32}$ unbalancing in mt-tRNA$^{Ser(UCN)}$ and mt-tRNA^{Thr} affects respiratory complex assembly
(A) Mitochondrial lysates from METTL8 WT, METTL8 KO and METTL8 overexpressing (WT$_{OE}$) Flp-In TREx293 cell lines were separated by blue native (BN) page and analyzed by liquid chromatography-tandem mass spectrometry (LC-MS/MS) analysis. Assembly of the complex I and II submodules are shown to the side of the panel. Structural complex I assembly (bottom) and complex II assembly (left panel) are based on (Signes und Fernandez-Vizarra 2018),(Sánchez-Caballero et al. 2016) and (Barros und McStay 2020) using crystal structures published in the Protein Data Base (PDB: 1zoy; 5ldw). PDB downloaded structures were modified in Pymol.
(B) Listed proteins were not detectable in LC-MS/MS analysis and are mapped to their related module. Additional proteins undetectable in Flp-In TREx METTL8 KO are highlighted in red.
(C) Crystal structure of complex I with highlighted proteins missing in METTL8 KO as described in (B).

Since all mt-tRNA$^{Ser(UCN)}$ or mt-tRNA^{Thr} codons are randomly distributed in all 13 mitochondrially encoded transcripts and their translation, not considering ND4L and ND6 is not significantly impaired (Figure 2.9A and B), we teamed up with Markus Hafner and James Marks (RNA Molecular Biology Group, Laboratory of Muscle Stem Cells and Gene Regulation, National Institute of Arthritis and Musculoskeletal and Skin Diseases, Bethesda, MD, 20892, USA) and performed an unbiased translation monitoring approach using ribosome profiling. Mitochondrial ribosome profiling allows us to identify codons causing ribosome pausing or accumulation. Ribosome protected fragments (RPF) were generated by MNase digestion and sucrose gradient centrifugation (Figure 2.20A). After cloning and deep sequencing, RPFs were aligned to the mitochondrial genome considering the mitochondrial ribosomal acceptor (A), peptidyl (P) and exit (E) site. When we compared the RPFs of METTL8 KO with METTL8 WT, we observed a clearly enrichment of serine(UCN) codons in the P site (Figure 2.20B) suggesting that the ribosome paused during translation elongation specifically on serine codons when the corresponding tRNA is unmodified. Interestingly, no effect was detectable for threonine codons under these conditions suggesting that the m^3C_{32} modification of mt-tRNA^{Thr} is dispensable for translation. However, during METTL8 overexpression, ribosomes accumulate at threonine codons in the A site meaning that the decoding takes more time as usual and might be marred (Figure 2.20C). This might be caused by a lower mt-tRNA^{Thr} expression level detected in our Northern Blot (Figure 2.4B and C). Since both mt-tRNAs decode cognate and near-cognate codons, we specified the affected codons at nucleotide level (Figure 2.20D and E). In the absence of METTL8, the mt-tRNA$^{Ser(UCN)}$ cognate codon UCA was the highest significantly enriched codon in the P site and A site compared to the near-cognate codons UCG and UCU (Figure 2.20D). During METTL8 up-regulation, ribosomes accumulated preferentially at the mt-tRNA^{Thr} near-cognate codon ACC in the A site (Figure 2.20E). Further, we asked whether all encoded UCA and ACC codons are affected by METTL8 expression level. Our analysis revealed that UCA codons harboring paused ribosomes were flanked downstream with the purines A or G in the P and A site (Figure 2.20F). Parallel, we did not observe an enrichment for any adjacent upstream nucleotides (data not shown). ACC codons were equally flanked downstream with the nucleotide A in the ribosomal A site (Figure 2.20G, left panel), which might be a sequencing bias considering the individual codon frequency (Figure 2.20G, right panel). Everything included, we postulate that decoding or translation elongation of specific serine(UCN) and threonine codons is marred, if a certain nucleotide context is given. When we mapped the strongest ribosome stalling events over all 13 mitochondrial encoded transcripts, we observed that ND6 harbored two of the three strongest stalling events at position 20 and 24 both containing UCU codons (Figure 2.20F and data not shown). The stalling event occurs in the ribosomal P site, when the UCU codon is upstream to a following UCU codon (position 20) and the UCU codons is flanked with a downstream proline codon (position 24). Taken together, we assumed that the missing mt-tRNA$^{Ser(UCN)}$ methylation caused by the absence of METTL8 impairs ND6 translation potentially leading to an alternative complex I assembly.

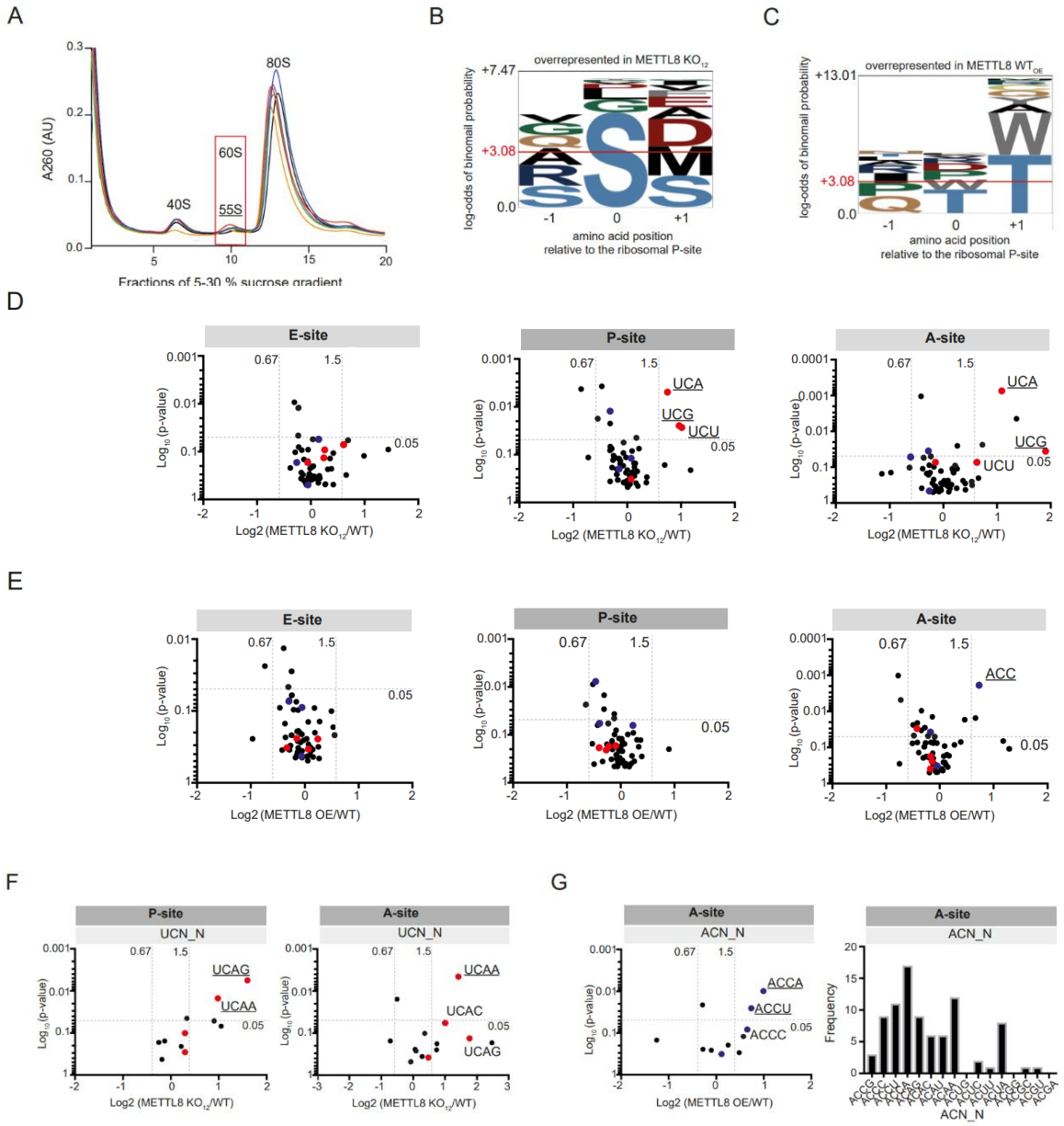

Figure 2.20: m^3C_{32} unbalancing in mt-tRNA$^{Ser(UCN)}$ and mt-tRNA^{Thr} affects translation dynamics
(A) Ribosome footprinting of METTL8 WT, METTL8 KO and METTL8 overexpressing Flp-In TREx cell lines. MNase treated ribosomes were separated by sucrose density centrifugation. Monosomes were isolated, sub-cloned and sequenced.
(B) Amino acid overrepresentation at positions relative to the P-site in Flp-In TREx293 METTL8 KO cells. Horizontal red line indicates significantly overrepresentation.
(C) Amino acid overrepresentation at positions relative to the P-site in Flp-In TREx293 cells overexpressing METTL8. Horizontal red line indicates significantly overrepresentation.
(D) Ribosomal redistribution in E, P and A site of Flp-In TREx293 METTL8 KO cells based on the codon. Red dots represent mt-tRNA$^{Ser(UCN)}$ codons, mt-tRNA^{Thr} codons are highlighted in blue. Significant overrepresented codons are underlined.
(E) Ribosomal redistribution in E, P and A site of Flp-In TREx293 cells overexpressing METTL8 based on the codon. Red dots represent mt-tRNA$^{Ser(UCN)}$ codons, mt-tRNA^{Thr} codons are highlighted in blue. Significant over- and underrepresented codons are underlined.

(F) Ribosome stalling in the P and A site of Flp-In TREx293 METTL8 KO cells based on the UCN codon and the nucleotide downstream**.** Left: UCN codons with overrepresented downstream nucleotides in the P site. Right: UCN codons with overrepresented downstream stream nucleotides in the A site. Significantly enriched mt-tRNA$^{Ser(UCN)}$ codons are highlighted in red and underlined.
(G) Ribosome stalling in the A site of Flp-In TREx293 cells overexpressing METTL8 based on the ACC codon and the nucleotide downstream**.** Left: ACC codons with overrepresented downstream nucleotides. Significantly enriched mt-tRNA^{Thr} codons are highlighted in blue and underlined. Right: frequency of mt-tRNA^{Thr} quadruplets with an additional downstream nucleotide (ACN_N).

3 DISCUSSION

In all kingdoms of life RNAs, in particular tRNAs, rRNAs and snRNAs are heavily modified. Chemical modified residues in tRNAs, for example, are crucial for tRNA structure, aminoacylation as well as ribosomal binding including decoding and translation elongation (Suzuki 2021). In the last years, tRNA modifications and their modifying enzymes were characterized in detail and interesting aspects of their biological function were unraveled. Several studies demonstrated that loss of the tRNA modifying enzymes and their matching modifications cause human diseases and promote cancer (Bohnsack und Sloan 2018; Chujo und Tomizawa 2021; Delaunay und Frye 2019b; Suzuki 2021)

Up to now, the human m^3C_{32} modifying enzyme of the mitochondrial tRNAs $tRNA^{Ser(UCN)}$ and $tRNA^{Thr}$ has been unknown (Bohnsack und Sloan 2018; Suzuki und Suzuki 2014; Suzuki et al. 2020). In our study we identified the methyltransferase like protein 8 (METTL8) as the m^3C methyltransferase acting on these mt-tRNAs. We further revealed that METTL8 methylation activity on mt-$tRNA^{Ser(UCN)}$ depends on the A_{37} modification status, which has to be isopentenylated (i^6A) prior to m^3C_{32} methylation. Most likely, a structural rearrangement of the anticodon loop by the i^6A modification allows METTL8 to recognize and catalyze position 32 of the mt-$tRNA^{Ser(UCN)}$ (Cabello-Villegas et al. 2002; Ganichkin et al. 2011; Murphy, 4th. et al. 2004; Weixlbaumer et al. 2007). This mechanism was indirectly shown as well for mt-$tRNA^{Thr}$. Studies of the mitochondrial t^6A_{37} modification demonstrated that loss of the mitochondrial t^6A modifying enzymes OSGEPL1 and YRDC leads to mt-$tRNA^{Thr}$ hypomodification at position 37 and additionally 32, which usually encode for m^3C (Lin et al. 2018).

Interestingly, prior studies postulated that METTL8 modifies mRNAs in the cytoplasm and RNAs within R-loops in the nucleus (Xu et al. 2017; Zhang et al. 2020). We could not confirm in our unbiased m^3C sequencing approach using AlkAnilineSeq any cytoplasmic or nuclear substrates. Nevertheless, we cannot exclude an alternative METTL8 function in other cellular compartments regarding that AlkAnilineSeq might not pick very low abundant transcripts. Furthermore, two of seven METTL8 isoforms do not contain a mitochondrial targeting sequence (MTS) and METTL8 contains an N terminally nuclear localization signal (NLS) in addition, which was triggered when we de-activated the MTS by modifying essential residues within the MTS. A MTS-mutated METTL8 mis-localized to nucleoli, which might be a hint for an alternative METTL8 function even though the mis-localization affected the cell viability negatively. To clarify a role of METTL8 apart from the mitochondrial function, further investigations of METTL8 isoforms are needed.

Mammalian mitochondria contain several copies of the circular double-stranded DNA genome (mtDNA) encoding 13 subunits of the OXPHOS machinery embedded in the inner membrane. Theses 13 mRNAs are translated by the mtDNA-encoded mitochondrial tRNA pool containing 22 different mitochondrial tRNAs (mt-tRNAs) including isoacceptors for the amino acids leucine and serine. Noticeably, the serine isoaccepetors belong, according to their cloverleaf structure, to different mt-tRNA classes and differ in their modification status meaning only mt-tRNA$^{Ser(UCN)}$ is methylated at position C_{32} (Anderson et al. 1981; Anderson et al. 1982). Surprisingly, in our AlkAnilineSeq approach we observed surprisingly that the C_{32} methylation status of the mt-tRNA$^{Ser(UCN)}$ pool is not 100 % and varies under different METTL8 conditions. Even if METTL8 was overexpressed, the mt-tRNA$^{Ser(UCN)}$ pool was not 100 % methylated suggesting the m^3C_{32} modification plays a pivotal role under specific conditions. Generally, the modification status of position C_{32} is dispensable for aminoacylation. Beyond that, though, it remains unclear, how the partial methylation of the mt-tRNA$^{Ser(UCN)}$ pool is regulated. We revealed in our methylation assay that METTL8 activity on C_{32} of mt-tRNA$^{Ser(UCN)}$ relies on the prior modified i^6A_{37} residue. However, nothing is known about a partial isopentenlyated mt-tRNA$^{Ser(UCN)}$ pool, which would be consistent with the partial m^3C_{32} methylation. Considering that the i^6A_{37} modification is highly conserved and indispensable for proper tRNA function (Fakruddin et al. 2018; Wei et al. 2011), it can be assumed that the mt-tRNA$^{Ser(UCN)}$ pool is fully isopentenlyated. Therefore, METTL8 activity on C_{32} in mt-tRNA$^{Ser(UCN)}$ needs to be blocked. A further anticodon loop arrangement might be such a regulatory element, which inhibits METTL8 activity on C_{32}. The 2-metylathio-*N*^{6}-isopentenyladenosine ($ms^2i^6A_{37}$) hypermodification, catalyzed by the ms^2 modifying enzyme CDK5RAP1, may introduce this arrangement and might block METTL8 activity on position C_{32}. In such a scenario, the ms^2 group affects the steric position of the U_{33} residue, which is essential for METTL8 catalytic activity on C_{32} (data not shown) and parallel face-to face arranged to C_{32}. The offset orientation of U_{33} is incompatible with the METTL8 catalytic active site and thus inhibits the C_{32} methylation in mt-tRNA$^{Ser(UCN)}$. However, this model has to be further analyzed. Of note, the mt-tRNA^{Thr} pool is fully methylated and position 37 not hypermodified.

The remarkable circumstances of the mt-tRNA$^{Ser(UCN)}$ methylation were further analyzed by ribosome profiling. In the absence of METTL8, mitoribosomes paused particularly on the mt-tRNA$^{Ser(UCN)}$ cognate codon UCA and near-cognate codons UCG/U preferentially in the P and A site suggesting that decoding of and translation elongation through these codons require m^3C_{32}. When we zoom in the nearer nucleotide context, we observed ribosome accumulation in the P and A site on UCA codons flanked downstream by purine bases. The stalling events on mt-tRNA$^{Ser(UCN)}$ near-cognate codons UCG and UCU seem independent of the nucleotide context, which might be based on the thermodynamically less stable wobble base pairing in contrary to the mt-tRNA$^{Ser(UCN)}$ cognate codon UCA forming Watson-Crick base pairing. All this data lead us to speculate that the m^3C_{32} modification of mt-tRNA$^{Ser(UCN)}$

promote decoding and translation elongation of the mt-tRNA$^{Ser(UCN)}$ cognate codon UCA, when flanked by a bulky purine. We further speculate that the m^3C_{32} modification destabilizes the Watson-Crick base pairing of the anticodon position 34 and the codon, which pushes for ribosome translocation especially when the codon residue A is involved in stacking interaction with the flanked A or G residue. Base stacking is a hydrophobic interaction shaping up between adjacent nucleotides and stabilizes nucleic acids originally known from 3D-DNA structures. Base-stacking interactions occur between pyrimidine-pyrimidine, purine-pyrimidine and purine-purine, but differ in their stability. Purine-purine stacking interactions are most stable. This hypothesis, however, needs to be further analyzed. Interestingly, when we analyzed the individual stalling events in the absence of METTL8 for all 13 mitochondrially encoded transcripts, we observed that ND6 contains two of the three strongest stalling events. The missing m^3C_{32} modification of the mt-tRNA$^{Ser(UCN)}$ affected the near-cognate codon UCU at position 20 and 24 either flanked by other UCU or proline codons. Our LC-MS/MS analysis, in which ND6 was reproducibly not detectable, confirmed an altered ND6 expression level. In this context, it has to be assessed weather ND6 expression level is lower than the detection threshold or ND6 is not expressed at all or an alternative ND6 product is generated by frameshifting. Although ribosomal frameshifting is rare, it can occur in the mitochondrial translation system by paused ribosomes either on downstream stable secondary structures or upstream slippery sequences, which might be present in ND6 (Temperley et al. 2010). We started LC-MS/MS analysis searching alternative ND6 products, but so far, we could not detect any.

In contrast to the partial methylation status of the mt-tRNA$^{Ser(UCN)}$ pool, the mt-tRNA^{Thr} pool is likely fully methylated (> 750 U), which is completly lost in METTL8 KO cells. Interestingly, we did not observe any stalling events on threonine codons under METTL8 KO conditions. Thus, we assumed either the methylation is not crucial for the translation cycle under tissue culture conditions or the increased mt-tRNA^{Thr} expression level we observed in Northern Blots might suppress long dwelling times on threonine codons. Strikingly, when METTL8 was overexpressed, we observed stalling events on mt-tRNA^{Thr} near-cognate codons ACC in the A site. That might be consistent with the strong reduced mt-tRNA^{Thr} expression level in METTL8 overexpressing cells and thus limited the availability of the tRNA. Taken together, METTL8 levels directly affect, in addition to its methylation activity, mt-tRNA^{Thr} expression level suggesting the mt-tRNA^{Thr} limitation might lead to an extended dwelling time of the ribosome at ACC codons in the A site. Interestingly, ACC codons appear randomly in almost all mitochondrial mRNAs except ND6. This data would support our model, in which METTL8 balance mitochondrial translation, in particular ND6 expression.

According to previous studies and the GEPIA database (Begik et al., 2020; Zhang et al., 2020), METTL8 is mis-expressed in a variety of cancer types. Even if METTL8 is upregulated in seven different types of cancer, METTL8 correlates with patient survival only in pancreatic cancer. Generally, cancer cells

spend a lot of energy on fast and aggressive progression (Tataranni et al. 2017). The massive demand of energy is provided by an enhanced glucose metabolism and/or respiratory chain activity. Since METTL8 triggers respiratory activity, METTL8 can be a benefit for cancer especially the highly aggressive and fast progressing pancreatic cancer. However, to link the partial methylation of mt-tRNA$^{Ser(UCN)}$ and the imbalance of the mt-tRNA^{Thr} expression to malignant cell metabolism is challenging. Furthermore, it has to be clarified why METTL8 is relevant for this specific form of pancreatic cancer needs to be clarified. PANC-1 cells are classified as respiratory-competent malignant cells, however their metabolic profile is not fully understood so far (Tataranni et al. 2017).Although OXPHOS generates much more ATP, cancer cells mainly activate glycolysis also due to the low oxygen levels in their environment. The increased proton leak and enhanced complex I activity in PANC-1 cells lead us to speculate that PANC-1 cells might use the higher respiratory activity not for generating ATP but for NADH recycling. The massive toxic amount of NADH generated by increased glycolysis is recycled by both the lactate dehydrogenase B (LDHB) and complex I. For this scenario, the complex I activity need to be increased and the respiratory chain itself need to be in an uncoupled mode. All this can be provided by high METTL8 levels affecting C_{32} methylation of mt-tRNA$^{Ser(UCN)}$ and mt-tRNA^{Thr} expression level, which balance the mitochondrial translation system and respiratory chain composition.

Although loss of METTL8 mis-regulates the mitochondrial translation, under cell culture conditions, METTL8 KO has no onerous consequences. METTL8 KO clones might suppress mitochondrial deficiency by adapting the nuclear background during the clonal selection (Deng et al. 2006). Especially, an ND6 defect can be rescued by an alternative background, which stabilize the remaining mtDNA-encoded subunits of complex I and recover complex I assembly by modified complex I subunits (Deng et al. 2006). Further, complex I assembly might not impaired in the absence of ND6, because loss of ND6 does not impair the further organization into high-molecular mass sub-complexes at all, although ND6 act as a linker for ND1- and ND2- containing sub-complexes (Perales-Clemente et al. 2010). Complex I assembly with non-regular subunits is known and already characterized (Perales-Clemente et al. 2010). However, loss of individual mt-encoded complex I subunits (ND subunits) results in different phenotypes. Defects in ND1, ND4 and ND6 alter complex I assembly, while loss of ND3 and ND5 affects complex I activity. In the absence of ND2 abnormal complex I intermediates accumulate. This data are consistent with our LC-MS/MS analysis after blue native gel electrophoresis.

Since mitochondrial function is crucial during early development, a mouse model for METTL8 function would be highly beneficial. METTL8 effects might be more pronounced, when cells are within their natural environment and progress.

4 MATERIAL AND METHODS

4.1 Reagents and Resources

4.1.1 Consumables and Chemicals

All chemicals, peptides and recombinant enzymes used in this work were obtained from Thermo Fisher Scientific, Sigma-Aldrich, Merck, Roth, AppliChem GmbH, Calbiochem, Invitrogen, GE Healthcare (Cytiva), BioRad, Serva and New England BioLabs. The individual allocation of resources are described in the Methods Details (4.4).

Radiochemicals were acquired from Hartmann Analytic GmbH and Perkin Elmer, the scintillation cocktail from Zinsser Analytic.

Oligonucleotides were synthesized by Metabion GmbH.

4.1.2 Antibodies

Used antibodies are listed in Table 4.1.

Table 4.1: Antibodies

Antibody	Source
Mouse monoclonal anti-HA.11 antibody (clone 16B2)	Covance
Mouse monoclonal anti-beta actin antibody (ab6276)	Abcam
Mouse monoclonal anti-GAPDH (GT239)	GeneTEx
Mouse monoclonal anti-p54[nrb]	BD Transduction Laboratories
Mouse monoclonal anti-FLAG®M2 (F3165)	Sigma
Rabbit polyclonal anti-TOM20 (FL-145)	Santa Cruz Biotechnologies

Rat monoclonal anti-METTL8 antibody (clone 16A7)	this paper
Rat monoclonal anti-METTL8 antibody (clone 19A10)	this paper
Goat polyclonal anti-mouse IgG, IRDye 800CW conjugated antibody	LI-COR Bioscience
Goat polyclonal anti-rabbit IgG, IRDye 800CW conjugated antibody	LI-COR Bioscience

4.1.3 Bacterial strains and human cell lines

Bacterial strains and human cell lines are listed in Table 4.2 and 4.3.

Table 4.2: Bacterial strains

Bacterial strain	**Source**
Escherichia coli Rosetta™ (DE3) competent cells	Novagen
XL1 blue competent cells	our lab

Table 4.3: Human cell lines

Experimental models: human cell line	**Source**
Flp-In™TREx™ -293	ATCC
Flp-In™TREx™ -293 METTL8 -/- clone C12_05	this work
Flp-In™TREx™ -293 METTL8 -/- clone C07_05	this work
Flp-In™TREx™ -293 METTL8-F/H	this work

Flp-In™TREx™ -293 METTL8 -/- // METTL8-F/H D230A	this work
Flp-In™TREx™ -293 METTL8 -/- // METTL8-F/H F253A	this work
Flp-In™TREx™ -293 METTL8 -/- // METTL8-F/H D260A	this work
Flp-In™TREx™ -293 METTL8 -/- // METTL8-F/H D272A	this work
Flp-In™TREx™ -293 METTL8 -/- // METTL8-F/H L299A	this work
Flp-In™TREx™ -293 METTL8 -/- // METTL8-F/H I4Q	this work
Flp-In™TREx™ -293 METTL8 -/- // METTL8-F/H I4,9Q	this work
Flp-In™TREx™ -293 METTL8 -/- // METTL8-F/H I4,9L12Q	this work
Flp-In™TREx™ -293 F/H-METTL2	this work
PANC-1	ATCC
PANC-1 METTL8 -/- clone C13_13	this work
PANC-1 METTL8 -/- clone C13-24	this work
CAPAN-1	ATCC
A-549	ATCC
HeLa S3	ATCC
P3X63Ag8.653 myeloma cells	ATCC

4.1.4 Recombinant DNA

Generated plasmids are listed in Table 4.4.

Table 4.4: Plasmids

Plasmid	Source
pcDNA™5/FRT/TO modified with N-terminal F/H-tag	Invitrogen
pOG44	Invitrogen
pcDNA™5/FRT/TO METTL8-F/H	this work
pcDNA™5/FRT/TO METTL8-F/H D230A	this work
pcDNA™5/FRT/TO METTL8-F/H F253A	this work
pcDNA™5/FRT/TO METTL8-F/H D260A	this work
pcDNA™5/FRT/TO METTL8-F/H D272A	this work
pcDNA™5/FRT/TO METTL8-F/H L299A	this work
pcDNA™5/FRT/TO METTL8-F/H I4Q	this work
pcDNA™5/FRT/TO METTL8-F/H I4/9Q	this work
pcDNA™5/FRT/TO METTL8-F/H I4/9 L12Q	this work
pcDNA™5/FRT/TO F/H-METTL2	this work
pIRES-VP5 modified	(Meister und Tuschl 2004)
pIRES-VP5 METTL8-EGFP	this work
pIRES-VP5 METTL8-EGFP I4Q	this work
pIRES-VP5 METTL8-EGFP I4/9Q	this work
pIRES-VP5 METTL8-EGFP I4/9 L12Q	this work

pIRES-VP5 F/H-METTL2	this work
pIRES-VP5 F/H-METTL8-F/H	this work
pETM14 TRIT1-GST	this work
pETM14 METTL8-GST	this work

4.1.5 Critical commercial assays

Used commercial assays are listed in Table 4.5.

Table 4.5: Commercial assays

Commercial assays	**Source**
Lipofectamin™ 2000	Invitrogen
Phusion® High-Fidelity DNA Polymerase	New England BioLabs®
NucleoSpin Gel and PCR Clean-up kit	Macherey-Nagel
NucleoSpin Mini Plasmid, Mini kit	Macherey-Nagel
NucleoBond Xtra Midi EF, Midi kit	Macherey-Nagel
MiSeq reagent Kit V3 (150 cycles)	Illumina
SuperScript™ III First-Strand Synthesis System	Invitrogen
First-strand cDNA synthesis kit	Thermo Fisher Scientific
Takyon™ No ROX SYBR 2x MasterMix blue dTTP	Eurogentec
T4 Polynucleotide Kinase (T4 PNK) kit – Buffer B	Thermo Fisher Scientific
Next Small RNA kit	New England BioLabs®

SERVA*Gel*™ Native Gel Starter Kit	Serva

4.1.6 Software and Algorithm

Used software is listed in Table 4.6.

Table 4.6: Software and Algorithm

Software and algorithm	**Source**
Quantity One Software	BioRad
Data Analysis 4.2	Bruker Daltonics
Protein Scape 3.1.3	Bruker Daltonics
Mascot 2.5.1	Matrix Science
Uniprot	https://www.uniprot.org/
PyMOL	
MitoFates	http://mitf.cbrc.jp/MitoFates/cgi-bin/top.cgi
RCSB Protein Data Bank (PDB)	https://www.rcsb.org/
Clustal Omega	https://www.ebi.ac.uk/Tools/msa/clustalo/
PrimerX	http://www.bioinformatics.org/primerx/
NCBI database	https://www.ncbi.nlm.nih.gov/
pLOGO	https://plogo.uconn.edu/
UCSC Genome Browser	https://genome.ucsc.edu/
Odyssey	LI-CORE

Zen10 Microscope Software	Zeiss
DatLab	Oroboros Instruments

4.1.7 Deposit data

Deposit data are listed in Table 4.7.

Table 4.7: Deposit data with corresponding database and accession number

Deposit data/ experiment	**Database/Accession Number**
Alk-Aniline-Seq	ENA: PRJEB45091
mitoRibosome Profiling	GEO: GSE180400

4.1.8 Others

Critical equipment is listed in Table 4.8.

Table 4.8: Critical equipment

Equipment	**Source**
LSM 710, AxioObserver microscope with a C-Apochromat 63x/1.20 W Korr M27 objective	Zeiss
Zeiss Axiovert200M microscope	Zeiss
Multimode-Microplate reader Mithras LB 940	Berthold Technologies
CFX96real-Time System BioRad	BioRad
Personal Molecular Imager™ System	BioRad
Multipurpose Scintillation Counter	Beckmann Coulter LS6500

Potter S Homogenizer	I B. Braun Biotech International
UltiMate 3000 RSLCnano System	Thermo Fisher Scientific
C18 Acclaim Pepmap100 preconcentration column	Thermo Fisher Scientific
Acclaim Pepmap100 C18 nano column	Thermo Fisher Scientific
maXis plus UHR-QTOF System	Bruker Daltonics
CaptiveSpray nanoflow electrospray source	Bruker Daltonics

4.2 Oligonucleotides

4.2.1 DNA oligonucleotide sequences for cloning and mutagenesis

Used DNA oligonucleotide sequences are listed in Table 4.9.

Table 4.9: DNA oligonucleotide sequences for cloning and mutagenesis. Construct name, orientation and sequences are indicated.

Construct name	**Sequence 5`- 3`**
METTL8//2-F/H in VP5 FLAG/HA N-terminal	
METTL8-WT NheI F	AGTGCTAGCATGAATATGATTTGGAGAA ATTCC
METTL8-WT EcoRI R	ACTGAATTCTCAAGCGTAATCGGGCACG TCATAAGGGTACTTGTCATCGTCGTCCTT GTAGTCGTCTTGTGAA

METTL2B NheI F	AGTGCTAGCGCCGGCTCCTACCCTGAAG G
METTL2B BglII R	ACTAGATCTAGCTGGTGCTGGACAGAAG G

sgRNA METTL8 in pX459 // 150 bp PCR Primer + barcode annealing site

METTL8-BbsI F	CACCGAGAGAAGCTAGTAAATACT
METTL8-BbsI R	AAACAGTATTTACTAGCTTCTCTC
PCR sgRNA METTL8 F	GTTCAGAGTTCTACAGTCCGACGATCCA ATTACGATCCTTGAAAAAC
PCR sgRNA METTL8 R	CCTTGGCACCCGAGAATTCCAACAATTA TCAAGACAGTAGCTAATAG

METTL8-eGFP in VP5 FLAG/HA C-terminal

eGFP-NheI F	AGTGCTAGCGTGAGCAAGGGCGAGGAG CTG
eGFP-EcoRI R	AGTGAATTCTTACTTGTACAGCTCGTCCA TGC
METTL8-WT FseI F	AGTGGCCGGCCATGAATATGATTTGGAG AAATTCC
METTL8- WT AscI R	AGTGGCGCGCCGTCTTGTGAAAGGAGTG
METTL8-I4 FseI F	AGTGGCCGGCCATGAATATGCAATGGAG AAATTC
METTL8-I4 AscI R	AGTGGCGCGCCGTCTTGTGAAAGGAGTG
METTL8-I4/9 FseI F	AGTGGCCGGCCATGAATATGCAATGGAG AAATTC
METTL8-I4/9 AscI R	AGTGGCGCGCCGTCTTGTGAAAGGAGTG
METTL8-I4/9//L12 FseI F	AGTGGCCGGCCATGAATATGCAATGGAG AAATTC
METTL8-I4/9//L12 AscI R	AGTGGCGCGCCGTCTTGTGAAAGGAGTG

site-directed mutagenesis Primer

METTL8-I4 F	CGCTAGCATGAATATGCAATGGAGAAATTC
METTL8-I4 R	GAATTTCTCCATTGCATATTCATGCTAGCG
METTL8-I4/9 F	GCAATGGAGAAATTCCCAATCTTGTCTAAGGCTAG
METTL8-I4/9 R	CTAGCCTTAGACAAGATTGGGAATTTCTCCATTGC
METTL8-I4/9//L12 F	GCAATGGAGAAATTCCCAATCTTGTCAAAGGCTAG
METTL8-I4/9//L12 R	CTAGCCTTTGACAAGATTGGGAATTTCTCCATTGC
METTL8-D230A F	CTTTCTGTATTGTTGTGCTTTTGCTTCTGGAGCTG
METTL8-D230A R	CAGCTCCAGAAGCAAAAGCACAACAATACAGAAAG

METTL8//TRIT1-GST with Shine-Dalgarno Sequence in modified pETM14

METTL8-GST XbaI F	AGTTCTAGATAAGAAGGAGATATACCATGCAAAGTGGTTACCACCCAG
METTL8-GST NheI R	AGTGCTAGCGTCTTGTGAAAGGAGTGTAG
TRIT1-GST NcoI F	AGTCCATGGTAAGAAGGAGATATACCATGCTACCTCTTGTAGTGATTCTC
TRIT1-GST NheI R	AGTGCTAGCAACGCTGCATTTCAGCTCTTGATC

METTL8-F/H in pcDNA 5/FRT/TO

METTL8-WT AscI F	AGTGGCGCGCCATGAATATGATTTGGAGAAATTCC
METTL8-WT FseI R	GGTATCTACACTCCTTTCACAAGACGACTACAAGGACGACGATGACAAGTACCCTTATGACGTGCCCGATTACGCTTGAGGCCGGCCAGT

Library cloning	
3`Adapter	TGGAATTCTCGGGTGCCAAGG
5`Adapter	GUUCAGAGUUCUACAGUCCGACGAUC
RT 3` Primer	GCCTTGGCACCCGAGAATTCCA
5` PCR Primer	AATGATACGGCGACCACCGAGATCTACA CGTTCAGAGTTCTACAGTCCGACGATC
3` True Seq PCR Primer	ACCTTAAGAGCCCACGGTTCCTTGAGGT CAGTG######TAGAGCATACGGCAGAAG ACGAAC ##### = Barcode

4.2.2 DNA oligonucleotide sequences for qPCR

Used DNA oligonucleotide sequences are listed in Table 4.10.

Table 4.10: DNA oligonucleotide sequences for qPCR. Construct name, orientation and sequences are indicated

Construct name	**Sequence 5`- 3`**
qPCR mt-ND1 F	CAAAGGCCCCAACGTTGTAG
qPCR mt-ND1 R	CGGGTTTTAGGGGCTCTTTG
qPCR mt-ND2 F	GCACCACGACCCTACTACTA
qPCR mt-ND2 R	CTAGGGAGAGGAGGGTGGAT
qPCR mt-ND3 F	GACTACCACAACTCAACGGC
qPCR mt-ND3 R	TTATGGAGAAAGGGACGCGG
qPCR mt-ND4L F	TCGCTCACACCTCATATCCTC
qPCR mt-ND4L R	AAGAGGGAGTGGGTGTTGAG

qPCR mt-ND4 F	GCTCCCTTCCCCTACTCATC
qPCR mt-ND4 R	TCTTGGGCAGTGAGAGTGAG
qPCR mt-ND5 F	AAAACCTGCCCCTACTCCTC
qPCR mt-ND5 R	GGTGGAGATTTGGTGCTGTG
qPCR mt-ND6 F	GGGTGGTGGTTGTGGTAAAC
qPCR mt-ND6 R	GATCCTCCCGAATCAACCCT
qPCR mt-COI F	TCCCCTAATAATCGGTGCCC
qPCR mt-COI R	GGAGTAGGAGAGAGGGAGGT
qPCR mt-COII F	CAACGATCCCTCCCTTACCA
qPCR mt-COII R	AGATTAGTCCGCCGTAGTCG
qPCR mt-COIII F	ATGATGGCGCGATGTAACAC
qPCR mt-COIII R	TCCCGTATCGAAGGCCTTTT
qPCR mt-ATP6 F	TTCGCTTCATTCATTGCCCC
qPCR mt-ATP6 R	GGTGGGGATCAATAGAGGGG
qPCR mt-ATP8 F	CTCCCTCACCAAAGCCCATA
qPCR mt-ATP8 R	GGGGCAATGAATGAAGCGAA
qPCR mt-CYB F	TGAAACTTCGGCTCACTCCT
qPCR mt-CYB R	TTGAGGCGTCTGGTGAGTAG

4.2.3 Northern Blot probes

Used DNA oligonucleotide sequences are listed in Table 4.11.

Table 4.11: DNA oligonucleotide sequences for Northern Blots. Construct name, orientation and sequences are indicated

Construct name	**Sequence 5`- 3`**
mt-tRNA$^{Ser(UCN)}$	CCCCATGGCCTCCATGACTTT
mt-tRNA^{Arg}	TATGATTATCATAATTTAATG
mt-tRNA^{Trp}	ATTAAGTATTGCAACTTACTG
mt-tRNA^{Thr}	CCGGTTTACAAGACTGGTGTA
mt-tRNA^{Ile}	AATAAGGGGGTTTAAGCTCCT
mt-tRNA^{Lys}	TGTAAAGAGGTGTTGGTTCTCTT
tRNA$^{Thr(AGT)}$	TCGAACCCAGGATCTCCTGTT

4.2.4 DNA oligonucleotide sequences for mt-tRNA *in vitro* transcription

Used DNA oligonucleotide sequences are listed in Table 4.12.

Table 4.12: DNA oligonucleotide sequences for mt-tRNA in vitro transcription. Construct name, orientation and sequences are indicated

Construct name	**Sequence 5`- 3`**
T7 promotor sequence + *mt-tRNA DNA nucleotide sequence*	
	AGTATAATACGACTCACTATAGG…….
mt-tRNA$^{Ser(UCN)}$ F	GAAAAAGTCATGGAGGCCATGGGGTTGGCTTG AAACCAGCTTTGGGGGGTTCGATTCCTTCCTTT TTTG
mt-tRNA$^{Ser(UCN)}$ R	CAAAAAAGGAAGGAATCGAACCCCCCAAAGC TGGTTTCAAGCCAACCCCATGGCCTCCATGACT TTTTC
mt-tRNA$^{Ser(UCN)}$ C32G mutant F	GAAAAAGTCATGGAGGCCATGGGGTTGGGTTG AAACCAGCTTTGGGGGGTTCGATTCCTTCCTTT TTTG
mt-tRNA$^{Ser(UCN)}$ C32G mutant R	CAAAAAAGGAAGGAATCGAACCCCCCAAAGC TGGTTTCAACCCAACCCCATGGCCTCCATGACT TTTTC
mt-tRNA$^{Ser(AGY)}$ F	GAGAAAGCTCACAAGAACTGCTAACTCATGCC CCCATGTCTAACAACATGGCTTTCTCA
mt-tRNA$^{Ser(AGY)}$ R	TGAGAAAGCCATGTTGTTAGACATGGGGGCAT GAGTTAGCAGTTCTTGTGAGCTTTCTC
mt-tRNA^{Phe} F	GTTTATGTAGCTTACCTCCTCAAAGCAATACAC TGAAAATGTTTAGACGGGCTCACATCACCCCA TAAACA
mt-tRNA^{Phe} R	TGTTTATGGGGTGATGTGAGCCCGTCTAAACA TTTTCAGTGTATTGCTTTGAGGAGGTAAGCTAC ATAAAC
mt-tRNA^{Trp} F	AGAAATTTAGGTTAAATACAGACCAAGAGCCT TCAAAGCCCTCAGTAAGTTGCAATACTTAATTT CTG

mt-tRNA$^{Trp\ R}$	CAGAAATTAAGTATTGCAACTTACTGAGGGCT TTGAAGGCTCTTGGTCTGTATTTAACCTAAATT TCT

4.3 Experimental Models and Subject Details

4.3.1 Generation of inducible Flp-In™ T-REx™ 293 cell stable cell lines

Inducible Flp-In™ T-REx™ 293 cell lines stably expressing F/H-METTL2B// METTL8-F/H constructs were generated by co-transfection of pcDNA™5/FRT/TO harboring F/H-METTL2B //METTL8-F/H constructs and pOG44 plasmid. Transfection was carried out by Lipofectamin™ 2000 (Invitrogen) reagent according to the manufacture`s protocol. Cells grown in 24-wells were transfected at 80-90 % confluence using 100 ng pcDNA™5/FRT/TO and 900 ng pOG44 plasmid. To select transfectants, cells were cultured in medium supplemented with 15 µg/ml blasticidin and 150 µg/ml hygromycin B.

4.3.2 Generation of METTL8 knockout cell lines

METTL8 knockout was generated in Flp-In™ T-REx™293 and PANC-1 cell lines by CRISPR/Cas9-directed genome editing. The site-directed frameshift in *METTL8* was guided by the *METTL8* complementary sgRNA (5`-CACCGAGAGAAGCTAGTAAATACT-`3) embedded in a pX459 backbone. Cells were transfected twice by Lipofectamin™ 2000 (Invitrogen) with an intermediary puromycin selection round of 12-16 hours, which was skipped for PANC-1 cells. After transfection and recovering step, cells were separated into single clones. Flp-In™ T-REx™ 293 METTL8 KO clones were analyzed by sequencing strategy and validated by western blotting. For sequencing, genomic DNA of clonal cell lines was extracted by 0.2 mg/ml ProteinaseK (AppliChem) in 500 µl ProteinaseK buffer (200 mM Tris/HCl pH 7.5, 300 mM NaCl, 25 mM EDTA, 2 % [w/v] SDS) at 50 °C overnight. DNA was precipitated by addition of 400 µl 2-propanol and centrifugation at 20 000 g and 4 °C for at least 30 minutes. Pellet was washed twice with 70 % EtOH [v/v], dried 10 minutes at 50 °C and dissolved in 50 µl water. 150 bp region comprising sgRNA annealing site was amplified in a 50 µl PCR reaction (1x Phusion HF Buffer, 200 µM dNTPs, 2x 0.5 µM specific primer, 3 % [v/v] DMSO, 3 µl purified DNA, 1 U Phusion® High-Fidelity DNA Polymerase) (New England BioLabs®). DNA region was amplified by thermocycling and amplicons were purified by a 2 % [w/v] agarose gel, followed by a NucleoSpin Gel and PCR Clean-up Kit (Macherey-Nagel). In a second PCR round, purified amplicons were attached to barcodes of the Illumina TrueSeq-System and sequenced by a MiSeq-sequencing platform. Genotypes of the utilized METTL8 KO cell lines are given below.

METTL8 KO clone	Allele	Genotype
C12_05	1	Insertion 1 nt
	2	Insertion 1 nt
C07_05	1	Deletion 5 nt
	2	Deletion 1 nt

PANC-1 METTL8 KO clones were tested directly by western blotting.

4.3.3 General Cell culture conditions

Cell lines and adherent HeLa S3 were grown in Dulbecco's modified Eagle's medium (DMEM; Sigma Aldrich) supplemented with 10 % fetal bovine serum (FBS; Gibco) under standard conditions at 37 °C in 5 % CO_2 atmosphere. Medium for Flp-In™ T-REx™ 293 cells was completed with 15 µg/ml blasticidin (Gibco) and 100 µg/ml zeocin (Invitrogen), medium for Flp-In™ T-REx™ 293 cell stably expressing METTL2B or METTL8 constructs with 15 µg/ml blasticidin (Gibco) and 150 µg/ml hygromycin B (Invitrogen). HeLa cells were treated with antibiotics penicillin (100 U/ml) and streptomycin (100 µg/ml) (Sigma) and expanded in spinner flasks and Joklik`s medium (Sigma Aldrich) supplemented with 10 % fetal bovine serum (FBS; Gibco) at 37 °C.

Name	Tissue	Sex	Disease	Identifier ATCC®
Flp-In™ T-REx™ 293	embryonic kidney	fetus		CRL-1573™
PANC-1	pancreas/duct	male	epithelioid carcinoma	CRL-1649™
CAPAN-1	pancreas/derived from metastatic site: liver	male	adenocarcinoma	HTB-79™
A549	lung	male	carcinoma	CCL-185™
HeLa	cervix	female	adenocarcinoma	CCL-2™
HeLa S3	cervix	female	adenocarcinoma	CCL-2.2™

4.4 Methods Details

4.4.1 Immunofluorescence

Flp-In™ T-REx™ 293 cells stably expressing METTL8-F/H were grown on coverslips without blasticidin and hygromycinB. Expression was induced by 1 µg/ml tetracycline 24 h before fixation with ice cold aceton at -20 °C for 7 minutes (Alshammari et al. 2016).

Glass slides were incubated in blocking solution (1x TBS, 6 % [w/v] BSA, 0.1 % [v/v] Tween-20) at room temperature (RT) for 1 h, followed by overnight incubation at 4 °C with primary antibody (1x PBS, 3 % [w/v] BSA, 0.1 % [v/v] Tween-20). In the next step glass slides incubated with secondary antibody (1x PBS, 3 % [w/v] BSA, 0.1 % [v/v] Tween-20) at RT for 1 h. Between fixation and antibody treatments five 1x PBS washing steps of 10 minutes were performed. Terminally coverslips were rinsed with water and mounted by using ProLong™ Gold Antifade Mountant with DAPI (Life Technologies). Images were recorded on a Zeiss Axiovert200M microscope and analyzed using Fiji. Used antibodies were listed below.

Primary Antibody	**Dilution**	**Source**	**Secondary Antibody**
α-FLAG®M2	1:100-200	mouse, mAb	Alexa Fluor® 488 goat-α-mouse IgG (H+L)
α-TOM20	1:100-200	rabbit, pAb	Alexa Fluor® 555 goat-α-rabbit IgG (H+L)
α-METTL8 (MEL8 16A7; 19A10)	1:50-100	rat, mAb	Alexa Fluor® 488 goat-α-rat IgG (H+L)

4.4.2 Live cell Imaging

To analyze the subcellular localization of METTL8-EGFP constructs containing MTS mutations, live cell imaging was performed. Flp-In™ T-REx™ 293 cells were grown in 15 cm dishes and normal DMEM medium on coated coverslips (97 % [v/v] Ham`s F12 Nutrient Mixture, 1 % [w/v] Fibronectin Solution (Bovine),1 % [w/v] Collagen solution from calf skin, 0.05 % [w/v] BSA, 1 % [v/v] Penicillin-Streptomycin). Cells at 60-70 % confluence were transfected by calcium phosphate (2x HEPES-buffered saline, 2.5 M $CaCl_2$, 10 µg DNA) and grown for additional 48 h under standard conditions. Ahead visualization, cells were washed trice with warm 1x PBS, stained with 1 µg/ml Hoechst 33342 and 133 nM MitoTracker™ Deep Red FM (Invitrogen) in normal growth medium for 20 minutes under standard

conditions. Cells were rinsed twice in warm 1x PBS and analyzed on a LSM 710, AxioObserver microscope with a C-Apochromat 63x/1.20 W Korr M27 objective. For detection following filter were used: 450-517 nm (Hoechst 33342), 493-549 nm (EGFP), 638-755 nm (Red FM). Images were analyzed by the software Zen 2011 (Carl Zeiss).

4.4.3 High-resolution Respirometry by Oxygraph-2k

Oxygen consumptions rate was recorded by Oxygraph-2k (O2k; Oroboros Instruments) at 37 °C. Before analysis start, O2k was cleaned and equilibrated with air saturated MIR05 growth medium (20 mM HEPES, 10 mM KH_2PO_4, 20 mM Taurine, 60 mM Lactobionic acid, 3 mM $MgCl_2$, 0.5 mM EGTA, 0.1 % [w/v] BSA) under stirring at 700 rpm. Cells at 70-80 % confluence were washed with warm PBS and detached by trypsin, which was inactivated after desired incubation time by adding DMEM supplemented with 10 % FBS. Cells were centrifuged at 400 g and RT for 10 minutes, resuspended in MIR05 growth medium and adjusted to a concentration of 0.5x 10^6 cell/ml. For high resolution respirometry analysis 2 ml cell suspension was used and applied to the adapted Substrate-Uncoupler-Inhibitor-Titration Protocol - 001 O2 ce-pce D004 (SUIT; SUIT-001 O2 ce-pce D004). After monitoring routine respiration, plasma membrane was permeabilized by an optimal Digitonin (Merck) concentration depending on cell line.

Cell line	**Digitonin [nM]**
Flp-In™ T-REx™ 293 METTL8 WT	8.1
Flp-In™ T-REx™ 293 METTL8 KO	8.1
Flp-In™ T-REx™ 293 METTL8 WT_{OE}	8.1
Flp-In™ T-REx™ 293 METTL8 D230A	8.1
PANC-1 METTL8 WT	6.1
PANC-1 METTL8 KO	4.1

LEAK respiration with NADH-linked substrates Glutamate (10 mM; Sigma Aldrich) and Malate (2 mM; Sigma Aldrich) was detected first before stimulating OXPHOS capacity with saturating ADP (5 mM; Calbiochem). Cytochrome *c* (10 µM; Sigma Aldrich) evaluated the integrity of the mitochondrial outer membrane and supported the validity of the respiratory activity. By addition of succinate (10 mM;

Sigma Aldrich) the TCA cycle function was reconstituted. After monitoring LEAK respiration in present of ADP by oligomycin (2 mM; Sigma Aldrich), the electron transfer (ET) capacity was stimulated by titration of the uncoupler FCCP (Sigma Aldrich). Rotenone (2 mM; Sigma Aldrich) inhibited complex I and set apart the succinate pathway control state. Terminally complex III was blocked by antimycin (1 mM; Sigma Aldrich) to detect the residual oxygen consumption due to oxidative side reactions.

4.4.4 Proliferation Assay

For proliferation assay 1x 10^3 Flp-In™ T-REx™ 293 cells or 2.5 x 10^3 PANC-1 cells were seeded without any antibiotics in 96-well plates in DMEM without pyruvate and monitored five days under standard conditions. 96-well plates used for Flp-In™ T-REx™ 293 cells were coated with 50 µg/ml Poly-D lysine (Sigma Aldrich) in PBS before. METTL8-F/H expression in Flp-In™ T-REx™ -293 cells was induced by 1 µg/ml tetracycline (AppliChem). After desired incubation time, cells were fixed with 50 µl crystal violet solution (0.5 % [w/v] crystal violet in 20 % [v/v] MeOH) at RT for 10 minutes. Fixed cells were washed twice with 100 µl warm water followed by two further PBS washing steps of two minutes. Lastly cells were rinsed with water and air dried. Cells were quantified by crystal violet intensity detected at 590 nm using a Multimode-Microplate reader Mithras LB 940 (Berthold Technologies). Crystal violet was eluted from the cells before by 50 µl 0.1 M sodium citrate in 50 % [v/v] EtOH.

4.4.5 Plasmids

Open reading frame (ORF) of METTL2B (GenBank: NM_018396.2), METTL8 (GenBank: NM_024770.4) and TRIT1 (GenBank: NM_017646.5) were amplified from Flp-In™ T-REx™ 293 cDNA (SuperScript™ III First-Strand Synthesis System - Invitrogen) using target specific primer with appropriate restriction sites (Table 4.9) in a 50 µl PCR reaction (1x Phusion HF Buffer, 200 µM dNTPs, 2x 0.5 µM specific primer, 3 % [v/v] DMSO, 0.5 µl cDNA, 1 U Phusion® High-Fidelity DNA Polymerase) (New England BioLabs®). METTL2B amplicon was cloned into a modified pIRES-VP5 backbone encoding a N terminal FLAG/HA tag using the restrictions enzymes NheI/BglII. METTL8 cDNA was cloned into a pcDNA5/FRT/TO plasmid encoding a modified pIRES-VP5 backbone using the restriction enzymes NheI/EcoRI. METTL8 cDNA used for pIRES-VP5 cloning was linked to FLAG/HA tag C terminally by PCR amplification before cloning into the modified pIRES-VP5 plasmid encoding an N terminal FLAG/HA tag. Mutations in METTL8 sequence were introduced by site-directed mutagenesis. DpnI digestion at 37 °C for at least 3 h extracted plasmids with incorporated mutation/s. METTL8-EGFP constructs were set up in two consecutive steps. EGFP amplicon, amplified

from a random EGFP vector, was imbedded into a modified pIRES-VP5 backbone by using the restriction enzymes NheI/EcoRI. Thereupon METTL8 DNA, amplified from the corresponding VP5 plasmid, were inserted N-terminally by FseI/AscI. For generating tetracycline inducible Flp-In™ T-REx™-293 expression cell lines, METTL8-F/H was inserted into a modified pCDNA™5/FRT/TO vector by AscI/FseI. Recombinant proteins fused to a GST tag at their C-terminus were expressed from a modified pETM14 backbone without an N terminal 6x His-tag and 3C-site. METTL8 was combined to GST C-terminally by using XbaI/NheI. TRIT1-GST fusion protein was generated by NcoI/NheI. For CRISPR/Cas9-directed genome editing, chimeric guideRNA (sgRNA) complementary to the nearer *METTL8* N-terminus was embedded into the backbone vector pX459. DNA oligonucleotides were phosphorylated in a 10 µl Polynucleotide Kinase (PNK) reaction (2x 100 µM DNA oligonucleotide,1x T4 DNA Ligation Buffer, T4 PNK) (Thermo Fisher Scientific) at 37 °C for 30 minutes, boiled up to 95 °C and annealed during cooling down to 25 °C. BbsI digested pX459 backbone and annealed DNA oligonucleotides were ligated at RT for 1 h. All plasmids and their target sequence were verified by Sanger Sequencing.

4.4.6 cDNA Synthesis and RNA analysis by Quantitative Real Time RT-PCR

Total volume of RNA isolated from METTL8 immunoprecipitations were reversed transcripted by First-strand cDNA synthesis kit (Thermo Fisher Scientific) using random and mt-tRNA$^{Ser(UCN)}$ specific primer. Fluorometric amplification was performed by Takyon™ No ROX SYBR 2x MasterMix blue dTTP (Eurogentec) with mt-mRNA and mt-tRNASer$^{(UCN)}$ specific primer and CFX96real-Time System (BioRad). Primer sequences are listed in Table 4.10.

4.4.7 RNA Immunoprecipitation

METTL8-RNA interaction was analyzed by RNA-immunoprecipitation (RIP). Verification of METTL8-RNA interaction was done by either qPCR or Northern Blotting. Flp-In™ T-REx™ 293 METTL8 WT and KO cells were expanded in normal growth medium (DMEM supplemented with 10 % FBS), Flp-In™ T-REx™ 293 cells stably expressing METTL8-F/H were grown overnight in normal growth medium supplemented with 1 µg/ml tetracycline. Cells of 5x 15 cm dishes were harvested and lysed in 1 ml NP-40 lysis buffer (20 mM Tris/HCl pH 8, 137 mM NaCl, 10 % glycerol, 1 % [v/v] NP-40, 2 mM EDTA, 1 mM AEBSF and 1 mM DTT) on ice for 30 minutes. For Northern Blot analysis, living cells were irritated by 280 nm UV light before (120 mJ/cm^2)(Strategene). Cell lysates were cleared at 20 000 g and 4 °C for 30 minutes. Afterwards, samples were adjusted to the same concentration and 10 % of the lysate was used as input sample. For immunoprecipitation 50 µl Protein G Sepharose slurry

(GE Healthcare) were used and equilibrated in lysis buffer (20 mM Tris/HCl pH 8, 137 mM NaCl, 10 % glycerol, 1 % [v/v] NP-40, 2 mM EDTA, 1 mM AEBSF and 1 mM DTT). Beads were incubated with 1 ml protein lysate and 5 µg mAb α-METTL8 at 4 °C overnight with rotation. Antibody coupling to protein G was carried out in parallel. FLAG/HA tagged proteins were immunoprecipitated by ANTI-FLAG M2 Affinity Gel (Sigma Aldrich). Next day beads were washed trice with washing buffer (50 mM Tris/HCl pH 8, 300 - 1000 mM NaCl, 0.1 % [v/v] NP-40, 1.5 mM $MgCl_2$, 1 mM AEBSF,1 mM DTT). After transferring beads into a new reaction tube, beads were washed twice again and terminally cleansed in PBS. To isolate the METTL8 bound RNA, proteins were digested first by 6 U/ml ProteinaseK (Thermo Fisher Scientific) in 200 µl ProteinaseK buffer (200 mM Tris/HCl pH 7.5, 300 mM NaCl, 25 mM EDTA, 2 % [w/v] SDS) at 50 °C for 30 minutes while mild shaking. Subsequently RNA was extracted by Roti® Phenol/Chloroform/Isoamylalcohol (Roth) and ethanol precipitation. Total RNA of input samples was purified by TRIzol (Invitrogen).

4.4.8 Northern Blotting including ^{32}P –oligonucleotide labeling

0.5 µg total RNA and RNA derived from METTL8 IP were separated on a 6 % urea-PAGE running at 400 V in 1x TBE buffer. After electrophoresis, RNA quality was checked by EtBr staining first and transferred onto a water equilibrated Hybond™ -N membrane (GE Healthcare) at 20 V for 45 minutes by semi dry blotting (SD Semi-Dry Transfer Cell, Bio-RAD). 1-ethyl-3-(3-dimethylaminopropyl) -carbodiimide hydrochloride (EDC) (160 mM EDC, 130 mM 1-methylimidazol, adjusted to pH 8 by HCl) crosslinked RNA to the membrane at 50 °C in 1 h. Crosslink was completed with UV light at 254 nm (120 mJ/cm^2) (Stratagene). Membrane was rinsed with water and air dried. Meanwhile 20 pmol of DNA oligonucleotide (Table 4.11) were 5` end labeled by using 0.5 U/ml PNK (Thermo Fisher Scientific) and 20 mC_i γ-^{32}P-ATP (Hartmann Analytic). PNK reaction was carried out in PNK Buffer A (Thermo Fisher Scientific) 30 minutes at 37 °C and stopped by addition of 18 mM EDTA. [^{32}P] radiolabelled DNA was purified by illustra™ MicroSpin G-25 column (GE Healthcare) and mixed with hybridization solution (20 mM sodium phosphate buffer pH 7.2, 5x SSC, 1 % [w/v] SDS, 2 % [v/v] Denhardt's solution). Hybridization between RNA and radioactive labelled DNA was carrying out overnight at 50 °C. After 12-15 h membrane was washed twice with washing solution I (5x SSC, 1 % [w/v] SDS) and once with washing solution II (1x SSC, 1 % [w/v] SDS) at 50 °C for 10 minutes. Radioactive signals were detected by storage phosphor screens and Personal Molecular Imager™ System (BioRad) with Quantity One Software (version 4.6.9, Bio-Rad). Membrane was interrogated several times with different probes by consecutive stripping and re-probing. For stripping, membrane was washed twice in hot 0.1 % [w/v] SDS solution for 10 minutes with agitation and cleaned with hot water for another 10 minutes.

4.4.9 Aminoacylation Assay

RNA for aminoacylation assay was extracted by TRIzol (Invitrogen). To keep charged tRNAs, all steps were performed on ice and RNA was treated under acid conditions. Aminoacylated RNA was dissolved in 10 mM NaOAc/ HOAc (pH 4.8) at 37 °C for 5 minutes. Deacylated RNA was resuspended in 0.2 M Tris/HCl pH 9.5 and dissolved 1 h at 37 °C. 10 µg of either charged or uncharged RNA was mixed with acid denaturing sample buffer (90 % [v/v] formamide, 0.1 M NaOAc/ HOAc (pH 4.8), 0.05 % [w/v] bromophenol blue and 0.05 % [w/v] xylene cyanol) and separated on a 6 % urea-PAGE containing 0.1 M NaOAc/ OHAc (pH 4.8). Electrophoresis was running at 100 V and 4 °C in 0.1 M NaOAc/ OHAc (pH 4.8) overnight. Separated RNA was transferred onto a water equilibrated Hybond™ -N membrane (GE Healthcare) at 20 V for 30 minutes by semi dry blotting (SD Semi-Dry Transfer Cell, Bio-RAD). RNA crosslinking and visualization were performed according to Northern blotting.

4.4.10 AlkAnilineSeq

Analysis of m^3C residues in human cytoplasmic and mitochondrial tRNAs was performed as described previously (Marchand et al. 2018). In brief, total RNA sample was subjected to partial alkaline hydrolysis in bicarbonate buffer (96 °C, pH 9.2), the reaction was stopped by ethanol precipitation. RNA fragments were extensively de-phosphorylated by Antarctic phosphatase and subjected to aniline cleavage (1M pH 4.5, 15 min in the dark). Resulting fragments having a 5'-phosphate at N+1 nucleotide were converted to a sequencing library using NEBNext Small RNA kit. Sequencing was performed in single-read 50 nt (SR50) mode on HiSeq1000 (Illumina). Sequencing reads were trimmed to remove adapter sequence and aligned to human tRNA reference sequence (both cytoplasmic and mitochondrial tRNAs). Normalized cleavage is calculated as a 1000x ratio of reads starting at a given position to total number of sequencing reads mapped to a given RNA. Please notice that the calibration curve for modification rate to Normalized cleavage is non-linear and shows very high sensitivity for very low modification rates.

4.4.11 *In vitro* Transcription of mt-tRNAs

tRNAs were transcribed by T7 RNA polymerase. 100 µM 5` and 3` DNA oligonucleotides linked to T7 promotor sequence (Table 4.12) (Metabion) were boiled up at 95 °C for 30 seconds in 1x T4 DNA Ligation Buffer (Thermo Fisher Scientific) and annealed by cooling down to 25 °C. Annealed DNA oligonucleotides were transcribed in a 1 ml transcription reaction (30 mM Tris pH 8.0, 10 mM DTT, 0.01 % [v/v] Triton X-100, 25 mM $MgCl_2$, 2 mM spermidine, 30 % [v/v] DMSO, 5 mM ATP, 5 mM

CTP, 5 mM UTP, 5 mM GTP, 0.4 U/ml thermostable inorganic pyrophosphatase (NEB) and 0.1 mg/ml T7-polymerase) overnight at 37 °C. After 12-14 h transcription reaction was mixed with 2x RNA denaturing sample buffer and purified by a 6 % urea-PAGE. RNA was visualized by UV shadowing, cut out and extracted by RNA elution buffer (300 mM NaCl, 2 mM EDTA) overnight with agitation at 4 °C. By adding 0.7 volume 2-propanol RNA precipitated at -20 °C overnight. RNA was pelleted at 20 000 g and 4 °C for at least 30 minutes, washed twice with 80 % [v/v] ethanol, dried at 37 °C for 5 minutes and dissolved in water at 65 °C for 5 minutes.

4.4.12 *In vitro* m^3C design on mt-$tRNA^{Ser(UCN)}$ (Isopentenylation//Methylation)

m^3C incorporation on mt-$tRNA^{Ser(UCN)}$ catalyzed by METTL8 depends on an isopentenylation reaction at A_{37} (i^6A_{37}). N^6-isopentenyladenosine was introduce in 1 µM mt-tRNA by 250 nM TRIT1 and 10 µM γ,γ-Dimethylallyl pyrophosphate (DMAPP)(Sigma Aldrich). Reaction was carried out in isopentenylation buffer (50 mM Tris/HCl pH 7.5, 5 mM $MgCl_2$, 100 µM β-mercaptoethanol, 0.2 U/ml RiboLock RNase Inhibitor (Thermo Fisher Scientific)) at 37 °C for 1 h (Lamichhane et al. 2013). Modified RNA was isolated by TRIzol extraction (Invitrogen) according to the manufacture`s protocol. RNA pellet was resuspended in 10 µl water and used for the consecutive methylation assay. m^3C incorporation was performed by 250 nM METTL8 in methylation buffer (10 mM Tris/HCl pH 7.5, 100 mM KCl, 1.8 mM $MgCl_2$, 5 % [v/v] Glycerol, 0.1 mg/ml BSA, 1 mM DTT, 0.2 U/mL RiboLock RNase Inhibitor (Thermo Fisher Scientific), 10 nC_i/µl SAM[^{3}H] (Hartmann Analytic)) at 37 °C for 1 h. m^3C modified tRNA was purified by TRIzol extraction (Invitrogen) according to the manufacture`s protocol and resuspended in 25 µl water (65 °C for 5 minutes). RNA was mixed with 10 ml scintillations cocktail (Zinsser Analytic) and measured by a multipurpose scintillation counter (Beckmann Coulter LS6500). Activity was counted per minute (c.p.m.).

4.4.13 Generation of monoclonal Antibodies

A peptide comprising amino acids $_{149}$VPDEKNHYEKSSG $_{161}$ from human METTL8 protein was synthesized and coupled to ovalbumin (Peps4LS, Heidelberg, Germany). Lou/c rats were immunized subcutaneously and intraperitoneally with a mixture of 50 µg OVA-peptide, 5 nmol CPG oligonucleotide (Tib Molbiol, Berlin), 500 µl PBS and 500 µl *Incomplete Freund's* adjuvant (IFA). Eight week later, a boost injection without IFA was given three days before fusion of rat spleen cells with P3X63Ag8.653 myeloma cells using standard procedures. Hybridoma supernatants were screened by ELISA for binding to biotinylated METTL8 peptide on avidin-coated ELISA plates. Positive supernatants were further validated in immunoprecipitations and Western blot analysis. Hybridoma cells

from selected supernatants were subcloned twice by limiting dilution to obtain stable monoclonal cell lines. Experiments in this work were performed with supernatants from monoclonal antibody clones MEL8 19A10 and 16A7(both rat IgG2c/k).

4.4.14 Cell lysis – Immunoprecipitation – Western Blotting

Cells for immunoprecipitation were generally broken up by 1 ml NP-40 lysis buffer (20 mM Tris/HCl pH 8, 137 mM NaCl, 10 % glycerol, 1 % [v/v] NP-40, 2 mM EDTA, 1 mM AEBSF and 1 mM DTT). PANC-1, CAPAN-1 and A459 cells were disrupted by glass beads additionally. Cells were lysed 30 minutes on ice and centrifuged at 20 000 g at 4 °C for 30 minutes.

Lysates were adjusted to the same protein concentration by Bradford assay. For immunoprecipitation 50 µl Protein G Sepharose slurry (GE Healthcare) was used and equilibrated in NP-40 lysis buffer. Protein lysates adjusted to the same protein concentration by Bradford were incubated with equilibrated Protein G Sepharose and 5 µg mAb α-METTL8 at 4 °C overnight with agitation. 10 % of the protein lysate was used as input control. F/H tagged proteins were immunoprecipitated by ANTI-FLAG M2 Affinity Gel (Sigma Aldrich). In the next step beads were washed trice with washing buffer (50 mM Tris/HCl pH 8, 300 mM NaCl, 0.1 % [v/v] NP-40, 1.5 mM $MgCl_2$, 1 mM AEBSF,1 mM DTT). After the third washing step beads were transferred into a new reaction tube and washed twice again. Immunoprecipitated proteins were eluted by 5x SDS loading buffer. Input samples were mixed with 1x SDS loading buffer. Samples were boiled at 95 °C for 5 minutes and separated by a 10 % SDS-PAGE. Proteins were transferred onto a nitrocellulose membrane (0.45 µm, GE Healthcare) by semi dry blotting (SD Semi-Dry Transfer Cell, Bio-RAD). Nitrocellulose membrane was blocked in 5 % [w/v] milk at RT for 15-60 minutes and subsequently incubated with primary antibody overnight at 4 °C with agitation. Secondary antibody was applied afterwards for 1 h at RT. Between and after antibody application membrane was washed 3x with 1x TBST for 10 minutes with agitation. Used antibodies were listed below. Signals were detected by Odyssey Infrared Imaging System (LI-COR Biosciences). Gels for LC-MS/MS analysis were stained by Coomassie Blue (0.25 % [w/v] Coomassie Brilliant Blue R250 (#1610400, Bio-Rad),10 % [v/v] acetic acid, 30 % [v/v] ethanol) and cleansed afterwards with destainer (10 % [v/v] acetic acid, 30 % [v/v] ethanol).

Primary Antibody	Dilution 5 % [w/v]	Source	Incubation	Secondary Antibody
α-HA.11	1:1000 / milk	mouse, mAb	o/n // 4 °C	IRDye® 800CW Goat α-mouse IgG
α- β Actin	1:10000 / milk	mouse, mAb	o/n // 4 °C	IRDye® 800CW Goat α-mouse IgG
α-METTL8	1:500 / milk	rat, mAb	o/n // 4 °C	IRDye® 800CW Goat α-rat IgG
α-TIMM44	1:3000 / milk	rabbit, pAb	o/n // 4 °C	IRDye® 800CW Goat α-rabbit IgG
α-GAPDH	1:1000 / milk	mouse, mAb	o/n // 4 °C	IRDye® 800CW Goat α-mouse IgG
α- p54[nrb54]	1:1000 / milk	mouse, mAb	o/n // 4 °C	IRDye® 800CW Goat α-mouse IgG

4.4.15 Protein expression and purification

METTL8 (aa. 22-407) and TRIT1 (aa. 23-467) were expressed as GST-fusion protein from pETM-14 vector in *E.coli* Rosetta without mitochondrial targeting sequence (MTS). Bacteria were grown to an OD_{600} of 0.5 and cool down at 4 °C until OD_{600} of 0.6. Protein expression was subsequently induced by 100 µM IPTG. TRIT1-GST was expressed 6 hours at 37 °C, METTL8-GST overnight at 23 °C. Bacteria pellet was resuspended in lysis buffer (20 mM Tris/HCl pH 8, 1 M NaCl, 0.2 mM EDTA, 1 mM DTT) and sonicated 3x 5 minutes (duty cycle 50 %, output control 5) with a consecutive break of 5 minutes on ice. Lysate was cleared by centrifugation at 50 000 g and 4 °C for 45 minutes. Before performing GST-pulldown by using a 6 ml GST-column (GE Healthcare), supernatant was passed through a filter with a diameter of 45 µm (Roth). To remove proteins bound unspecifically, column was washed industriously with lysis buffer and protein of interest was finally eluted with 50 mM Tris/HCl pH 8 and 10 mM Glutathion. The eluate was concentrated to a volume of 0.5-1 ml by Vivaspin® 20 ultrafiltration device (MWCO 30 000, Sartorius) and loaded on a Superdex™ 200 10/30 GL (GE Healthcare) equilibrated with 25 mM Tris/HCl pH 8 and 150 mM NaCl. Peak fractions were analyzed by a 10 % SDS-PAGE, pooled, adjusted to 50 % [v/v] glycerol and stored at -80 °C.

4.4.16 Mitochondrial Preparation

Flp-In™ T-REx™-293 cells from a confluent 15 cm dish were resuspended in 1 ml trehalose buffer (10 mM HEPES/KOH pH 6.9, 10 mM KCl, 300 mM trehalose, 0.1 % [w/v] BSA, 0.2 % [w/v] Digitonin) and gently disrupted by using a Potter S Homogenizer (B. Braun Biotech International – sartorius group). Up down movement of the PTFE plungers at 700 rpm ruptured the cell membrane, which was subsequently pelletized at 800 g for 7 minutes at 4 °C. In this centrifugation step nuclei were sediment as well. To separate mitochondria from the cytosol, supernatant was centrifuged at 10 000 g and 4 °C for 10 minutes. Mitochondria were washed trice with trehalose buffer and pelletized at 10 000 g and 4 °C for 5 minutes. To reduce contaminants, mitochondria were resuspended in 1 ml trehalose buffer containing 3 µU/ml ProteinaseK (Thermo Fisher Scientific) and incubated 20 minutes on ice. The reaction was stopped by 2 µg/ ml Aprotinin (Roche), 1 mM AEBSF and centrifugation (10 000 g at 4 °C, 5 minutes). After two washing steps with trehalose buffer, mitochondria were used in BN experiments.

4.4.17 Blue Native Gel Electrophoresis (BN)

120 µg mitochondria were resuspended in 100 µl non-denaturing buffer (Tris/HCl pH 8, 1 mM sucrose, 1 %, [w/v] Digitonin) and solubilized 30 minutes on ice. Insoluble proteins were pelletized at 20 000 g and 4 °C for 30 minutes. Native protein migration was performed by using SERVA*Gel*™ Native Gel Starter Kit. Solubilized mitochondrial proteins were mixed with 2x Sample buffer for BN and separated on a SERVA*Gel*™ N 3-12 (vertical native gel 3-12 %). Electrophoresis was running 120 minutes at 50-200 V in anode and blue cathode buffer. Blue cathode buffer was exchanged after 2/3 of the electrophoresis. For LC-MS/MS analysis, proteins were fixed in 20 % [w/v] trichloroacetic acid (TCA) at RT for 30 minutes and stained with Coomassie blue (0.1 % [w/v] Coomassie Brilliant Blue R250 (# 1610400, Bio-Rad), 10 % [v/v] acetic acid, 45 % [v/v] ethanol). After 30 minutes, gel was cleansed 2x 60 minutes with destainer (20 % [v/v] ethanol, 5 % [v/v] acetic acid, 1 % [w/v] glycerol) and prepared for LC-MS/MS analysis.

4.4.18 Protein Analysis by Mass Spectrometry

For mass spectrometric analysis of proteins gel lanes were cut into consecutive slices. The gel slices were then transferred into 2ml micro tubes (Eppendorf) and washed with 50 mM NH_4HCO_3, 50mM NH_4HCO_3/acetonitrile (3/1) and 50mM NH_4HCO_3/acetonitrile (1/1) while shaking gently in an orbital shaker (VXR basic Vibrax, IKA). Gel pieces were lyophilized after shrinking by 100% acetonitrile. To

block cysteines, reduction with DTT was carried out for 30 min at 57°C followed by an alkylation step with iodoacetamide for 30 min at room temperature in the dark. Subsequently, gel slices were washed and lyophilized again as described above. Proteins were subjected to *in gel* tryptic digest overnight at 37°C with approximately 2 µg trypsin per 100 µl gel volume (Trypsin Gold, mass spectrometry grade, Promega). Peptides were eluted twice with 100 mM NH_4HCO_3 followed by an additional extraction with 50 mM NH_4HCO_3 in 50% acetonitrile. Prior to LC-MS/MS analysis, combined eluates were lyophilized and reconstituted in 20 µl of 1 % formic acid. Separation of peptides by reversed-phase chromatography was carried out on an UltiMate 3000 RSLCnano System (Thermo Scientific, Dreieich) which was equipped with a C18 Acclaim Pepmap100 preconcentration column (100µm i.D.x20mm, Thermo Fisher) in front of an Acclaim Pepmap100 C18 nano column (75 µm i.d. × 150 mm, Thermo Fisher). A linear gradient of 4% to 40% acetonitrile in 0.1% formic acid over 90 min was used to separate peptides at a flow rate of 300 nl/min. The LC-system was coupled on-line to a maXis plus UHR-QTOF System (Bruker Daltonics, Bremen) via a CaptiveSpray nanoflow electrospray source (Bruker Daltonics). Data-dependent acquisition of MS/MS spectra by CID fragmentation was performed at a resolution of minimum 60000 for MS and MS/MS scans, respectively. The MS spectra rate of the precursor scan was 2 Hz processing a mass range between m/z 175 and m/z 2000. Via the Compass 1.7 acquisition and processing software (Bruker Daltonics) a dynamic method with a fixed cycle time of 3 s and a m/z dependent collision energy adjustment between 34 and 55 eV was applied. Raw data processing was performed in Data Analysis 4.2 (Bruker Daltonics), and Protein Scape 3.1.3 (Bruker Daltonics) in connection with Mascot 2.5.1 (Matrix Science) facilitated database searching of the Swiss-Prot *Homo sapiens* database (release-2020_01, 220420 entries). Search parameters were as follows: enzyme specificity trypsin with 1 missed cleavage allowed, precursor tolerance 0.02 Da, MS/MS tolerance 0.04 Da, carbamidomethylation or propionamide modification of cysteine, oxidation of methionine, deamidation of asparagine and glutamine were set as variable modifications. Mascot peptide ion-score cut-off was set 15. If necessary, fragment spectra were validated manually. Protein list compilation was done using the Protein Extractor function of Protein Scape.

4.4.19 Metabolite analysis by gas chromatography – mass spectrometry

Intermediates of glycolysis and TCA cycle were analyzed by gas chromatography coupled to mass spectrometry (GC-MS). To harvest the cells for analysis, the cell culture supernatant was removed and cells were washed three times with PBS and then scrapped with cold 80% methanol. The suspension was collected, the cell culture dish was washed with 80 % methanol and the combined sample was stored at −80 °C. For further sample preparation, the sample suspension was thawed and 10 µl of an aqueous internal standard mix containing stable isotope labeled analogs of the analytes was added. The sample was vortexed, and centrifuged (9560 g, 5min, 4 °C). The supernatant was collected and the pellet was

resuspended twice in 200 µL 80% methanol with in-between supernatant collection. The last wash was centrifuged at a higher speed (13800 g). All supernatants were combined and dried in a vacuum evaporator (CombiDancer, Hettich AG, Bach, Switzerland). Sample residues were dissolved in 100 µl pure water and an aliquot was transferred into a flat bottom insert in a 1.5-ml glass vial. The aliquot was evaporated to dryness and then subjected to methoximation and silylation for GC-MS analysis using the derivatization protocol and instrumental setup previously described (Dettmer et al. 2011). A Rxi-5ms column (30m, 0.25mm ID, 0.25µm film thickness, Restek, Bad Homburg Germany) with a 2-m guard column was used. The temperature program started at 50 °C (0.5 min), followed by a ramp of 5°C/min to 120 °C, then 8 °C/min to 300 °C, and the final temperature was held for 5 min. The carrier gas was helium with a flow rate of 0.7 ml/min. The mass spectrometer was operated in full scan mode with a scan range of 50 to 550 m/z. An injection volume of 1 µl with splitless injection at 280°C was used. For analysis of cell culture supernatants, 10 µl of the supernatant and 10 µl of the aqueous internal standard mix were transferred into a flat bottom insert in a 1.5-ml glass vial, dried and subjected to derivatization and GC-MS analysis as described.

Quantification was performed using calibration curves based on the area ratio of the endogenous compound to the stable isotope labeled standard (Mass Hunter Quantitative Analysis, version B.07.01/build 7.1.524.0, Agilent Technologies). Data were normalized to total protein. Protein amount was determined using a fluorescence assay as recently described (Berger et al. 2021).

4.4.20 ^{35}S-methionine metabolic labelling of mitochondrial proteins

In order to label newly synthesized mitochondrially expressed proteins, the previously published protocol was used (Pearce et al. 2017). Briefly, cells at approximately 80% confluency were incubated in methionine/cysteine-free medium for 10 min before the medium was replaced with methionine/cysteine-free medium containing 10% dialyzed FCS and emetine dihydrochloride (100 µg/ml) to inhibit cytosolic translation. Following a 20 min incubation, 120 µCi/ml of [^{35}S]-methionine (Perkin Elmer) was added and the cells were incubated for 30 min. After washing with PBS, cells were lysed, and 30 µg of protein was loaded on 10–20% Tris- glycine SDS-PAGE gels. Dried gels were visualized with a PhosphorImager system.

4.4.21 Ribosome Profiling of Mitochondria

Cells were grown in T-75 flasks to 70% confluence in DMEM media and METTL8 overexpression was induced with 2 µg/mL of doxycycline 24 hours prior to collection. Cells were washed once with ice cold PBS, flash frozen on liquid nitrogen and stored at -80°C until lysis. 667 µL of 1.5x Lysis buffer (30 mM

Tris–HCl pH 7.8, 150 mM KCl, 15 mM $MgCl_2$, 1.5 mM DTT, 1.5% triton X-100, 0.15% NP40, 1× complete phosphatase and protease inhibitors) was added to each flask and cells were collected with a cell scraper while flasks thawed on an ice slurry. ~1 ml of lysate was transferred to a chilled 1.5 ml tube, gently passed through a 27-gauge needle 10 times, and spun at 5,000 g for 10 minutes at 4°C. Digestion was carried out by adding 1,500 U of MNase, 10 µl of SUPErase•In, and $CaCl_2$ to a final concentration of 5mM to 400 µL of lysate and incubating at 22°C for 1 h. Digestion was stopped by adding EGTA to a final concentration of 6 mM. Lysate was loaded onto a 5-30% sucrose gradient (20mM Tris–HCl pH 7.8, 100 mM KCl, 10 mM $MgCl_2$, and 1 mM DTT and spun for 2.5 h at 40,000 rpm in an SW40 rotor. The 55S mitoribosome fraction was collected using a BioComp Fractionator. Footprints were isolated through SDS/hot phenol/chloroform extraction.

Following each step, footprints or PCR products were cleaned by either Zymo's Oligo Clean and Concentrator or DNA Clean and Concentrator, respectively. Small RNAs were size selected using the Purelink miRNA isolation kit. 3' ends were dephosphorylated with NEB Quick CIP and 3' adapter ligation was carried out with Rnl2(1-249)K227Q ligase over night at 4°C. 3' adapter: 5'-rAppNNTGACTGTGGAATTCTCGGGTGCCAAGG-L, where the underlined sequence is the library barcode. Barcoded footprint libraries were then combined and phosphorylated by PNK. Footprints were then ligated to a 5' DNA-RNA adapter with RNA Ligase. 5'(aminolinker)GTTCAGAGTTCTACAGTCCGACGATCrNrNrNrN. Reverse transcription was carried out with SuperScript IV. RT Primer GCCTTGGCACCCGAGAATTCCA. Libraries were initially amplified by PCR using the RT primer and a short 5' primer, CTTCAGAGTTCTACAGTCCGACGA. Footprints were size selected by a Pippen Prep, 3% C gel. Sizes of 74-94 were selected, corresponding to footprint sizes of 15-35. Libraries were then amplified with long indexing primers and sequenced.

Ribosome profiling analysis

Deduplicated reads were mapped to a chrM transcriptome based on the hg38 genome. P site positioning was determined by Plastid, measuring from the start codons of ND4 and ATP6. Changes in relative ribosomal occupancy was measured by first determining the proportion of ribosome density at each codon relative to the total density in the encompassing gene. Then fold change is then calculated dividing the relative ribosomal density at each position in the experimental dataset by the WT control.

pLOGO analysis

pLOGO (O'Shea et al. 2013) backgrounds were the E, P, and A site sequences of all codons that had ribosomal density in both the experimental and control datasets. Foregrounds were defined as the E, P, and A sites that had a fold change greater than 2.

5 APPENDIX

5.1 List of Figures

5.2 List of Tables

5.3 List of Abbreviations

µg	Microgramm
µl	Microliter
µm	Micrometer
µM	Micromolar
µU	Microunits
A	Adenine
AEBSF	4-(2-Aminoethyl) benzenesulfonyl *f*uoride hydrochloride
Ala	Alanine
Arg	Arginine
A site	Acceptor site
Asn	Asparagine
Asp	Aspartate
ATP	Adenosine triphosphate
BSA	Bovine Serum Albumin
$CaCl_2$	Calcium chloride
cDNA	complementary DNA
CDS	Coding sequence
Cm	2`-*O*-Methylcytosine
cm^2	square centimeter

CO_2	Carbon dioxide
CTP	Cytidine triphosphate
Cys	Cysteine
DAPI	4′,6-Diamidin-2-phenylindole
DLBC	Diffuse large B cell carcinoma
DMAPP	γ,γ-Dimethylallyl pyrophosphate
DMEM	Dulbecco's modified Eagle's medium
DMSO	Dimethyl sulfoxide
DTT	Dithiothreitol
E site	Exit site
EDC	1-Ethyl-3-(3-dimethylaminopropyl) - carbodiimide hydrochloride
EDTA	Ethylenediaminetetraacetic acid
EGTA	Ethylene glycol-bis(β-aminoethyl ether)-N,N,N′,N′-tetraacetic acid
ER	Endoplasmatic reticulum
ET	Electron transfer
EtBr	Ethidium bromide
EtOH	Ethanol
ETS	Electron transport system
F/H	FLAG/HA
$FADH_2$	Flavin adenine dinucleotide
FBS	Fetal bovine serum
FCCP	Carbonyl caynid 4-(trifluoromethoxy)phenylhydrazone
FCS	Fetal Calb serum
G	Guanine
GBM	Glioblastoma
GC-MS	gas chromatography coupled to mass spectrometry
GEPIA	Gene Expression Profiling Interactive Analysis
Gln	Glutamine
Glu	Glutamate
Gm	2`-*O*-Methylguanosine
GST	Glutathione S-transferase
GTP	Guanosine triphosphate
h	Hour
HEPES	4-(2-Hydroxyethyl)-1-piperazineethanesulfonic acid
hESCs	Emybryonic human stem cells
HF	High Fidelity
His	Histidine
HOAc	Acetic acid
IF	Immunofluorescence
Ile	Isoleucines
IP	Immunoprecipitation
IPTG	Isopropyl-β-D-thiogalactopyranoside
KCl	Potassium chloride
KH_2PO_4	Potassium dihydrogenphosphate
KO	Knock out
KOH	Potassium hydroxid
LC-MS/MS	Liquid Chromatography with tandem mass spectrometry
LDHB	Lactate dehydrogenase B
Leu	Leucine
LGG	Low grade glioma
LUSC	Lung squamous cell carcinoma
Lys	Lysine
m	Meter
M	Molar
m/z	mass to charge ratio

m^1A	N^1-Methyladenosine
m^1G	N^1-Methylguanosine
$m^1\Psi$	N^1-Methylpseudouridine
m^2A	N^2-Methyladenosine
m^3C	3-Methylcytosine
m^3U	N^3-Methyluridine
$m^3\Psi$	N^3-Methylpseudouridine
m^5C	5-Methylcytosine
m^6A	N^6-Methyladenosine
mAb	monoclonal Antibody
mC_i	Millicurie
mcm^5s^2U	5-Methoxycarbonylmethyl-2-thiouridine
MELAS	Mitochondrial myopathy, encephalopathy, lactic acidosis and stroke-like episodes
MeOH	Methanol
MERRF	Myoclonus epilepsy with ragged red fibers
METTL3	Methyltransferase-like 3 protein
METTL8	Methyltransferase like protein 8
Mg^2	Magnesium ion
$MgCl_2$	Magnesium chloride
min	Minute
mJ	Millijoule
ml	Milliliter
mm	Millimeter
mM	Millimolar
mRNA	messenger RNA
ms^2hn^6A	2-methylthio-N^6-hydroxynorvalylcarbamoyladenosine
ms^2i^6A	2-Methylthio-N^6-isopentenyladenosine
ms^2io^6A	2-Methylthio-N^6-(cis-hydroxy)isopentenyl adenosine
ms^2t^6A	2-Methylthio-N^6-threonylcarbamoyladenosine
MTases	Methyltransferase
MTC	m^6A Mehyltransferase supercomplex
mtDNA	mitochondrial DNA genome
MTS	Mitochondrial targeting sequence
mt-tRNA	mitochondrial tRNA
NaCl	Sodium chloride
NADH	Nicotinamide adenine dinucleotide
NaOAc	Sodium acetate
NH_4HCO_3	Ammonium bicarbonate
NLS	Nuclear localization sequence
nm	Nanometer
nM	Nanomolar
nmol	Nanomol
OD	Optical density
ORF	Open reading frame
OXPHOS	Oxidative phosphorylation system
P	Phosphorus-32
P site	Peptidyl site
PAAD	Pancreatic adenocarcinoma
PAGE	Polyacrylamide gel electrophoresis
PBS	Phosphate Buffer Saline
PCR	Polymerase chain reaction
Phe	Phenylalanine
PK	Proteinase K
PKMTs	Protein lysine methyltransferases

pmol	Pikomol
PNK	Polynucleotide Kinase
PTFE	Polytetrafluoroethylene
PTM	Protein methyltransferase
Q	Queuine
RFM	Rossmann-fold MTases
RIP	RNA-immunoprecipitation
ROS	Reactive oxygen species
RPF	Ribosome protected fragments
rpm	Rounds per minute
rRNA	ribosomal RNA
RT	Room temperature
SAH	*S*-Adenosyl-homocysteine
SAM or AdoMet	*S*-Adensoyl-methionine
SDS	Sodium dodecyl sulfate
SED	Standard error of difference
Ser	Serine
sgRNA	single guide RNA
snRNA	small nuclear RNA
SSC	Sodium chloride-sodium citrate
STAD	Stomach adenocarcinoma
SUIT protocol	Substrate-uncoupler-inhibitor titration protocol
t^6A_{37}	N^6-Treonylcarbamoyladeonsine
TBE	Tris-Borate EDTA
TBS	Tris Buffer Saline
TBST	Tris Buffered Saline + Tween
TCA	Trichloroacetic acid
TCA cyle	Tricarboxlic acid cycle
TCGA	The Cancer Genome Atlas
Thr	Threonine
THYM	Thyroid carcinoma
Tris/HCl	Tris-(hydroxymethyl)-aminomethan/hydrochlorid
TRMU	Methylaminomethyl-2-thiouridylatemethyltransferase
tRNA	transfer RNA
$tRNA^{Trp}$	Tryptophan
Tyr	Tyrosine
U	Units, Uridine
UPR	Unfolded protein response
UTP	Uridine triphosphate
UTR	3` untranslated region
UV	Ultra violet
V	Volt
Val	Valine
w/v	weight/volume
WT	wilde type
$\tau m^5s\,^2U$	5-Taurinomethyl-2-thiouridine
τm^5U	5-Taurinomethyluridine
Ψ	Pseudouridine

5.4 References

Abbasi-Moheb, Lia; Mertel, Sara; Gonsior, Melanie; Nouri-Vahid, Leyla; Kahrizi, Kimia; Cirak, Sebahattin et al. (2012): Mutations in NSUN2 cause autosomal-recessive intellectual disability. In: *American journal of human genetics* 90 (5), S. 847–855. DOI: 10.1016/j.ajhg.2012.03.021.

Abe, Y.; Shodai, T.; Muto, T.; Mihara, K.; Torii, H.; Nishikawa, S. et al. (2000): Structural basis of presequence recognition by the mitochondrial protein import receptor Tom20. In: *Cell* 100 (5), S. 551–560. DOI: 10.1016/s0092-8674(00)80691-1.

Agris, Paul F.; Vendeix, Franck A. P.; Graham, William D. (2007): tRNA's wobble decoding of the genome. 40 years of modification. In: *Journal of molecular biology* 366 (1), S. 1–13. DOI: 10.1016/j.jmb.2006.11.046.

Alexandrov, Andrei; Chernyakov, Irina; Gu, Weifeng; Hiley, Shawna L.; Hughes, Timothy R.; Grayhack, Elizabeth J.; Phizicky, Eric M. (2006): Rapid tRNA decay can result from lack of nonessential modifications. In: *Molecular cell* 21 (1), S. 87–96. DOI: 10.1016/j.molcel.2005.10.036.

Alshammari, Musaad A.; Alshammari, Tahani K.; Laezza, Fernanda (2016): Improved Methods for Fluorescence Microscopy Detection of Macromolecules at the Axon Initial Segment. In: *Frontiers in cellular neuroscience* 10, S. 5. DOI: 10.3389/fncel.2016.00005.

Anderson, S.; Bankier, A. T.; Barrell, B. G.; Bruijn, M. H. de; Coulson, A. R.; Drouin, J. et al. (1981): Sequence and organization of the human mitochondrial genome. In: *Nature* 290 (5806), S. 457–465. DOI: 10.1038/290457a0.

Anderson, S.; Bruijn, M. H. de; Coulson, A. R.; Eperon, I. C.; Sanger, F.; Young, I. G. (1982): Complete sequence of bovine mitochondrial DNA. Conserved features of the mammalian mitochondrial genome. In: *Journal of molecular biology* 156 (4), S. 683–717. DOI: 10.1016/0022-2836(82)90137-1.

Arimbasseri, Aneeshkumar G.; Iben, James; Wei, Fan-Yan; Rijal, Keshab; Tomizawa, Kazuhito; Hafner, Markus; Maraia, Richard J. (2016): Evolving specificity of tRNA 3-methyl-cytidine-32 (m3C32) modification. A subset of tRNAsSer requires N6-isopentenylation of A37. In: *RNA (New York, N.Y.)* 22 (9), S. 1400–1410. DOI: 10.1261/rna.056259.116.

Arragain, Simon; Handelman, Samuel K.; Forouhar, Farhad; Wei, Fan-Yan; Tomizawa, Kazuhito; Hunt, John F. et al. (2010): Identification of eukaryotic and prokaryotic methylthiotransferase for biosynthesis of 2-methylthio-N6-threonylcarbamoyladenosine in tRNA. In: *The Journal of biological chemistry* 285 (37), S. 28425–28433. DOI: 10.1074/jbc.M110.106831.

Barros, Mario H.; McStay, Gavin P. (2020): Modular biogenesis of mitochondrial respiratory complexes. In: *Mitochondrion* 50, S. 94–114. DOI: 10.1016/j.mito.2019.10.008.

Batista, Pedro J.; Molinie, Benoit; Wang, Jinkai; Qu, Kun; Zhang, Jiajing; Li, Lingjie et al. (2014): m(6)A RNA modification controls cell fate transition in mammalian embryonic stem cells. In: *Cell stem cell* 15 (6), S. 707–719. DOI: 10.1016/j.stem.2014.09.019.

Begik, Oguzhan; Lucas, Morghan C.; Liu, Huanle; Ramirez, Jose Miguel; Mattick, John S.; Novoa, Eva Maria (2020): Integrative analyses of the RNA modification machinery reveal tissue- and cancer-specific signatures. In: *Genome biology* 21 (1), S. 97. DOI: 10.1186/s13059-020-02009-z.

Bento-Abreu, Andre; Jager, Gunilla; Swinnen, Bart; Rué, Laura; Hendrickx, Stijn; Jones, Ashley et al. (2018): Elongator subunit 3 (ELP3) modifies ALS through tRNA modification. In: *Human molecular genetics* 27 (7), S. 1276–1289. DOI: 10.1093/hmg/ddy043.

Berger, Raffaela S.; Wachsmuth, Christian J.; Waldhier, Magdalena C.; Renner-Sattler, Kathrin; Thomas, Simone; Chaturvedi, Anuhar et al. (2021): Lactonization of the Oncometabolite D-2-Hydroxyglutarate Produces a Novel Endogenous Metabolite. In: *Cancers* 13 (8). DOI: 10.3390/cancers13081756.

Blanco, Sandra; Dietmann, Sabine; Flores, Joana V.; Hussain, Shobbir; Kutter, Claudia; Humphreys, Peter et al. (2014): Aberrant methylation of tRNAs links cellular stress to neuro-developmental disorders. In: *The EMBO journal* 33 (18), S. 2020–2039. DOI: 10.15252/embj.201489282.

Boccaletto, Pietro; Machnicka, Magdalena A.; Purta, Elzbieta; Piatkowski, Pawel; Baginski, Blazej; Wirecki, Tomasz K. et al. (2018): MODOMICS. A database of RNA modification pathways. 2017 update. In: *Nucleic acids research* 46 (D1), D303-D307. DOI: 10.1093/nar/gkx1030.

Bohnsack, Markus T.; Sloan, Katherine E. (2018): The mitochondrial epitranscriptome. The roles of RNA modifications in mitochondrial translation and human disease. In: *Cellular and molecular life sciences : CMLS* 75 (2), S. 241–260. DOI: 10.1007/s00018-017-2598-6.

Bokar, J. A.; Rath-Shambaugh, M. E.; Ludwiczak, R.; Narayan, P.; Rottman, F. (1994): Characterization and partial purification of mRNA N6-adenosine methyltransferase from HeLa cell nuclei. Internal mRNA methylation requires a multisubunit complex. In: *The Journal of biological chemistry* 269 (26), S. 17697–17704.

Bokar, J. A.; Shambaugh, M. E.; Polayes, D.; Matera, A. G.; Rottman, F. M. (1997): Purification and cDNA cloning of the AdoMet-binding subunit of the human mRNA (N6-adenosine)-methyltransferase. In: *RNA (New York, N.Y.)* 3 (11), S. 1233–1247.

Cabello-Villegas, Javier; Winkler, Malcolm E.; Nikonowicz, Edward P. (2002): Solution conformations of unmodified and A(37)N(6)-dimethylallyl modified anticodon stem-loops of Escherichia coli tRNA(Phe). In: *Journal of molecular biology* 319 (5), S. 1015–1034. DOI: 10.1016/S0022-2836(02)00382-0.

Cantara, William A.; Crain, Pamela F.; Rozenski, Jef; McCloskey, James A.; Harris, Kimberly A.; Zhang, Xiaonong et al. (2011): The RNA Modification Database, RNAMDB. 2011 update. In: *Nucleic acids research* 39 (Database issue), D195-201. DOI: 10.1093/nar/gkq1028.

Chan, Clement T. Y.; Deng, Wenjun; Li, Fugen; DeMott, Michael S.; Babu, I. Ramesh; Begley, Thomas J.; Dedon, Peter C. (2015): Highly Predictive Reprogramming of tRNA Modifications Is Linked to Selective Expression of Codon-Biased Genes. In: *Chemical research in toxicology* 28 (5), S. 978–988. DOI: 10.1021/acs.chemrestox.5b00004.

Chan, Clement T. Y.; Dyavaiah, Madhu; DeMott, Michael S.; Taghizadeh, Koli; Dedon, Peter C.; Begley, Thomas J. (2010): A quantitative systems approach reveals dynamic control of tRNA modifications during cellular stress. In: *PLoS genetics* 6 (12), e1001247. DOI: 10.1371/journal.pgen.1001247.

Chatterjee, Biswanath; Shen, Che-Kun James; Majumder, Pritha (2021): RNA Modifications and RNA Metabolism in Neurological Disease Pathogenesis. In: *International journal of molecular sciences* 22 (21). DOI: 10.3390/ijms222111870.

Chujo, Takeshi; Tomizawa, Kazuhito (2021): Human transfer RNA modopathies. Diseases caused by aberrations in transfer RNA modifications. In: *The FEBS journal. DOI:* 10.1111/febs.15736.

Cload, S. T.; Liu, D. R.; Froland, W. A.; Schultz, P. G. (1996): Development of improved tRNAs for in vitro biosynthesis of proteins containing unnatural amino acids. In: *Chemistry & biology* 3 (12), S. 1033–1038. DOI: 10.1016/s1074-5521(96)90169-6.

Cohen, Julie S.; Srivastava, Siddharth; Farwell, Kelly D.; Lu, Hsiao-Mei; Zeng, Wenqi; Lu, Hong et al. (2015): ELP2 is a novel gene implicated in neurodevelopmental disabilities. In: *American journal of medical genetics. Part A* 167 (6), S. 1391–1395. DOI: 10.1002/ajmg.a.36935.

Cosentino, Cristina; Toivonen, Sanna; Diaz Villamil, Esteban; Atta, Mohamed; Ravanat, Jean-Luc; Demine, Stéphane et al. (2018): Pancreatic β-cell tRNA hypomethylation and fragmentation link TRMT10A deficiency with diabetes. In: *Nucleic acids research* 46 (19), S. 10302–10318. DOI: 10.1093/nar/gky839.

Crécy-Lagard, Valérie de; Boccaletto, Pietro; Mangleburg, Carl G.; Sharma, Puneet; Lowe, Todd M.; Leidel, Sebastian A.; Bujnicki, Janusz M. (2019): Matching tRNA modifications in humans to their known and predicted enzymes. In: *Nucleic acids research* 47 (5), S. 2143–2159. DOI: 10.1093/nar/gkz011.

Crécy-Lagard, Valérie de; Brochier-Armanet, Céline; Urbonavicius, Jaunius; Fernandez, Bernard; Phillips, Gabriela; Lyons, Benjamin et al. (2010): Biosynthesis of wyosine derivatives in tRNA. An ancient and highly diverse pathway in Archaea. In: *Molecular biology and evolution* 27 (9), S. 2062–2077. DOI: 10.1093/molbev/msq096.

Dai, Ling; Xing, Lianxi; Gong, Pingyuan; Zhang, Kejin; Gao, Xiaocai; Zheng, Zijian et al. (2008): Positive association of the FTSJ1 gene polymorphisms with nonsyndromic X-linked mental retardation in young Chinese male subjects. In: *Journal of human genetics* 53 (7), S. 592–597. DOI: 10.1007/s10038-008-0287-x.

Damon, Jadyn R.; Pincus, David; Ploegh, Hidde L. (2015): tRNA thiolation links translation to stress responses in Saccharomyces cerevisiae. In: *Molecular biology of the cell* 26 (2), S. 270–282. DOI: 10.1091/mbc.E14-06-1145.

Davarniya, Behzad; Hu, Hao; Kahrizi, Kimia; Musante, Luciana; Fattahi, Zohreh; Hosseini, Masoumeh et al. (2015): The Role of a Novel TRMT1 Gene Mutation and Rare GRM1 Gene Defect in Intellectual Disability in Two Azeri Families. In: *PloS one* 10 (8), e0129631. DOI: 10.1371/journal.pone.0129631.

Delaunay, Sylvain; Frye, Michaela (2019a): RNA modifications regulating cell fate in cancer. In: *Nature cell biology* 21 (5), S. 552–559. DOI: 10.1038/s41556-019-0319-0.

Delaunay, Sylvain; Frye, Michaela (2019b): RNA modifications regulating cell fate in cancer. In: *Nature cell biology* 21 (5), S. 552–559. DOI: 10.1038/s41556-019-0319-0.

Deng, Jian-Hong; Li, Youfen; Park, Jeong Soon; Wu, Jun; Hu, Peiqing; Lechleiter, James; Bai, Yidong (2006): Nuclear suppression of mitochondrial defects in cells without the ND6 subunit. In: *Molecular and cellular biology* 26 (3), S. 1077–1086. DOI: 10.1128/MCB.26.3.1077-1086.2006.

Deng, Xiaolan; Su, Rui; Weng, Hengyou; Huang, Huilin; Li, Zejuan; Chen, Jianjun (2018): RNA N(6)-methyladenosine modification in cancers. Current status and perspectives. In: *Cell research* 28 (5), S. 507–517. DOI: 10.1038/s41422-018-0034-6.

Dettmer, Katja; Nürnberger, Nadine; Kaspar, Hannelore; Gruber, Michael A.; Almstetter, Martin F.; Oefner, Peter J. (2011): Metabolite extraction from adherently growing mammalian cells for metabolomics studies. Optimization of harvesting and extraction protocols. In: *Analytical and bioanalytical chemistry* 399 (3), S. 1127–1139. DOI: 10.1007/s00216-010-4425-x.

Dominissini, Dan; Moshitch-Moshkovitz, Sharon; Schwartz, Schraga; Salmon-Divon, Mali; Ungar, Lior; Osenberg, Sivan et al. (2012): Topology of the human and mouse m6A RNA methylomes revealed by m6A-seq. In: *Nature* 485 (7397), S. 201–206. DOI: 10.1038/nature11112.

Edvardson, Simon; Prunetti, Laurence; Arraf, Aiman; Haas, Drago; Bacusmo, Jo Marie; Hu, Jennifer F. et al. (2017): tRNA N6-adenosine threonylcarbamoyltransferase defect due to KAE1/TCS3 (OSGEP) mutation manifest by neurodegeneration and renal tubulopathy. In: *European journal of human genetics : EJHG* 25 (5), S. 545–551. DOI: 10.1038/ejhg.2017.30.

El Yacoubi, Basma; Bailly, Marc; Crécy-Lagard, Valérie de (2012): Biosynthesis and function of posttranscriptional modifications of transfer RNAs. In: *Annual review of genetics* 46, S. 69–95. DOI: 10.1146/annurev-genet-110711-155641.

Endres, Lauren; Dedon, Peter C.; Begley, Thomas J. (2015): Codon-biased translation can be regulated by wobble-base tRNA modification systems during cellular stress responses. In: *RNA biology* 12 (6), S. 603–614. DOI: 10.1080/15476286.2015.1031947.

Esberg, Anders; Huang, Bo; Johansson, Marcus J. O.; Byström, Anders S. (2006): Elevated levels of two tRNA species bypass the requirement for elongator complex in transcription and exocytosis. In: *Molecular cell* 24 (1), S. 139–148. DOI: 10.1016/j.molcel.2006.07.031.

Esteve-Puig, Rosaura; Bueno-Costa, Alberto; Esteller, Manel (2020): Writers, readers and erasers of RNA modifications in cancer. In: *Cancer letters* 474, S. 127–137. DOI: 10.1016/j.canlet.2020.01.021.

Fakruddin, Md; Wei, Fan-Yan; Suzuki, Takeo; Asano, Kana; Kaieda, Takashi; Omori, Akiko et al. (2018): Defective Mitochondrial tRNA Taurine Modification Activates Global Proteostress and Leads to Mitochondrial Disease. In: *Cell reports* 22 (2), S. 482–496. DOI: 10.1016/j.celrep.2017.12.051.

Flores, Joana V.; Cordero-Espinoza, Lucía; Oeztuerk-Winder, Feride; Andersson-Rolf, Amanda; Selmi, Tommaso; Blanco, Sandra et al. (2017): Cytosine-5 RNA Methylation Regulates Neural Stem Cell Differentiation and Motility. In: *Stem cell reports* 8 (1), S. 112–124. DOI: 10.1016/j.stemcr.2016.11.014.

Friederich, M. W.; Gast, F. U.; Vacano, E.; Hagerman, P. J. (1995): Determination of the angle between the anticodon and aminoacyl acceptor stems of yeast phenylalanyl tRNA in solution. In: *Proceedings of the National Academy of Sciences of the United States of America* 92 (11), S. 4803–4807. DOI: 10.1073/pnas.92.11.4803.

Friederich, M. W.; Hagerman, P. J. (1997): The angle between the anticodon and aminoacyl acceptor stems of yeast tRNA(Phe) is strongly modulated by magnesium ions. In: *Biochemistry* 36 (20), S. 6090–6099. DOI: 10.1021/bi970066f.

Friederich, M. W.; Vacano, E.; Hagerman, P. J. (1998): Global flexibility of tertiary structure in RNA. Yeast tRNAPhe as a model system. In: *Proceedings of the National Academy of Sciences of the United States of America* 95 (7), S. 3572–3577. DOI: 10.1073/pnas.95.7.3572.

Fukasawa, Yoshinori; Tsuji, Junko; Fu, Szu-Chin; Tomii, Kentaro; Horton, Paul; Imai, Kenichiro (2015): MitoFates. Improved prediction of mitochondrial targeting sequences and their cleavage sites. In: *Molecular & cellular proteomics : MCP* 14 (4), S. 1113–1126. DOI: 10.1074/mcp.M114.043083.

Fustin, Jean-Michel; Doi, Masao; Yamaguchi, Yoshiaki; Hida, Hayashi; Nishimura, Shinichi; Yoshida, Minoru et al. (2013): RNA-methylation-dependent RNA processing controls the speed of the circadian clock. In: *Cell* 155 (4), S. 793–806. DOI: 10.1016/j.cell.2013.10.026.

Ganichkin, Oleg M.; Anedchenko, Ekaterina A.; Wahl, Markus C. (2011): Crystal structure analysis reveals functional flexibility in the selenocysteine-specific tRNA from mouse. In: *PloS one* 6 (5), e20032. DOI: 10.1371/journal.pone.0020032.

Geula, Shay; Moshitch-Moshkovitz, Sharon; Dominissini, Dan; Mansour, Abed AlFatah; Kol, Nitzan; Salmon-Divon, Mali et al. (2015): Stem cells. m6A mRNA methylation facilitates resolution of naïve pluripotency toward differentiation. In: *Science (New York, N.Y.)* 347 (6225), S. 1002–1006. DOI: 10.1126/science.1261417.

Guan, Min-Xin; Yan, Qingfeng; Li, Xiaoming; Bykhovskaya, Yelena; Gallo-Teran, Jaime; Hajek, Petr et al. (2006): Mutation in TRMU related to transfer RNA modification modulates the phenotypic expression of the deafness-associated mitochondrial 12S ribosomal RNA mutations. In: *American journal of human genetics* 79 (2), S. 291–302. DOI: 10.1086/506389.

Guy, Michael P.; Shaw, Marie; Weiner, Catherine L.; Hobson, Lynne; Stark, Zornitza; Rose, Katherine et al. (2015): Defects in tRNA Anticodon Loop 2'-O-Methylation Are Implicated in Nonsyndromic X-Linked Intellectual Disability due to Mutations in FTSJ1. In: *Human mutation* 36 (12), S. 1176–1187. DOI: 10.1002/humu.22897.

Guzzi, Nicola; Cieśla, Maciej; Ngoc, Phuong Cao Thi; Lang, Stefan; Arora, Sonali; Dimitriou, Marios et al. (2018): Pseudouridylation of tRNA-Derived Fragments Steers Translational Control in Stem Cells. In: *Cell* 173 (5), 1204-1216.e26. DOI: 10.1016/j.cell.2018.03.008.

Hasler, Daniele; Lehmann, Gerhard; Murakawa, Yasuhiro; Klironomos, Filippos; Jakob, Leonhard; Grässer, Friedrich A. et al. (2016): The Lupus Autoantigen La Prevents Mis-channeling of tRNA Fragments into the Human MicroRNA Pathway. In: *Molecular cell* 63 (1), S. 110–124. DOI: 10.1016/j.molcel.2016.05.026.

Heijne, G. von (1986): Mitochondrial targeting sequences may form amphiphilic helices. In: *The EMBO journal* 5 (6), S. 1335–1342.

Helm, M.; Brulé, H.; Degoul, F.; Cepanec, C.; Leroux, J. P.; Giegé, R.; Florentz, C. (1998): The presence of modified nucleotides is required for cloverleaf folding of a human mitochondrial tRNA. In: *Nucleic acids research* 26 (7), S. 1636–1643. DOI: 10.1093/nar/26.7.1636.

Helm, M.; Giegé, R.; Florentz, C. (1999): A Watson-Crick base-pair-disrupting methyl group (m1A9) is sufficient for cloverleaf folding of human mitochondrial tRNALys. In: *Biochemistry* 38 (40), S. 13338–13346. DOI: 10.1021/bi991061g.

Helm, Mark (2006): Post-transcriptional nucleotide modification and alternative folding of RNA. In: *Nucleic acids research* 34 (2), S. 721–733. DOI: 10.1093/nar/gkj471.

Hou, Ya-Ming; Gamper, Howard; Yang, Wei (2015): Post-transcriptional modifications to tRNA--a response to the genetic code degeneracy. In: *RNA (New York, N.Y.)* 21 (4), S. 642–644. DOI: 10.1261/rna.049825.115.

Hua, Wenfeng; Zhao, Yuan; Jin, Xiaohan; Yu, Danyang; He, Jing; Xie, Dan; Duan, Ping (2018): METTL3 promotes ovarian carcinoma growth and invasion through the regulation of AXL translation

and epithelial to mesenchymal transition. In: *Gynecologic oncology* 151 (2), S. 356–365. DOI: 10.1016/j.ygyno.2018.09.015.

Huang, Huilin; Weng, Hengyou; Deng, Xiaolan; Chen, Jianjun (2020): RNA Modifications in Cancer. Functions, Mechanisms, and Therapeutic Implications. In: *Annual Review of Cancer Biology* 4 (1), S. 221–240. DOI: 10.1146/annurev-cancerbio-030419-033357.

Huang, Shi-Qiong; Sun, Bao; Xiong, Zong-Ping; Shu, Yan; Zhou, Hong-Hao; Zhang, Wei et al. (2018): The dysregulation of tRNAs and tRNA derivatives in cancer. In: *Journal of experimental & clinical cancer research : CR* 37 (1), S. 101. DOI: 10.1186/s13046-018-0745-z.

Huber, Sabrina M.; Leonardi, Andrea; Dedon, Peter C.; Begley, Thomas J. (2019): The Versatile Roles of the tRNA Epitranscriptome during Cellular Responses to Toxic Exposures and Environmental Stress. In: *Toxics* 7 (1). DOI: 10.3390/toxics7010017.

Jia, Guifang; Fu, Ye; Zhao, Xu; Dai, Qing; Zheng, Guanqun; Yang, Ying et al. (2011): N6-methyladenosine in nuclear RNA is a major substrate of the obesity-associated FTO. In: *Nature chemical biology* 7 (12), S. 885–887. DOI: 10.1038/nchembio.687.

Kadaba, Sujatha; Krueger, Anna; Trice, Tamyra; Krecic, Annette M.; Hinnebusch, Alan G.; Anderson, James (2004): Nuclear surveillance and degradation of hypomodified initiator tRNAMet in S. cerevisiae. In: *Genes & development* 18 (11), S. 1227–1240. DOI: 10.1101/gad.1183804.

Kimura, Satoshi; Miyauchi, Kenjyo; Ikeuchi, Yoshiho; Thiaville, Patrick C.; Crécy-Lagard, Valérie de; Suzuki, Tsutomu (2014): Discovery of the β-barrel-type RNA methyltransferase responsible for N6-methylation of N6-threonylcarbamoyladenosine in tRNAs. In: *Nucleic acids research* 42 (14), S. 9350–9365. DOI: 10.1093/nar/gku618.

Kirchner, Sebastian; Ignatova, Zoya (2015): Emerging roles of tRNA in adaptive translation, signalling dynamics and disease. In: *Nature reviews. Genetics* 16 (2), S. 98–112. DOI: 10.1038/nrg3861.

Kobayashi, Y.; Momoi, M. Y.; Tominaga, K.; Momoi, T.; Nihei, K.; Yanagisawa, M. et al. (1990): A point mutation in the mitochondrial tRNA(Leu)(UUR) gene in MELAS (mitochondrial myopathy, encephalopathy, lactic acidosis and stroke-like episodes). In: *Biochemical and biophysical research communications* 173 (3), S. 816–822. DOI: 10.1016/s0006-291x(05)80860-5.

Krüger, M. K.; Sørensen, M. A. (1998): Aminoacylation of hypomodified tRNAGlu in vivo. In: *Journal of molecular biology* 284 (3), S. 609–620. DOI: 10.1006/jmbi.1998.2197.

Lamichhane, Tek N.; Blewett, Nathan H.; Crawford, Amanda K.; Cherkasova, Vera A.; Iben, James R.; Begley, Thomas J. et al. (2013): Lack of tRNA modification isopentenyl-A37 alters mRNA decoding and causes metabolic deficiencies in fission yeast. In: *Molecular and cellular biology* 33 (15), S. 2918–2929. DOI: 10.1128/MCB.00278-13.

Lee, Yong Sun; Shibata, Yoshiyuki; Malhotra, Ankit; Dutta, Anindya (2009): A novel class of small RNAs. TRNA-derived RNA fragments (tRFs). In: *Genes & development* 23 (22), S. 2639–2649. DOI: 10.1101/gad.1837609.

Lin, Huan; Miyauchi, Kenjyo; Harada, Tai; Okita, Ryo; Takeshita, Eri; Komaki, Hirofumi et al. (2018): CO(2)-sensitive tRNA modification associated with human mitochondrial disease. In: *Nature communications* 9 (1), S. 1875. DOI: 10.1038/s41467-018-04250-4.

Lin, Shuibin; Choe, Junho; Du, Peng; Triboulet, Robinson; Gregory, Richard I. (2016): The m(6)A Methyltransferase METTL3 Promotes Translation in Human Cancer Cells. In: *Molecular cell* 62 (3), S. 335–345. DOI: 10.1016/j.molcel.2016.03.021.

Liu, Fange; Clark, Wesley; Luo, Guanzheng; Wang, Xiaoyun; Fu, Ye; Wei, Jiangbo et al. (2016): ALKBH1-Mediated tRNA Demethylation Regulates Translation. In: *Cell* 167 (3), 816-828.e16. DOI: 10.1016/j.cell.2016.09.038.

Liu, Jianzhao; Yue, Yanan; Han, Dali; Wang, Xiao; Fu, Ye; Zhang, Liang et al. (2014): A METTL3-METTL14 complex mediates mammalian nuclear RNA N6-adenosine methylation. In: *Nature chemical biology* 10 (2), S. 93–95. DOI: 10.1038/nchembio.1432.

Liu, Nian; Parisien, Marc; Dai, Qing; Zheng, Guanqun; He, Chuan; Pan, Tao (2013): Probing N6-methyladenosine RNA modification status at single nucleotide resolution in mRNA and long noncoding RNA. In: *RNA (New York, N.Y.)* 19 (12), S. 1848–1856. DOI: 10.1261/rna.041178.113.

Lorenz, Christian; Lünse, Christina E.; Mörl, Mario (2017): tRNA Modifications. Impact on Structure and Thermal Adaptation. In: *Biomolecules* 7 (2). DOI: 10.3390/biom7020035.

Machnicka, Magdalena A.; Milanowska, Kaja; Osman Oglou, Okan; Purta, Elzbieta; Kurkowska, Malgorzata; Olchowik, Anna et al. (2013): MODOMICS. A database of RNA modification pathways--2013 update. In: *Nucleic acids research* 41 (Database issue), D262-7. DOI: 10.1093/nar/gks1007.

Machnicka, Magdalena A.; Olchowik, Anna; Grosjean, Henri; Bujnicki, Janusz M. (2014): Distribution and frequencies of post-transcriptional modifications in tRNAs. In: *RNA biology* 11 (12), S. 1619–1629. DOI: 10.4161/15476286.2014.992273.

Marchand, Virginie; Ayadi, Lilia; Ernst, Felix G. M.; Hertler, Jasmin; Bourguignon-Igel, Valérie; Galvanin, Adeline et al. (2018): AlkAniline-Seq. Profiling of m(7) G and m(3) C RNA Modifications at Single Nucleotide Resolution. In: *Angewandte Chemie (International ed. in English)* 57 (51), S. 16785–16790. DOI: 10.1002/anie.201810946.

Martens-Uzunova, Elena S.; Böttcher, René; Croce, Carlo M.; Jenster, Guido; Visakorpi, Tapio; Calin, George A. (2014): Long noncoding RNA in prostate, bladder, and kidney cancer. In: *European urology* 65 (6), S. 1140–1151. DOI: 10.1016/j.eururo.2013.12.003.

Maute, Roy L.; Schneider, Christof; Sumazin, Pavel; Holmes, Antony; Califano, Andrea; Basso, Katia; Dalla-Favera, Riccardo (2013): tRNA-derived microRNA modulates proliferation and the DNA damage response and is down-regulated in B cell lymphoma. In: *Proceedings of the National Academy of Sciences of the United States of America* 110 (4), S. 1404–1409. DOI: 10.1073/pnas.1206761110.

Meister, Gunter; Tuschl, Thomas (2004): Mechanisms of gene silencing by double-stranded RNA. In: *Nature* 431 (7006), S. 343–349. DOI: 10.1038/nature02873.

Meng, Feilong; Cang, Xiaohui; Peng, Yanyan; Li, Ronghua; Zhang, Zhengyue; Li, Fushan et al. (2017): Biochemical Evidence for a Nuclear Modifier Allele (A10S) in TRMU (Methylaminomethyl-2-thiouridylate-methyltransferase) Related to Mitochondrial tRNA Modification in the Phenotypic Manifestation of Deafness-associated 12S rRNA Mutation. In: *The Journal of biological chemistry* 292 (7), S. 2881–2892. DOI: 10.1074/jbc.M116.749374.

Meyer, Kate D.; Saletore, Yogesh; Zumbo, Paul; Elemento, Olivier; Mason, Christopher E.; Jaffrey, Samie R. (2012): Comprehensive analysis of mRNA methylation reveals enrichment in 3' UTRs and near stop codons. In: *Cell* 149 (7), S. 1635–1646. DOI: 10.1016/j.cell.2012.05.003.

Miyauchi, Kenjyo; Kimura, Satoshi; Suzuki, Tsutomu (2013): A cyclic form of N6-threonylcarbamoyladenosine as a widely distributed tRNA hypermodification. In: *Nature chemical biology* 9 (2), S. 105–111. DOI: 10.1038/nchembio.1137.

Morris, R. C.; Brown, K. G.; Elliott, M. S. (1999): The effect of queuosine on tRNA structure and function. In: *Journal of biomolecular structure & dynamics* 16 (4), S. 757–774. DOI: 10.1080/07391102.1999.10508291.

Motorin, Yuri; Helm, Mark (2010): tRNA stabilization by modified nucleotides. In: *Biochemistry* 49 (24), S. 4934–4944. DOI: 10.1021/bi100408z.

Motorin, Yuri; Helm, Mark (2011): RNA nucleotide methylation. In: *Wiley interdisciplinary reviews. RNA* 2 (5), S. 611–631. DOI: 10.1002/wrna.79.

Mugridge, Jeffrey S.; Coller, Jeff; Gross, John D. (2018): Structural and molecular mechanisms for the control of eukaryotic 5'-3' mRNA decay. In: *Nature structural & molecular biology* 25 (12), S. 1077–1085. DOI: 10.1038/s41594-018-0164-z.

Murphy, Frank V., 4th.; Ramakrishnan, Venki; Malkiewicz, Andrzej; Agris, Paul F. (2004): The role of modifications in codon discrimination by tRNA(Lys)UUU. In: *Nature structural & molecular biology* 11 (12), S. 1186–1191. DOI: 10.1038/nsmb861.

O'Shea, Joseph P.; Chou, Michael F.; Quader, Saad A.; Ryan, James K.; Church, George M.; Schwartz, Daniel (2013): pLogo. A probabilistic approach to visualizing sequence motifs. In: *Nature methods* 10 (12), S. 1211–1212. DOI: 10.1038/nmeth.2646.

Palmer, Colin J.; Bruckner, Raphael J.; Paulo, Joao A.; Kazak, Lawrence; Long, Jonathan Z.; Mina, Amir I. et al. (2017): Cdkal1, a type 2 diabetes susceptibility gene, regulates mitochondrial function in adipose tissue. In: *Molecular metabolism* 6 (10), S. 1212–1225. DOI: 10.1016/j.molmet.2017.07.013.

Pan, Yutian; Ma, Pei; Liu, Yu; Li, Wei; Shu, Yongqian (2018): Multiple functions of m(6)A RNA methylation in cancer. In: *Journal of hematology & oncology* 11 (1), S. 48. DOI: 10.1186/s13045-018-0590-8.

Parnell, Amber A.; Nobrega, Aliza K. de; Lyons, Lisa C. (2021): Translating around the clock. Multi-level regulation of post-transcriptional processes by the circadian clock. In: *Cellular signalling* 80, S. 109904. DOI: 10.1016/j.cellsig.2020.109904.

Patil, Deepak P.; Chen, Chun-Kan; Pickering, Brian F.; Chow, Amy; Jackson, Constanza; Guttman, Mitchell; Jaffrey, Samie R. (2016): m(6)A RNA methylation promotes XIST-mediated transcriptional repression. In: *Nature* 537 (7620), S. 369–373. DOI: 10.1038/nature19342.

Pearce, Sarah F.; Rorbach, Joanna; van Haute, Lindsey; D'Souza, Aaron R.; Rebelo-Guiomar, Pedro; Powell, Christopher A. et al. (2017): Maturation of selected human mitochondrial tRNAs requires deadenylation. In: *eLife* 6. DOI: 10.7554/eLife.27596.

Perales-Clemente, Ester; Fernández-Vizarra, Erika; Acín-Pérez, Rebeca; Movilla, Nieves; Bayona-Bafaluy, María Pilar; Moreno-Loshuertos, Raquel et al. (2010): Five entry points of the mitochondrially encoded subunits in mammalian complex I assembly. In: *Molecular and cellular biology* 30 (12), S. 3038–3047. DOI: 10.1128/MCB.00025-10.

Ping, Xiao-Li; Sun, Bao-Fa; Wang, Lu; Xiao, Wen; Yang, Xin; Wang, Wen-Jia et al. (2014): Mammalian WTAP is a regulatory subunit of the RNA N6-methyladenosine methyltransferase. In: *Cell research* 24 (2), S. 177–189. DOI: 10.1038/cr.2014.3.

Rapino, Francesca; Delaunay, Sylvain; Zhou, Zhaoli; Chariot, Alain; Close, Pierre (2017): tRNA Modification. Is Cancer Having a Wobble? In: *Trends in cancer* 3 (4), S. 249–252. DOI: 10.1016/j.trecan.2017.02.004.

Rezgui, Vanessa Anissa Nathalie; Tyagi, Kshitiz; Ranjan, Namit; Konevega, Andrey L.; Mittelstaet, Joerg; Rodnina, Marina V. et al. (2013): tRNA tKUUU, tQUUG, and tEUUC wobble position modifications fine-tune protein translation by promoting ribosome A-site binding. In: *Proceedings of the National Academy of Sciences of the United States of America* 110 (30), S. 12289–12294. DOI: 10.1073/pnas.1300781110.

Roise, D.; Horvath, S. J.; Tomich, J. M.; Richards, J. H.; Schatz, G. (1986): A chemically synthesized pre-sequence of an imported mitochondrial protein can form an amphiphilic helix and perturb natural and artificial phospholipid bilayers. In: *The EMBO journal* 5 (6), S. 1327–1334.

Roise, D.; Schatz, G. (1988): Mitochondrial presequences. In: *The Journal of biological chemistry* 263 (10), S. 4509–4511.

Roise, D.; Theiler, F.; Horvath, S. J.; Tomich, J. M.; Richards, J. H.; Allison, D. S.; Schatz, G. (1988): Amphiphilicity is essential for mitochondrial presequence function. In: *The EMBO journal* 7 (3), S. 649–653.

Rojas-Benítez, Diego; Eggers, Cristián; Glavic, Alvaro (2017): Modulation of the Proteostasis Machinery to Overcome Stress Caused by Diminished Levels of t6A-Modified tRNAs in Drosophila. In: *Biomolecules* 7 (1). DOI: 10.3390/biom7010025.

Roundtree, Ian A.; Evans, Molly E.; Pan, Tao; He, Chuan (2017): Dynamic RNA Modifications in Gene Expression Regulation. In: *Cell* 169 (7), S. 1187–1200. DOI: 10.1016/j.cell.2017.05.045.

Sánchez-Caballero, Laura; Guerrero-Castillo, Sergio; Nijtmans, Leo (2016): Unraveling the complexity of mitochondrial complex I assembly. A dynamic process. In: *Biochimica et biophysica acta* 1857 (7), S. 980–990. DOI: 10.1016/j.bbabio.2016.03.031.

Schaffer, Stephen W.; Jong, Chian Ju; Ito, Takashi; Azuma, Junichi (2014): Role of taurine in the pathologies of MELAS and MERRF. In: *Amino acids* 46 (1), S. 47–56. DOI: 10.1007/s00726-012-1414-8.

Schöller, Eva; Weichmann, Franziska; Treiber, Thomas; Ringle, Sam; Treiber, Nora; Flatley, Andrew et al. (2018): Interactions, localization, and phosphorylation of the m(6)A generating METTL3-METTL14-WTAP complex. In: *RNA (New York, N.Y.)* 24 (4), S. 499–512. DOI: 10.1261/rna.064063.117.

Schwartz, Schraga (2016): Cracking the epitranscriptome. In: *RNA (New York, N.Y.)* 22 (2), S. 169–174. DOI: 10.1261/rna.054502.115.

Schwartz, Schraga; Mumbach, Maxwell R.; Jovanovic, Marko; Wang, Tim; Maciag, Karolina; Bushkin, G. Guy et al. (2014): Perturbation of m6A writers reveals two distinct classes of mRNA methylation at internal and 5' sites. In: *Cell reports* 8 (1), S. 284–296. DOI: 10.1016/j.celrep.2014.05.048.

Shen, Yijing; Yu, Xiuchong; Zhu, Linwen; Li, Tianwen; Yan, Zhilong; Guo, Junming (2018): Transfer RNA-derived fragments and tRNA halves. Biogenesis, biological functions and their roles in diseases. In: *Journal of molecular medicine (Berlin, Germany)* 96 (11), S. 1167–1176. DOI: 10.1007/s00109-018-1693-y.

Signes, Alba; Fernandez-Vizarra, Erika (2018): Assembly of mammalian oxidative phosphorylation complexes I-V and supercomplexes. In: *Essays in biochemistry* 62 (3), S. 255–270. DOI: 10.1042/EBC20170098.

Simpson, Claire L.; Lemmens, Robin; Miskiewicz, Katarzyna; Broom, Wendy J.; Hansen, Valerie K.; van Vught, Paul W. J. et al. (2009): Variants of the elongator protein 3 (ELP3) gene are associated with motor neuron degeneration. In: *Human molecular genetics* 18 (3), S. 472–481. DOI: 10.1093/hmg/ddn375.

Soares, Ana Raquel; Santos, Manuel (2017): Discovery and function of transfer RNA-derived fragments and their role in disease. In: *Wiley interdisciplinary reviews. RNA* 8 (5). DOI: 10.1002/wrna.1423.

Struck, Anna-Winona; Thompson, Mark L.; Wong, Lu Shin; Micklefield, Jason (2012): S-adenosyl-methionine-dependent methyltransferases. Highly versatile enzymes in biocatalysis, biosynthesis and other biotechnological applications. In: *Chembiochem : a European journal of chemical biology* 13 (18), S. 2642–2655. DOI: 10.1002/cbic.201200556.

Suzuki, Takeo; Suzuki, Tsutomu (2014): A complete landscape of post-transcriptional modifications in mammalian mitochondrial tRNAs. In: *Nucleic acids research* 42 (11), S. 7346–7357. DOI: 10.1093/nar/gku390.

Suzuki, Takeo; Yashiro, Yuka; Kikuchi, Ittoku; Ishigami, Yuma; Saito, Hironori; Matsuzawa, Ikuya et al. (2020): Complete chemical structures of human mitochondrial tRNAs. In: *Nature communications* 11 (1), S. 4269. DOI: 10.1038/s41467-020-18068-6.

Suzuki, Tsutomu (2021): The expanding world of tRNA modifications and their disease relevance. In: *Nature reviews. Molecular cell biology* 22 (6), S. 375–392. DOI: 10.1038/s41580-021-00342-0.

Swinehart, William E.; Jackman, Jane E. (2015): Diversity in mechanism and function of tRNA methyltransferases. In: *RNA biology* 12 (4), S. 398–411. DOI: 10.1080/15476286.2015.1008358.

Takai, Kazuyuki; Yokoyama, Shigeyuki (2003): Roles of 5-substituents of tRNA wobble uridines in the recognition of purine-ending codons. In: *Nucleic acids research* 31 (22), S. 6383–6391. DOI: 10.1093/nar/gkg839.

Tataranni, Tiziana; Agriesti, Francesca; Ruggieri, Vitalba; Mazzoccoli, Carmela; Simeon, Vittorio; Laurenzana, Ilaria et al. (2017): Rewiring carbohydrate catabolism differentially affects survival of pancreatic cancer cell lines with diverse metabolic profiles. In: *Oncotarget* 8 (25), S. 41265–41281. DOI: 10.18632/oncotarget.17172.

Temperley, Richard; Richter, Ricarda; Dennerlein, Sven; Lightowlers, Robert N.; Chrzanowska-Lightowlers, Zofia M. (2010): Hungry codons promote frameshifting in human mitochondrial ribosomes. In: *Science (New York, N.Y.)* 327 (5963), S. 301. DOI: 10.1126/science.1180674.

Tudek, Agnieszka; Schmid, Manfred; Jensen, Torben Heick (2019): Escaping nuclear decay. The significance of mRNA export for gene expression. In: *Current genetics* 65 (2), S. 473–476. DOI: 10.1007/s00294-018-0913-x.

Tuorto, Francesca; Lyko, Frank (2016a): Genome recoding by tRNA modifications. In: *Open biology* 6 (12). DOI: 10.1098/rsob.160287.

Tuorto, Francesca; Lyko, Frank (2016b): Genome recoding by tRNA modifications. In: *Open biology* 6 (12). DOI: 10.1098/rsob.160287.

Varshney, U.; Lee, C. P.; RajBhandary, U. L. (1991): Direct analysis of aminoacylation levels of tRNAs in vivo. Application to studying recognition of Escherichia coli initiator tRNA mutants by glutaminyl-tRNA synthetase. In: *The Journal of biological chemistry* 266 (36), S. 24712–24718.

Vinayak, Manjula; Pathak, Chandramani (2009): Queuosine modification of tRNA. Its divergent role in cellular machinery. In: *Bioscience reports* 30 (2), S. 135–148. DOI: 10.1042/BSR20090057.

Wang, Yang; Li, Yue; Toth, Julia I.; Petroski, Matthew D.; Zhang, Zhaolei; Zhao, Jing Crystal (2014): N6-methyladenosine modification destabilizes developmental regulators in embryonic stem cells. In: *Nature cell biology* 16 (2), S. 191–198. DOI: 10.1038/ncb2902.

Wei, Fan-Yan; Suzuki, Takeo; Watanabe, Sayaka; Kimura, Satoshi; Kaitsuka, Taku; Fujimura, Atsushi et al. (2011): Deficit of tRNA(Lys) modification by Cdkal1 causes the development of type 2 diabetes in mice. In: *The Journal of clinical investigation* 121 (9), S. 3598–3608. DOI: 10.1172/JCI58056.

Weixlbaumer, Albert; Murphy, Frank V., 4th.; Dziergowska, Agnieszka; Malkiewicz, Andrzej; Vendeix, Franck A. P.; Agris, Paul F.; Ramakrishnan, V. (2007): Mechanism for expanding the decoding capacity of transfer RNAs by modification of uridines. In: *Nature structural & molecular biology* 14 (6), S. 498–502. DOI: 10.1038/nsmb1242.

Wen, Jing; Lv, Ruitu; Ma, Honghui; Shen, Hongjie; He, Chenxi; Wang, Jiahua et al. (2018): Zc3h13 Regulates Nuclear RNA m(6)A Methylation and Mouse Embryonic Stem Cell Self-Renewal. In: *Molecular cell* 69 (6), 1028-1038.e6. DOI: 10.1016/j.molcel.2018.02.015.

Xu, Luang; Liu, Xinyu; Sheng, Na; Oo, Kyaw Soe; Liang, Junxin; Chionh, Yok Hian et al. (2017): Three distinct 3-methylcytidine (m(3)C) methyltransferases modify tRNA and mRNA in mice and humans. In: *The Journal of biological chemistry* 292 (35), S. 14695–14703. DOI: 10.1074/jbc.M117.798298.

Yarham, John W.; Lamichhane, Tek N.; Pyle, Angela; Mattijssen, Sandy; Baruffini, Enrico; Bruni, Francesco et al. (2014): Defective i6A37 modification of mitochondrial and cytosolic tRNAs results from pathogenic mutations in TRIT1 and its substrate tRNA. In: *PLoS genetics* 10 (6), e1004424. DOI: 10.1371/journal.pgen.1004424.

Yeung, Man Lung; Bennasser, Yamina; Watashi, Koichi; Le, Shu-Yun; Houzet, Laurent; Jeang, Kuan-Teh (2009): Pyrosequencing of small non-coding RNAs in HIV-1 infected cells. Evidence for the processing of a viral-cellular double-stranded RNA hybrid. In: *Nucleic acids research* 37 (19), S. 6575–6586. DOI: 10.1093/nar/gkp707.

Yue, Yanan; Liu, Jun; Cui, Xiaolong; Cao, Jie; Luo, Guanzheng; Zhang, Zezhou et al. (2018): VIRMA mediates preferential m(6)A mRNA methylation in 3'UTR and near stop codon and associates with alternative polyadenylation. In: *Cell discovery* 4, S. 10. DOI: 10.1038/s41421-018-0019-0.

Zhang, Li-Hong; Zhang, Xue-Yun; Hu, Tao; Chen, Xin-Yun; Li, Jing-Jia; Raida, Manfred et al. (2020): The SUMOylated METTL8 Induces R-loop and Tumorigenesis via m3C. In: *iScience* 23 (3), S. 100968. DOI: 10.1016/j.isci.2020.100968.

Zheng, Guanqun; Dahl, John Arne; Niu, Yamei; Fedorcsak, Peter; Huang, Chun-Min; Li, Charles J. et al. (2013): ALKBH5 is a mammalian RNA demethylase that impacts RNA metabolism and mouse fertility. In: *Molecular cell* 49 (1), S. 18–29. DOI: 10.1016/j.molcel.2012.10.01